LOS ALAMOS SCIENTIFIC LABORATORY
of the
University of California

LOS ALAMOS • NEW MEXICO

Quarterly Status Report on the

Advanced Plutonium Fuels Program

October 1 to December 31, 1968

UNITED STATES
ATOMIC ENERGY COMMISSION
CONTRACT W-7405-ENG. 36

This LA...MS report presents the status of the LASL Advanced Plutonium Fuels Program. Previous Quarterly Status Reports in this series, all unclassified, are:

LA-3607-MS	LA-3745-MS	LA-3933-MS
LA-3650-MS	LA-3760-MS*	LA-3993-MS
LA-3686-MS	LA-3820-MS	LA-4073-MS
LA-3708-MS*	LA-3880-MS	

This report, like other special-purpose documents in the LA...MS series, has not been reviewed or verified for accuracy in the interest of prompt distribution.

*Advanced Reactor Technology (ART) Series.

Distributed: March 4, 1969

LA-4114-MS
SPECIAL DISTRIBUTION

LOS ALAMOS SCIENTIFIC LABORATORY
of the
University of California

LOS ALAMOS • NEW MEXICO

Quarterly Status Report on the

Advanced Plutonium Fuels Program

October 1 to December 31, 1968

FOREWORD

This is the tenth quarterly report on the Advanced Plutonium Fuels Program conducted at the Los Alamos Scientific Laboratory. The work is centered around problem areas associated with LMFBR development, though some of it has a broader applicability to general reactor technology.

Most of the investigations discussed here are of the continuing type. Results and conclusions described may therefore be changed or augmented as the work continues. Published reference to results cited in this report should not be made without obtaining explicit permission to do so from the person in charge of the work.

TABLE OF CONTENTS

TABLE OF CONTENTS
(continued)

PROJECT 401

EXAMINATION OF FAST REACTOR FUELS

Person in Charge: R. D. Baker
Principal Investigators: J. W. Schulte
J. A. Leary
C. F. Metz

I. INTRODUCTION

This project is directed toward the examination and comparison of the effects of neutron irradiation on LMFBR Program fuel materials. Irradiated materials are examined as requested by the Fuels and Materials Branch of DRD & T.

Another phase of this project is the development of an analytical chemistry program designed to assure the high-quality well-characterized fuel required by the LMFBR/FFTF Program. In close cooperation with PNL, an analytical program has been developed which has the following objectives:

1. To evaluate the present capabilities of potential fuel producers for making the analytical measurements on FFTF fuel that are necessary to assure the uniformly high quality fuel required by the LMFBR/FFTF Program.
2. To provide technical guidance to fuel producers, as may be required, to assure these capabilities are established at the level required by FFTF reactor fuel specifications.
3. To establish and conduct a monitoring program that will assure continuing technical competence of fuel producers for the analysis of FFTF fuel at the level required by fuel specifications.

II. HOT CELL EQUIPMENT DEVELOPMENT

Shipping Cask
(J. W. Schulte)

Design of the shielded cask for shipping irradiated fuel elements from EBR-II was completed. Engineering analyses were made which indicated the cask would withstand the hypothetical accident conditions listed in Chapter 0529 of the AEC Manual. Approval of this cask for shipping highly irradiated fissile material was received from the AEC's ALO Office. Estimates for fabrication of the cask are currently being obtained. Construction will commence upon receiving approval of the design from the Department of Transportation.

Argon Purification Unit
(C. E. Frantz, R. F. Velkinburg)

This unit was purchased for providing an inert atmosphere for the two grinding-polishing containment boxes as well as the blister which houses the metallograph. The purification unit was received in November. Minor deficiencies, noted in preliminary tests, have been corrected by using materials and instructions furnished by the manufacturer.

In-Cell Equipment
(G. R. Brewer, D. B. Court, E. L. Ekberg, F. J. Fitzgibbon, M. E. Lazarus, F. H. Newbury, T. Romanik, J. R. Trujillo)

Additional modifications to existing equipment were made to provide better measurements or increased through-put.

1. Dimensioning Equipment

Work continues on the design and procurement for the new profilometer which will be operated in the beta-gamma cells; thereby relieving some of the

congestion currently encountered in the disassembly cell where many other operations are carried out.

Several short standards have been made to provide assurance that the profilometer, presently in operation, is providing accurate data on the diameters currently being measured. A full length standard was fabricated to show that the profilometer is giving reliable and reproducible results over the entire length capability (ca. 48 in.). This standard will also be used to obtain data for a precision analysis on the profilometer.

2. Fission Gas Sampling and Void-Volume Determination

The equipment previously described was used successfully in obtaining fission gas samples from PNL, BNW, and UNC pins (and capsules). A program for the Olivetti-Underwood Computer has been written to perform gas volume calculations. Calculations which previously took 3 hr can now be completed in less than 20 min on the new machine.

3. Cut-Off Saw

Using a standard tool post grinder as the basic unit, a high speed cut-off saw was designed and installed for obtaining transverse sections of fuel pins. This unit will be used on both mixed oxide and carbide fuels. It will supplement the slitting saw installed as original equipment.

4. Other Support Equipment

Progress has also been made on the following items:

a. Design of transfer cart for shielded electron microprobe cask.
b. Gamma scanning installation at DP West.
c. Installation of carbon evaporator for microprobe samples.
d. Improved design for containers in which to remove fuel pin samples and sections from the alpha containment boxes.
e. Low temperature soldering capability to provide gastight containers suitable for long-term storage or shipping.

Differential Thermal Analysis
(D. B. Court)

Minor changes are being made to some of the equipment to make the remote operation less difficult. After these changes are completed, the system will be given a final check prior to calibrating the equipment. It will then be suitable for the analysis of irradiated fuels.

Heat Content Measurement
(C. E. Frantz)

The individual mechanical motions of the calorimeter and related equipment were tested and modified as required. The alpha-box has now been installed in the cell, and a check-out of the entire integrated system is now possible.

III. HOT CELL APPLICATIONS OF ANALYTICAL METHODS

Measurement of O_2 and N_2
(G. C. Swanson, J. W. Dahlby)

Calibration and testing was started on a LECO Nitrox-6 Analyzer for measurement of N_2 and O_2 in fuels at concentrations in either the ppm or percent ranges. This instrument is a combination of an inert-gas-fusion induction furnace and a simplified gas chromatograph. The sample is heated in a C crucible, the evolved N_2 and CO are trapped on molecular sieve cooled in liquid N_2, and the gases are then injected into the chromatograph where they are separated and measured.

Following suitable adjustments and flushings, the apparatus blank for N_2 was reduced to approximately 5 μg; the relative standard deviation was 1 percent in measuring this blank. Data for a calibration curve were obtained by repeated measurements of known quantities of added N_2 between 9.0 and 65.6 μg. More data are being obtained to extend the range to 100 μg of N_2 before a statistical evaluation of the data is made. Based upon present results, the relative standard deviation of the method at the lower limit of reliable measurement, 2 μg of N_2, is 50 percent. Organic and inorganic standards are being prepared for calibration of the instrument for measurement of O_2.

Thermogravimetric Determination of O/M Atom Ratios
(G. C. Swanson, J. W. Dahlby)

Modifications were made on a micro thermobalance (Fisher Model 360) to adapt it to hot-cell

gravimetric measurements of O/M atom ratios by Lyon's method on sintered mixed oxide samples weighing 0.1 to 0.5 g. Modifications included installation of Pt crucibles of 0.5-g capacity, changing the carrier gas flow pattern to improve purging of the balance chamber, and sealing of the balance compartment. A gas manifold system was installed to provide either dry He or He-H_2 mixtures to the furnace chamber. The system was checked by heating U metal in the sample pan for 24 hr at 1000°C in a stream of He. The U did not increase in weight, showing that the system was gastight and not contaminated with air.

Preliminary oxidation-reduction cycles using U metal samples showed that the calibration of the Cahn electrobalance is critical and dependent upon the sample size. The balance is being calibrated initially for 250-mg samples. For this sample size, weights can be measured to ±0.4 μg which corresponds to ± 0.0001 in the O/M ratio.

Shielded Electron Microprobe
(W. V. Cummings, E. A. Hakkila)

Installation of the shielded electron microprobe (Materials Analysis Corporation) is essentially complete, except for a few back-ordered items; check-out of the instrument was continued. The testing procedure showed unsatisfactory operation of an automatic valving assembly in the vacuum system, which was completely replaced by the vendor. The digital voltmeter, data coupler, one flow proportional counter, and a pre-amplifier were returned for exchange or repair. Temporary loss of these items did not put the probe completely out of operation, and testing was continued.

A vacuum evaporator for coating the mounted samples with thin, electrically conducting layers of either C or various metals was tested, and design work for installing the instrument in a hot cell was started. Also, work was initiated on design of a transfer cart for the microprobe cask. The cart will transport the cask from the sample preparation area in the hot cells to the shielded microprobe in an adjacent laboratory.

Measurement of U and Pu
(J. W. Dahlby, G. R. Waterbury)

Titration cells using magnetic stirrers were built and tested for controlled-potential coulometric titrations of U and Pu in a hot cell. Repeated titrations of known quantities of U and Fe, used as a stand-in for Pu, showed that the equipment functioned properly and that the methods were unbiased. Relative standard deviations for a single determination were 0.1 percent in measuring U and 0.05 percent in measuring Fe. In these determinations, the titration current was integrated while U(VI) was coulometrically reduced at a Hg electrode to U(IV) following a preliminary reduction of more-easily reduced impurities. Titration of the Fe or Pu involved a quantitative coulometric reduction to Fe(II) or Pu(III) at a Pt working electrode followed by an oxidation to Fe(III) or Pu(IV). The titration current was integrated during the oxidation.

The titration equipment was installed in a hot cell, and testing was started. Some difficulty was experienced in maintaining good electrical connections between the in-cell equipment and the external coulometers. Initial results for titrations of known amounts of U were high, and possible sources of the interference are being sought.

Spectrographic Analysis of Acid Insoluble Residue from Irradiated $(U,Pu)O_2$
(J. W. Dahlby, O. R. Simi)

A 0.1515-g sample of $(U,Pu)O_2$, having undergone approximately 12 percent burnup, was partially dissolved by repeated treatments with hot HNO_3-HF during a 60-hr period followed by heating with 6N HCl. The small quantity of insoluble residue was washed with water, dried, and analyzed semiquantitatively by a spectrographic method. As expected, the residue contained significant concentrations of Mo, Tc, Ru, Rh, and Pd. In addition, Ti, U, Ba, Mg, Al, Ca, Cr, Fe, Cu, B, Si, Mn, Co, Ni, Sr, and Sn were found at concentrations greater than 0.1 percent.

IV. EXAMINATION OF UNIRRADIATED FUELS

Thermal Conductivity
(K. W. R. Johnson)

The thermal conductivity of two specimens of pressed and sintered, 93 percent dense, single phase, stoichiometric $U_{0.8}Pu_{0.2}C$ was measured and results

are listed in Table 401-I.

Table 401-I

Thermal Conductivity of Single Phase $U_{0.8}Pu_{0.2}C$

Specimen No.	Temp., °C	Thermal Conductivity, cal/sec-cm-°C uncorr.(1)	corrected(2)	literature(3)
1	93	0.0311 ± 0.0005	0.0334	0.0342
	222	0.0340 ± 0.0010	0.0365	0.0344
	404	0.0376 ± 0.0002	0.0403	0.0348
2	44	0.0322 ± 0.0011	0.0346	0.0341
	120	0.0331 ± 0.0016	0.0356	0.0342
	226	0.0357 ± 0.0008	0.0384	0.0344

Notes: (1) Standard deviation (precision) indicated
(2) Corrected for porosity by $k_c = k_u/(1-P)$
(3) See reference 1

Specimens No. 1 and 2 differed only in that No. 1 contained some longitudinal surface cracks; apparently these caused a 5 percent reduction of the thermal conductivity.

It was necessary to terminate measurements prematurely for each specimen due to specimen oxidation. The source of this oxidation was traced to the sealant glands around the numerous electrical and thermocouple leads into the system. Appropriate modifications were made and a check of system at higher temperatures is in progress.

Plastic Deformation
(M. Tokar)

The compressive creep of mixed uranium-plutonium carbides is being studied to obtain information which can be used to analyze and predict the mechanical behavior of these materials under reactor operating conditions. Specimens of $U_{0.8}Pu_{0.2}C$ of about 95 percent of theoretical density are being tested at temperatures from 1200-1500°C and stresses of 2000, 4000, and 6000 psi in vacuo. The specimens, which are solid, right-circular cylinders, about 1/2 in. in diameter and 1/2 in. high, are currently single phase (Figure 401-1), but this study will, in the future, include an investigation of the effects of stoichiometry on creep rate.

Creep is highly structure sensitive and microstructural variables of interest here include the grain size and the amount, distribution, and shape of secondary

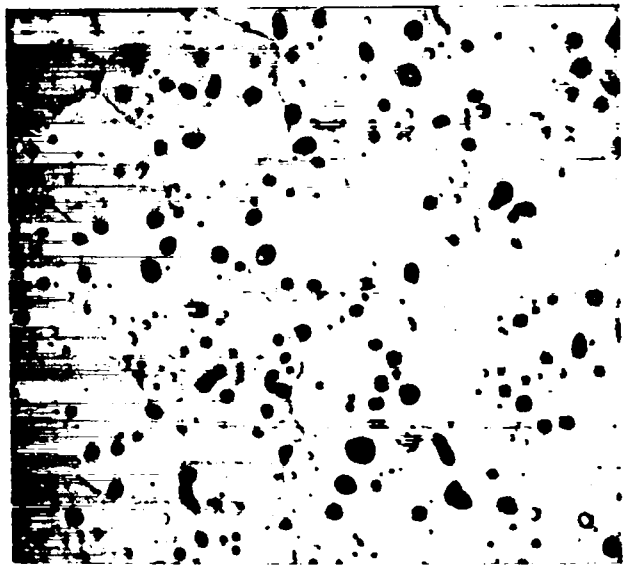

Figure 401-1. Typical $(U_{0.8}Pu_{0.2})C$ electrorefined with nitric, acetic, and lactic acids (1:1:1) 500X

phases and pores. Metallographic examination and density measurements of the creep specimens shows that the porosity is relatively unchanged by the creep test. Figure 401-2 is a photomicrograph of a specimen tested at 1400°C and 2000 psi for 45 hrs to a total deformation of 8.4 percent. The immersion density of this specimen after creep testing was 95.2 percent of theoretical. A

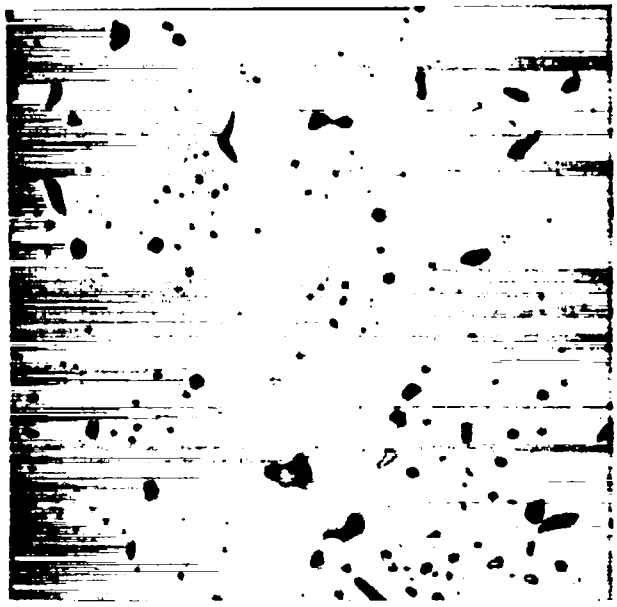

Figure 401-2. Unetched specimen of $U_{0.8}Pu_{0.2}C$ deformed 8.4 percent at 1400°C, 2000 psi. 500 X
95.2 percent of Theoretical Density

photomicrograph of a control sample (having 95.7 percent of theoretical density) is shown in Figure 401-3

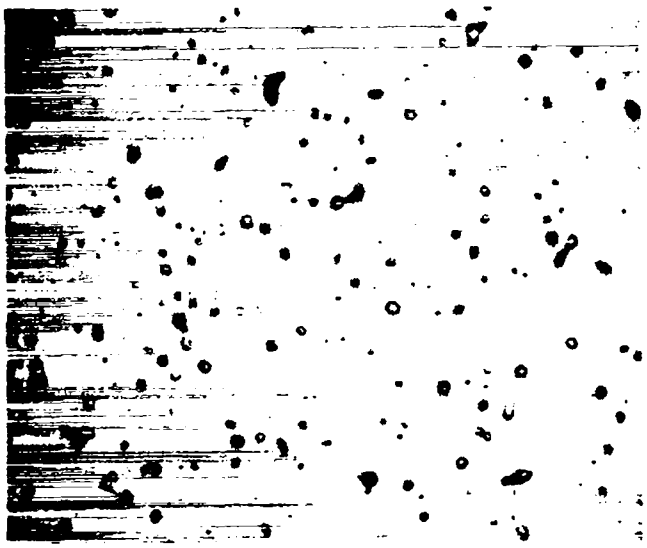

Figure 401-3. Unetched control specimen of $U_{0.8}Pu_{0.2}C$ 95.7 percent of Theoretical Density. 500X

The amount, distribution, and shape of the pores are evidently the same in the two specimens. Grain size measurements have also revealed that the grain size (average about 20 μm) does not change appreciably during the creep test.

A summation of the test conditions and results is given in Table 401-II

Table 401-II

Test Conditions and Minimum Creep Rates for 95 Percent Dense $U_{0.8}Pu_{0.2}C$

Temperature, °C	Stress, psi	Creep Rate, hr^{-1}	Total Time, hr	Total Deformation
1300	2000	3.39×10^{-5}	164	0.61
1300	4000	1.55×10^{-4}	84	3.0
1300	6000	5.9×10^{-4}	18	1.76
1400	2000	1.76×10^{-3}	27.5	7.03

Data of this type can be used to yield a solution to an equation of the form

$$\dot{\epsilon} = A \sigma \exp(-Q/RT)$$

where $\dot{\epsilon}$ is the creep rate, σ is the creep stress, A and n are constants and $-Q/RT$ is the usual Arrhenius term. The magnitude of the stress exponent (n) should yield information on the rate-controlling mechanism of creep. The value for n should be 1 for stress-directed vacancy migration (Nabarro-Herring creep) and should be 4.5 for dislocation climb. Likewise, the value of the activation energy Q can usually be associated with a creep mechanism. More data is being generated in order to determine these quantities.

The creep rates ($\dot{\epsilon}$) reported here for $U_{0.8}Pu_{0.2}C$ are in general somewhat higher than those reported by Norreys[2] or by Stellrecht, et al[3] for hyperstoichiometric UC. Aside from the obvious differences in composition, the test samples used by Stellrecht, et al contained substantial amounts of sesquicarbide (U_2C_3) and dicarbide. It is not clear from Norrey's paper what phases were present in his specimens. Since the higher carbides are harder than the monocarbide, specimens having a dispersion of U_2C_3 or UC_2 in a UC matrix could be expected to have a higher creep resistance than stoichiometric UC specimens.

Hot Hardness
(A. L. Gonzales)

A new molybdenum resistance heating element is being installed in order to increase the maximum working temperature.

Vacuum Cathodic Etcher
(A. L. Gonzales)

This instrument is located in the same enclosure as the hot hardness unit, and will be available for plutonium use at the same time.

V. REQUESTS FROM DRDT

Examination of WARD Carbides

Pellets of (U,Pu)C from seven WARD batches were received on December 26 for metallographic, electron microprobe, and chemical examination. In addition, one pellet from a batch of UC, and one pellet from each of two batches of $Cr_{23}C_6$ were received. Examinations are in progress.

Examination of Irradiated Peach Bottom Element
(R. J. Bard, K. A. Johnson, J. W. Schulte, G. R. Waterbury)

Investigations were made of several sections of sleeve and of portions of eight fuel compacts from a failed fuel element. Examinations included macrophotography, measurements of physical properties, chemical and spectrographic analyses, and metallography.

Meaningful correlations of chemical analyses for U and Th were made with data for bead loadings in the compacts, and techniques were developed to obtain chemical evidence, as well as metallographic, for the extent of bead coating damage. Based upon the results of the investigation, a mode of failure was postulated for the element. A final report describing the investigation was furnished to GGA and DRDT.

Examination of EBR-II Driver Fuel Rods
(J. H. Cappis)

The extensive investigation of six irradiated and five unirradiated EBR-II Driver Fuel Rods, which was mostly completed and reported previously in Reports LA-3993-MS and LA-4073-MS, was finished with the isotopic analyses of the final two samples as shown in the following table.

Mass Spectrometric Analyses of Uranium Isotopic Composition

Sample	U Isotope Concentration, %		
	235	234 + 236 + 238	234 + 236
0121H-27 (Unirrad.) Top	53.02	46.98	< 1.0%
SL 42-17 (Irrad.) Top	51.83	47.93	< 1.0%

Examination of Irradiated Pins and Capsules from Battelle Northwest Laboratory
(K. A. Johnson, J. W. Schulte, G. R. Waterbury, J. F. Torbert (GMX-1), D. Holm (K-1)

This work initiated in the preceding quarter, was continued with the following operations completed during this period:

1. Temperature measurements, radiation measurements, gamma scanning, x-ray radiography, and photography of the BNW 1-9 and -11 capsules.
2. Profilometry of 5 PNL and 2 BNW units.
3. Removal of cladding and hardware from PNL-1-16 and -18 and from BNW1-9 and -11.
4. NaK was removed from the BNW capsules. The NaK was drained from each inner capsule, and remaining traces were washed out with kerosene added from a polyethylene wash bottle. The kerosene wash from LASL-30 (BNW-1-9) was red-brown as it emerged from the pin. Small samples of the liquid, adsorbed on filter paper, were analyzed qualitatively by x-ray fluorescence for metallic constituents. Only the metals found in NaK and stainless steel were detected in significant quantity. It was subsequently found that the virgin kerosene in contact with NaK and air turned red-brown in color. The cause of the color was assumed to be a trace of an organic contaminant in the kerosene that turned red-brown when contacted by either NaK or its oxides or hydroxides.
5. Na was removed from the PNL-1-16 and -18 capsules by melting. Dowanol EB was used to remove the final trace of Na.
6. Gas samples were taken from all seven pins and from the two PNL capsules and the two BNW inner capsules.
7. Metallography was begun on transverse and longitudinal sections from three PNL pins and both BNW-1 units. Alpha and beta-gamma radiography were also started.
8. All the capsule hardware, monitoring wire, and pin hardware were returned to BNWL. In addition 1/2 in. long samples of fuel from PNL-1-15, -17 -19 and BNW-1-9, -11 were returned to BNWL for burnup analysis.
9. Data furnished to BNWL during this period included pertinent material from: radiography, profilometry, photography, gas-analysis, etc.

Examination of Irradiated Pins from United Nuclear
(E. L. Ekberg, F. J. Fitzgibbon, D. M. Holm (K-1), J. F. Torbert (GMX-1) J. R. Trujillo)

The following operations have been carried out thus far on UNC-87, UNC-89 and UNC-90 capsules and/or pins:

1. Temperature and radiation measurements.
2. Viewing and photography.
3. Radiography and gamma scanning.
4. Removal of Na from the capsules.
5. Profilometry of the pins will be completed early in January.
6. Metallography and related examinations will

be started at the conclusion of work on the PNL-1 and BNW-1 specimens.

7. Material resulting from the tests thus far is being provided to United Nuclear Personnel as it becomes available.

Schedule for Examination of Pins from Other Sources
(K. A. Johnson, J. W. Schulte, G. R. Waterbury)

1. Numec - Two pins are scheduled to be received at LASL about mid-January 1969.
2. Atomics International - The UC (W-doped) pellets were received in December; work on these specimens is expected to commence in January.
3. Westinghouse - Three multiple pin fuel elements will be shipped from GE Vallecitos to LASL about February 1.

VI. LMFBR/FFTF ANALYTICAL CHEMISTRY QUALITY CONTROL PROGRAM

A progress report, identified as CMB-1-861, which discusses the laboratory results obtained in Phase I of the LMFBR/FFTF Fuels Development Quality Control and Assurance Analytical Chemistry Program was prepared and sent to participants in the program. A second report, identified as CMB-1-862, was prepared, which discusses the recommendations for work to be done in Phase II by each participant. Both of these were discussed in a meeting at AEC Headquarters held November 24, 1968. In attendance at the meeting were G. W. Cunningham, C. E. Weber, K. Magnus. S. Rosen, J. Colby, and A. C. Millunzi, all of AEC Headquarters and B. R. Hayward, PNL, R. K. Zeigler and C. F. Metz of LASL. It was the concenses of opinion that Phase II should consist of a repetition of Phase I in its entirety if adequate supporting funds could be found.

The data generated in Phase I indicate clearly that none of the participants has an analytical laboratory capable of doing all of the analyses required in the complete characterization of FFTF fuel as required by the chemical specifications. This is due to several reasons such as lack of equipment, lack of methods and/or lack of appropriate standards. In some cases, a method may be adequate but certain parameters need to be standardized. Lack of common standards was also in evidence. In general, however, the results from Phase I operations were encouraging, and succeeded in bringing to light the imminent analytical problems.

Plans for Phase II were made and recommendations were sent to each participant. These plans will be executed following completion of contractural agreements which are being handled by PNL.

In preparation for Phase II operations, LASL has provided program participants with copies of methods for U assay, Pu assay, C, N, O, O/M ratio and halogens. PNL has provided program participants with copies of methods for H_2O gas evolution, density and homogeneity. In addition, LASL has continued to further the program by the following investigations.

Determination of C in Sintered $(U,Pu)O_2$ Pellets
(C. S. MacDougall, M. E. Smith, G. R. Waterbury)

Preliminary work showed that grinding of sintered $(U,Pu)O_2$ pellets was required before the C present was quantitatively oxidized at 900°C in a stream of O_2. Only the ground material was analyzed successfully by the usual combustion-capillary trap method. In order to avoid contamination of the sample by either CO_2 in the air or by tramp C materials, an investigation was made to establish optimum grinding conditions.

The investigation involved repeated measurements of C in samples prepared in various ways from one lot of sintered $(U,Pu)O_2$. First, six measurements were made on the unground oxide. An average value of 9 ppm C was obtained. The remainder of the lot was ground in an inert atmosphere. One-half of the powder was weighed and stored in air. Repeated measurements of C were made on each batch of powder during a period of several days. Ambiguous results were obtained. The experiments will be repeated using additional material.

Gas Evolution from Sintered $(U,Pu)O_2$ Fuel Material
(D. E. Vance, M. E. Smith)

One of the specifications under consideration for FFTF Fuel is the total gas evolution, including water vapor. An apparatus was constructed for measuring separately the quantities of H_2O evolved at 200°C and of other gases evolved as the sample is heated inductively

from 200° to 2000°C in a W crucible. The H_2O vapor is swept by He carrier gas through heated stainless steel conduit to a CEC moisture monitor, and the total quantity of H_2O is obtained by digital integration of the monitor signal. The system is evacuated, and gases evolved above 200°C are collected with a Toeppler pump. The volume and pressure of the collected gas sample are measured, and provision is made in the equipment design for sampling of the gas for mass spectrometric analysis.

A new type of induction furnace to heat the samples to temperatures as high as 2500°C is now being fabricated. The important new feature in this design is location of the induction coil inside the water jacket of the fused silica furnace tube. The diameter of the coil is smaller than that of an external coil, and induction coupling is increased.

Determination of U and Pu in $(U,Pu)O_2$ Fuel Material
(G. B. Nelson, W. W. Wilson, G. R. Waterbury)

Testing of previously reported controlled-potential coulometric and potentiometric titration methods was continued by repeatedly analyzing sintered $(U,Pu)O_2$ pellets for U and Pu without prior separation of these elements. The potentiometric method titrates Pu(VI) to Pu(IV) with standardized Fe(II) without interference from U. The U concentration is calculated by subtracting the Pu concentration from the total Pu and U measured by oxidizing with standard Ce(IV) the Pu(III) to (IV) and the U(IV) to (VI). The coulometric method measures the quantity of electricity to oxidize Pu(III) to Pu(IV), following electrolytic reduction of all Pu to the (III) oxidation state, or the quantity of electricity to reduce U(VI) to U(IV), following a pre-reduction of easily reduced impurities.

The results for ten to twelve measurements of each element by each method showed that the relative standard deviations of the coulometric titrations were 0.13 and 0.14 percent, respectively, in measuring U and Pu. The precisions (1 σ) for the potentiometric titrations were 0.06 and 0.08 relative percent in measuring U and Pu. The average U concentration by coulometry of 66.25 percent was slightly higher than the 66.13 percent obtained by potentiometric titration. The average Pu concentrations by the two methods were 22.06 and 22.05 percent. These analyses completed the the testing of the methods and preparation of a final report was started.

Determination of O_2 in $(U,Pu)O_2$ (Gas Chromatographic Method)
(D. E. Vance, M. E. Smith, C. S. MacDougall)

Investigation of an inert-gas-fusion method which utilizes a gas chromatographic finish was completed. A comparison was made between results obtained by this method and those obtained by a previously-described gravimetric method. In either method, 1 g of the oxide is mixed with 0.2 g C and pressed into a pellet which is heated by induction to 2000°C in a C crucible to evolve the O_2 as CO and CO_2. In the gravimetric method the gases are weighed as CO_2. For gas chromatographic measurement, the CO and CO_2 are mixed with Ne internal standard, and the chromatographic peaks are integrated electronically to provide a measure of the O_2.

Results for ten determinations by each method on one lot of powdered $(U,Pu)O_2$ were 11.88 percent O_2 with a relative standard deviation of 0.8 percent by the chromatographic measurement, and 11.80 percent with a relative standard deviation of 0.2 percent for the gravimetric method. Because of the substantially better precision by the gravimetric method, investigation of the chromatographic method was discontinued.

O/M Ratio
(J. W. Dahlby, G. R. Waterbury)

At present three methods are being used by various laboratories for the determination of the O/M atom ratio of mixed oxide fuel. These are referred to here as Lyon's Method, Chikalla's Method and the LASL Method. The first two of these are essentially thermogravimetric methods in which the sample is brought to a stoichiometric condition by heating for a specified period of time, in a specified atmosphere, and at a specified temperature. From the change in weight and the original weight of the sample the O/M atom ratio is calculated. Each of these methods gives reproducible results, but frequently they do not agree. Each is

sensitive to impurities if present in significant amounts. The LASL method is based on actual measurement of the oxygen, plutonium and uranium contents. It, too, is sensitive to the presence of certain impurities.

In an attempt to evaluate the three methods, equipment was set up to make this measurement on different portions of the same material. No data are available at this time.

Matrix Effects in the Emission Spectrographic Analysis of $(U,Pu)O_2$ Fuel Material
(W. M. Myers, C. B. Collier, R. T. Phelps)

It has been known for several years that the chemical and physical nature of the matrix of a sample analyzed by the carrier distillation technique of emission spectroscopy significantly influences the sensitivities for various impurity elements. For example, for the best results it is not wise to use a matrix of UO_2 for standards if PuO_2 is being analyzed for impurities. In case of mixtures, it is always good practice to prepare standards using the same matrix as the samples being analyzed.

In the case of the analysis of sintered $(U,Pu)O_2$ material, the standards should be prepared with a matrix similar in composition to the sample. This imposes very high purity requirements on the sintering operation. This sintering step could be avoided providing spectrographic standards prepared with a matrix consisting of a mechanical mixture of UO_2 and PuO_2, each of which can be prepared having high purity, showed about the same sensitivities for the various impurity elements as the sintered sample after grinding.

An investigation of this problem proved that indeed this was the case. This means that the problem of preparing spectrographic standards for use in this analysis is greatly simplified. Further, that it will not be necessary to ignite the $(U,Pu)O_2$, prior to analysis, to a mixture of U_3O_8 and PuO_2.

VII. REFERENCES

1. J. A. Leary, R. L. Thomas, A. E. Ogard, and G. C. Wonn, "Thermal Conductivity and Electrical Resistivity of UC, U Pu C, and PuC," Carbides in Nuclear Energy, Vol. 1, L. E. Russell, et al., Ed., 1964, Macmillan and Co., Ltd., London.

2. J. J. Norreys, "Compressive Creep in Uranium Monocarbide," ibid.

3. D. E. Stellrecht, M. S. Farkas, and D. P. Moak, "Compressive Creep of Uranium Carbide," J. Am. Ceram. Soc., 51 (8), 455-8, 1968.

PROJECT 462

SODIUM TECHNOLOGY

Person in Charge: D. B. Hall
Principal Investigators: G. H. Best
R. H. Perkins
E. O. Swickard

I. INTRODUCTION

For the successful operation of high temperature sodium systems contemplated for use in fast, central station reactor concepts, impurities in the sodium must be monitored and controlled. Nonradioactive impurities such as oxygen must be maintained at low concentration levels to limit corrosion processes. Radioactive impurities introduced into sodium from failed fuel elements should be removed to facilitate "contact maintenance" and to minimize safety and detection problems. To control the levels of these impurities, a knowledge of their behavior and interactions in sodium must be developed. Acquisition of this information has been subdivided in the LMFBR Program Plan into a number of task areas. The sodium technology program at LASL has projects which contributed to six of these areas. The broad tasks and current LASL projects within those areas are summarized below:

Task Area 1: Materials Compatibility

- A. Correlation of sodium and helium leaks.
- B. Study of carbon transport in thermal convection loops.

Task Area 2: Sodium Purification

- A. Study of sodium oxide kinetics in cold traps.
- B. Study of soluble getters for removal of impurities from sodium.
- C. Study of gas diffusion through metals into sodium.

Task Area 3: Fission Products in Sodium Systems

- A. Study of fission product distribution in loop experiments.
- B. Study of fission product gettering in capsule experiments.

Task Area 4: On-Line Monitoring Methods

- A. Plugging meter studies.
- B. DC resistivity meter studies.
- C. Evaluation of UNC EMF cells.

Task Area 5: Sampling and Analysis

- A. Vacuum distillation studies.
- B. Study of gamma ray activation analysis for C and O.
- C. Absorption spectrometry development for metal impurity analysis.
- D. Total carbon analysis development.
- E. Development of remotely operated distillation samplers for EBR-II.

Task Area 7: Cover Gas and Maintenance Atmospheres

- A. Development of a high temperature quadrupole mass spectrometer for cover gas analysis.

Details of the work in these programs are presented below.

II. MATERIALS COMPATIBILITY

A. Correlation of Sodium and Helium Leak
(D. C. Kirkpatrick, J. P. Brainard)

1. General

The correlation of sodium leak development with measured helium leak rates observed during acceptance testing provides information on the degree of component integrity which must be attained for safe, long-term sodium plant operation. No firm criteria now exist that establish acceptable levels of leak-tightness for various situations.

This study uses fabricated stainless steel leaks and leaks that occur naturally in stainless steel bar stock. Selected samples having a range of helium leak rates are incorporated into small sodium systems (cells) which are held at a predetermined temperature until sodium leakage occurs. From these observations it may be possible to establish, for mass spectrometer acceptance tests on sodium system components, the maximum tolerable helium rate which is consistent with adequate long-term containment of sodium by that component.

An interesting side effect from this work has been observation of the elusiveness of what are considered to be large leaks (10^{-5} to 10^{-6} atm cm^3/sec). Normal contaminants such as grease, water and some solvents can completely mask leaks of this size and invalidate a leak test, unless proper pretreatment of the component is performed; and in some cases this can involve firing of the component in a hydrogen atmosphere. If meaningful helium leak tests are to be performed on LMFBR components, procedures must be developed for treating and handling of the part prior to leak test.

2. Current Results

The four new cells, numbers five through eight, (Table 462-I) were raised to 650°C on October 3,

Table 462-I

Pretest Characteristics of Na Leaks

Cell No.	Type of Leak	Initial He Leak Rates (room temp.)
5	Porosity (in bar stock)	About 1 x 10^{-5} atm cm^3/sec
6	Solid Bar Stock sample	none (control specimen)
7	Porosity (in bar stock)	About 1 x 10^{-1} atm cm^3/sec
8	Porosity (in bar stock)	none (steel oxide plugged)

1968. Their reaction chambers were pre-oxidized in air for one day before sodium introduction. Cell 7, with the 10^{-1} atm cm^3/sec helium leak rate, leaked sodium immediately. About 25 cm^3 of sodium flowed within one day of operation. Since data are taken every day, 25 cm^3/24 h represents a minimum flow rate estimate. The 25 cm^3 could have flowed in a much shorter time. The 25 cm^3 is the maximum amount of sodium flow which can be observed since this is approximately the volume of the reaction chamber. Cell 5, with the initial helium leak rate of 7 x 10^{-6} atm cm^3/sec, leaked sodium in 18 days and flowed at the rate of 1 cm^3/day, or about 1 x 10^{-5} cm^3/sec. Cell 6, with the control, and Cell 8, with the stainless steel oxide plugged leak, have not leaked sodium during this quarter.

The two cells which leaked have been removed. An attempt will be made to remove the sodium and sodium oxide from these leaks and remeasure the helium leak rate. From this measurement the extent of the stainless steel corrosion in the leak may be indicated.

Cells 1 through 4 at 400°C still have not leaked sodium after 5800 h. The pretest leak sizes for the two noncontrol test cells were 1.1 and 1.7 x 10^{-4} atm cm^3/sec.

The fixed geometry leaks have been received. These leaks have a helium leak rate of about 10^{-3} atm cm^3/sec. The leak channel is a cylinder of 0.6 mil diam and 50 mil long in Type 304 stainless steel. These leaks will be exposed to sodium at several temperatures. By fixing a few of the experimental parameters, such as channel dimension, it may be possible to develop a theory about sodium leaks into air.

A third generation sodium leak cell is now in fabrication. The second generation reaction cell was designed to contain the leaking sodium so that sodium flow rate could be determined. The sodium vapor, however, condensed and plugged the mass spectrometer manifold. The third generation sodium leak cell will contain the leaking sodium at a much lower temperature and hence, effectively eliminate condensation.

Eight more ovens and controls for an additional eight sodium leak cells are now being set up. The eight new cells, which are of the third generation type, and their associated manifolds are now under fabrication. Four of these new cells will be operated with the fixed geometry leaks.

As a starting point in the sodium leak analysis, a simple mathematical model has been developed. This model assumes that a sodium oxide plug in the leak channel prevents sodium from leaking into air. The plug behavior has been studied using the assumption that sodium and oxygen diffuse through the plug and sodium oxide dissolves into the sodium. This

model neglects the effect of stainless steel corrosion. The results from the cells with the fixed geometry leaks will help to determine the worth of this model.

B. Study of Carbon Transport in Thermal Convection Loops
(J. C. Biery, C. R. Cushing)

1. General

Studies have indicated that the use of carbon beds may be useful in the gettering of ^{137}Cs in sodium systems. Carbon, however, is slightly soluble in sodium and can carburize austenitic stainless steels and refractory metals. Therefore, the purpose of this study is to determine the conditions under which carbon mass transfer rates are sufficiently low to allow the use of carbon beds in a sodium system.

The carbon transfer rates from carbon rods will be studied in thermal convection loops. The Type 304 or 316 stainless steel loop itself will serve as the carbon sink when these alloys are studied and vanadium alloy sleeves will serve as getters when vanadium is studied.

2. Current Results

The modifications to the steam generator sodium loop which will supply sodium to the thermal convection loop have been completed. The harp is attached to the supply system and final equipment adjustments are being made in preparation for a conditioning run at 500°C.

III. STUDY OF PURIFICATION METHODS FOR NONRADIOACTIVE IMPURITIES

A. Study of Na_2O Kinetics in Cold Traps
(C. C. McPheeters, J. C. Biery, R. Martinez)

1. General

In sodium coolant systems for future LMFBR's it will be necessary to use cold traps for removal and control of oxygen and other contaminants. These cold traps should be designed to handle adequately the impurity loads and to maintain the impurity concentration level below some specified upper limit. For economic reasons, cold traps must be the smallest and simplest designs which can meet the above requirements.

Knowledge of the mechanisms of impurity deposition in cold traps is necessary to reach the optimum design for a given sodium coolant system. The rate of mass transfer of impurity species to cold trap surfaces must be measured and the effect of various flow patterns, surface condition, and temperature on the mass transfer rates must be determined. The purpose of this study is to determine the effect of the above variables on the mass transfer coefficient for removal of oxygen from sodium systems. Knowledge of the mechanisms involved and the mass transfer coefficients will allow calculation of the rate of oxygen removal and the location of deposited oxides in the cold trap for any given system size and cold trap geometry. Proposed cold trap designs could be evaluated in terms of total oxide capacity and expected system cleanup rates.

Cold trap tests are being conducted with a 60-gal sodium system which has analytical capabilities including a vacuum distillation sampler, a plugging indicator, and two UNC oxygen meters. The cold trap tests consist of measurement of the rates of change of oxygen concentration in the system. Various cold trapping conditions of temperature and flow rates are tested to determine the effect of these variables on the oxygen removal rates. When the rate of change of oxygen concentration, the cold trap temperatures and the deposition surface area is known, an overall mass transfer coefficient can be calculated.

2. Current Results

The cold trap test loop has been shut down during this report period. Cold Trap No. 2 was installed and is being prepared for system startup. The second cold trap includes a NaK-cooled insert which can be removed for examination and species identification. Sodium flows downward in an annular space around the cool insert, and its temperature is lowered by removal of heat by the NaK. Beyond the end of the insert, the sodium enters a regenerative heat exchanger where some of the heat lost to the NaK is regained. The insert is provided with studs which can be used to anchor wire mesh in the annular flow passage. The effect of packing on the transfer of oxygen to the cold trap will be determined and compared with results from packless experiments. The shortened diffusion path due to the presence of packing may greatly increase the mass transfer coefficients.

B. Study of Soluble Getters for Removal of Impurities from Sodium
(G. E. Meadows, L. A. Waldschmidt, D. N. Rodgers)

1. General

For large sodium-cooled reactor systems, it may be desirable to use soluble getters for control of oxygen and other dissolved impurities in lieu of the more conventional hot and cold trapping techniques. The soluble getters of interest occur in the sodium coolant either naturally, as an impurity (calcium), or are produced during reactor operation (as with magnesium). The techniques for the controlled additions of these getters, maintenance of fixed getter levels, and the selective removal of depleted getter metals and other impurities from dynamic sodium systems must be developed if their usefulness is to be evaluated. The significant chemical reactions occurring in a sodium system containing these soluble getters must be understood and controlled. This mode of purity control has the potential for effectively controlling not only oxygen, but also carbon, hydrogen, nitrogen, and possible metallic impurities.

2. Current Results

a. Analytical Loop No. 1

In the first soluble getter run, Analytical Loop No. 1 was spiked with 1.2 g of metallic calcium. The calcium was added by the tea bag method to the bulk sodium tank. Under ideal conditions this weight of calcium would give ~50 ppm calcium in the sodium. At the time of the addition the bulk sodium tank was operating at 350°C, the full flow cold trap crystallizer tank temperature was 125°C, the oxygen concentration was 1.4 ± 0.3 ppm as determined by vacuum distillation, and the loop flow rate was ~1 gpm. During the runs, samples for vacuum distillation analysis for oxygen and calcium in the residues were taken from the outlet line of the crystallizer tank. Sampling was begun 2 h after the addition of the metallic calcium and continued until the dissolved oxygen value was again in equilibrium with the crystallizer tank. The crystallizer tank outlet sodium was deficient in dissolved oxygen for approximately 50 h. The lower values (0.3 ppm O) occurred during the first 6 h. The values for calcium were highest during this period (0.3 ppm Ca) and fell off to the system's original background (<0.1 ppm Ca) within 24 h. After the run, the tea bag was removed from the bulk tank and was analyzed for remaining calcium. The calcium had all dissolved.

The loop has now been prepared for a second calcium addition. The cold trap temperature has been raised to 225°C, and 1.13 g of calcium have been loaded into the charger mechanism. The addition should take place in January.

One of the purposes of this addition is to determine the steady state calcium level at the higher cold trap temperature. At the cold trap temperature of 125°C the calcium level was about 0.05 ppm, nearly the lower limit of detection.

It is planned to install a new cold trap with an optional bypass which will permit isothermal operation of the loop at low oxygen levels. With an isothermal loop an equilibrium soluble getter system can be run. Sufficient calcium can be added to getter any oxygen present and still maintain a calcium concentration in the bulk sodium. Optionally, the loop can be run with the cold trap converted to a calcium oxide system.

b. Analytical Loop No. 2

Construction of Analytical Loop No. 2 is about 90% complete. The sampling systems and cold trap are the major items to be completed. Detail drawings for the distillation sampler were finished and submitted to the main shop for fabrication. Nearly all the parts for the sampler have been received.

Design of the distillation sampler, cold trap side loop, and the cold trap itself is nearly complete. Although this side loop had been included in the original design, a change in design was felt necessary to produce a more flexible and efficient operation.

It has been decided to use the remaining available side loop for a plugging indicator; drawings of the latest LASL plugging indicator design have been submitted to the shop for fabrication.

The charging mechanism was assembled, leak checked, and then installed on the loop and operated. A modification had to be made on the frame structure which carries the overhead trolley so the center core could be removed without interfering with the rest of the piping. The modification was completed.

C. Study of Gas Diffusion Through Metals into Sodium
(J. P. Brainard, D. C. Kirkpatrick)

1. General

Very little quantitative information is available on the diffusion of gases in reactor system containment materials, although the phenomenon has been observed in several high temperature, liquid-metal-cooled systems. Diffusion of nitrogen through stainless steel in such systems may be misinterpreted as evidence of an air leak in the plumbing. If quantitative information on diffusion were available, the expected rate of nitrogen influx could be estimated, and the existence of small hard-to-find leaks might be substantiated or dismissed by comparing the expected and observed rates of nitrogen accumulation in the system.

A program for determining the diffusion rate of nitrogen in stainless steels has therefore been undertaken. In later phases of the program the diffusion of O and H in stainless steels will be studied.

2. Current Results

The support brackets and table for the experiment have been designed and fabricated. The apparatus has been assembled to check the dimensions. The diffusion cell and vacuum pump manifolds (out of the bakeable region) have been designed and are awaiting fabrication.

A relatively new method for determining bulk diffusion of impurities in metal is the use of nuclear magnetic resonance.[1] This involves analyzing plots of the resonance line width vs temperature. The advantage of this method is that surface effects are eliminated. The method is too new, however, to consider using at this time; but with the rapid advances in this field, it may be usable in the future.

IV. FISSION PRODUCTS IN SODIUM SYSTEMS

A. Study of Fission Product Distribution in Loop Experiments
(J. C. Clifford, J. Fellers)

1. General

The behavior of radioactivity released to sodium from failed or vented fuel elements may limit access to portions of the primary coolant system and may effect the consequences of a loss-of-coolant incident. Depending on the fission-product release fraction anticipated in either circumstance, it may be desirable to scavenge these species (as well as uranium and plutonium) from the coolant.

The immediate goals of this investigation are: (1) to identify sodium-soluble fission-product species and (2) to examine the effects of primary-coolant-system construction materials, design features, and operating conditions on these species.

2. Current Results

Studies of the distribution of long-lived fission products have been continued with major emphasis on ^{137}Cs.

a. ^{137}Cs Adsorption Loop

The deposition of ^{137}Cs from flowing sodium onto several metal surfaces is being studied using the forced-convection loop shown in Fig. 462-1.

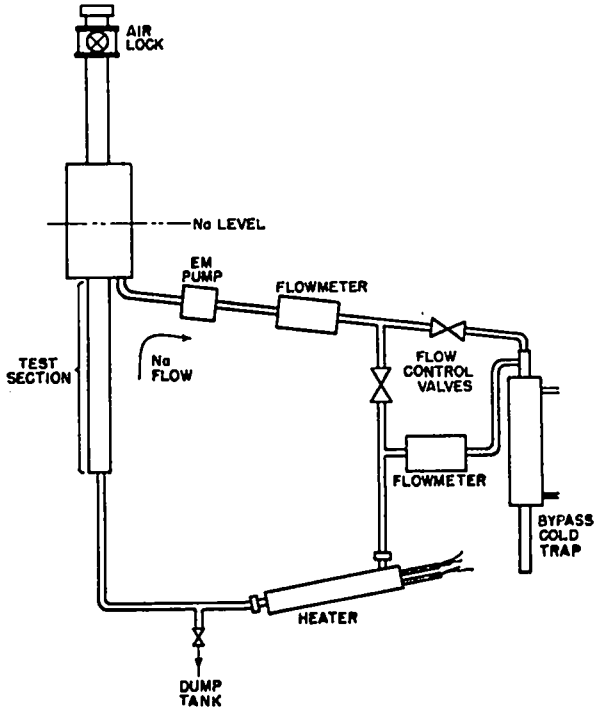

Fig. 462-1. Sodium loop for ^{137}Cs adsorption experiments.

Sodium containing 0.1 to 2 μCi ^{137}Cs/g Na flows upward through a 2-in. diam test column containing coils of metal foil fastened on a stringer. After leaving the test section, sodium passes through an expansion tank, a pump, a flowmeter, and a resistance heater. A cold trap on a bypass line provides

oxygen control for the loop. The loop contains approximately 5 lb of sodium flowing at a maxiumum rate of ~800 lb/h.

The metal specimens used in this study are made by winding a corrugated and a flat strip of 3-mil thick foil together on a nickel spindle and slipping a cylindrical sleeve over the bundle to prevent it from uncoiling. The finished bundle is 2 in. high, 1-1/8 in. in diam and contains ~85 in.^{2} of surface (Fig. 462-2). Four metals are being used

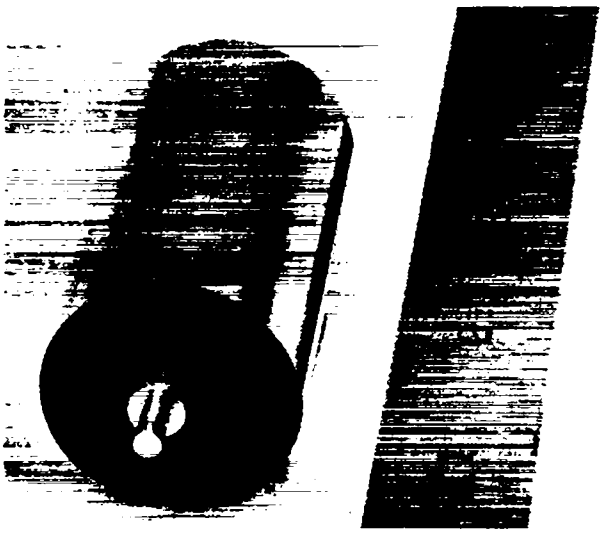

Fig. 462-2. Metal foil bundle used for ^{137}Cs adsorption experiments.

initially: C-1010 steel, Type 316 stainless steel, zirconium, and nickel. The foils are received and used in a cold worked state. The only surface preparation consists in removing grease and dirt ultrasonically. A stringer containing a bundle of each materials is assembled by pinning the spindles together and by adding upper and lower end pieces, which allow insertion of the stringer into the loop. An irradiated tab located in the lower end piece provides a reference point for gamma scanning.

The distribution of ^{137}Cs in the bundles and in the cold trap is determined by scanning the test section and trap with a collimated NaI(Tl) crystal and by fixed position counting of specific sections within the test column and cold trap. The scanner (Fig. 462-3) consists of a carriage, two upright shafts and a lead screw, and a yoke from which is suspended a 2000 lb lead shield. The shield houses a 3 x 3 in. NaI crystal and is equipped with replaceable collimators ranging from ½ in. slits and

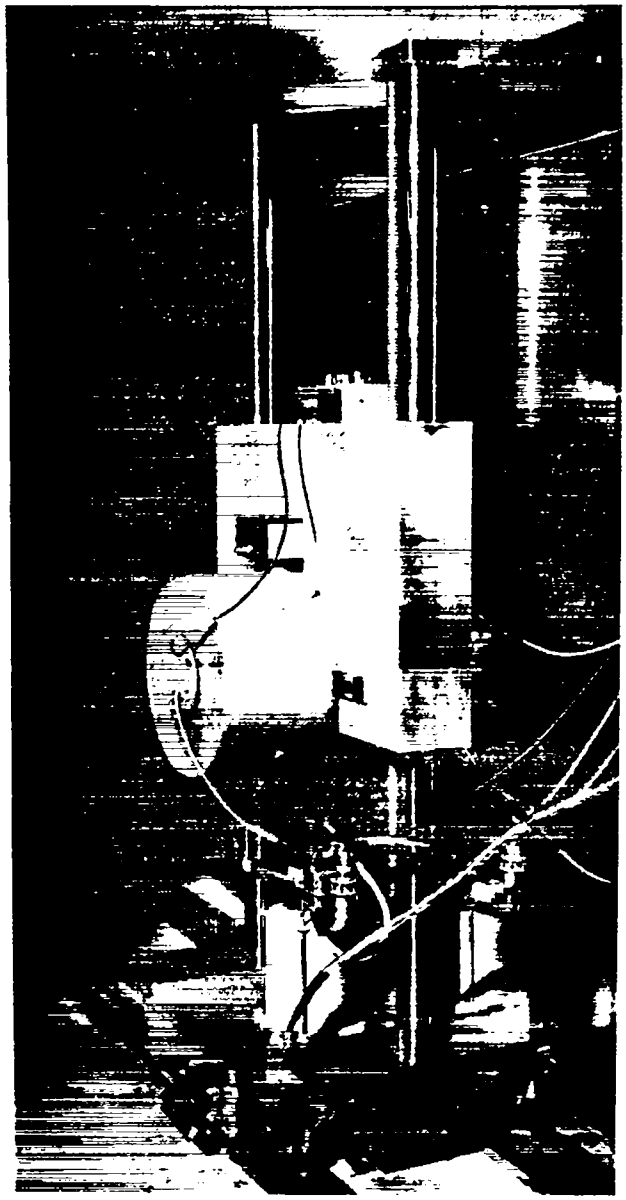

Fig. 462-3. Gamma Scanner

holes to 30-mil slits and holes. Vertical motion of the yoke and shield is provided by stepping motors, and vertical position is determined by a shaft encoder and readout. The carriage assembly moves in the horizontal plane on rails and is positioned manually using a lead screw and Veeder-Root mechanical readout. Positioning accuracy in both planes is 1 mil.

Experiments are prepared by adding ^{137}CsCl to the sodium at 500°C and allowing 3 days for dissolution. The temperatures in the loop and cold trap then are adjusted to the values for the experiment and another period of time, dependent on

operating temperature, is allowed for the system to approach equilibrium. At the start of an experiment, the test section is scanned to determine the activity level in the flowing sodium and on the walls, after which the foil bundles are lowered in place and the counting of specific bundle sections is begun. After the foil bundles have been equilibrated, they are removed from the loop, the stringer is disassembled, and the foils are analyzed for total ^{137}Cs by leaching each bundle and β-counting an aliquot of the solution. To establish initial and final ^{137}Cs concentrations in the flowing sodium, a 5-g sodium sample is taken from the loop prior to insertion and immediately after removal of the foil bundles. The activity level and distribution in the cold trap is determined before and after each test and several times during each test.

This experimental procedure was decided upon after extended observation had been made of ^{137}Cs behavior in small cold trapped systems. In general, half of the ^{137}Cs added to a cold trapped system was found in the flowing sodium, approximately a tenth deposited on the walls, and the remainder concentrated in the cold trap. (Partition of activity to the loop metal surfaces was a relatively rapid step requiring 200-500 h.) No differences in behavior were detected between ^{137}Cs extracted from irradiated metal fuel and that added as $^{137}CsCl$. Since metals appeared to be weak collectors of ^{137}Cs, it seemed that a loop containing several pounds of sodium could be equilibrated with ^{137}Cs and that metal specimens could be inserted and equlibrated without changing the cesium concentration in the flowing sodium by more than a few percent. As a first approximation, concentrations on this order can be ignored.

Three experiments have been completed using bundles of C-1010 steel, Type 316 stainless steel, zirconium, and nickel. In each case, the sodium temperature was 200°C and the flow velocity in the empty test section was 0.1 ft/sec, corresponding to a sodium Reynold's number of 2600. The oxygen level in the system was set by continuous operation of the bypass cold trap in the 110-120°C range. The initial ^{137}Cs concentration was in the range 0.5-1.5 μCi/g Na. Although the experiments have not yielded quantitative results that are consistent, a qualitative pattern is emerging. Figure 462-4

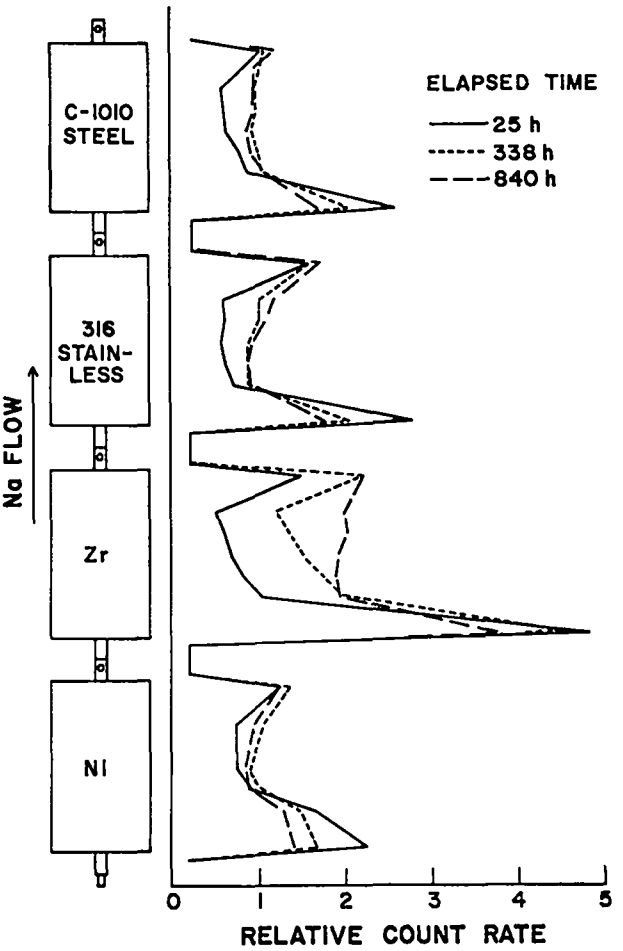

Fig. 462-4. Axial distribution of ^{137}Cs on metal surfaces contacted with cesium-contaminated, flowing sodium at 200°C.

shows the axial distribution of ^{137}Cs in all four foil bundles after 25, 338, and 840 h of operation during the latest experiment. The principal features are an activity maximum along the upstream edge of each bundle, a minimum near the center, and an increase near the downstream edge. As contact time increases, the upstream edge of each bundle gives up activity while the middle portion and trailing edge gain. The activity distributions also indicate that for some time after start the leading and trailing edges of each bundle acquire activity at a more rapid rate than sections in the middle of a bundle. This may be associated in part with flow disturbances at the ends of a bundle and in part with the fact that the bundle edges are the sheared, unannealed edges of the sheet stock.

Although no two regions in any bundle acquire activity at the same rate, the deposition process in all sections examined can be described by an

equation of the form $A = kt^x$, where A is ^{137}Cs activity, k and x are constants, and t is time. Although it varies with the materials and region, the time period over which this equation appears applicable is approximately 1 h to 200 h. An example of the time dependent behavior of the four metals at 200°C is shown in Fig. 462-5. The slopes of the

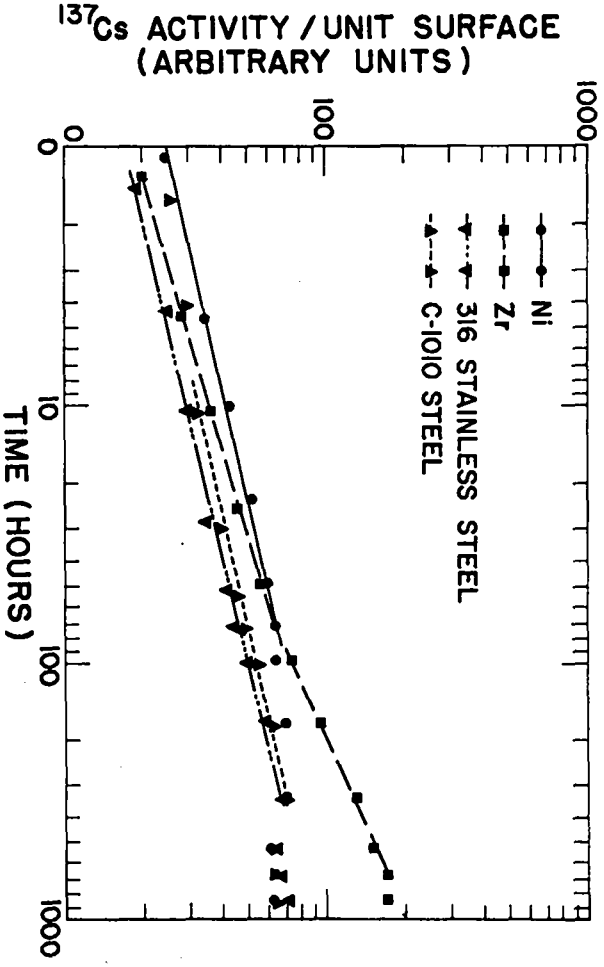

Fig. 462-5. Variation of ^{137}Cs activity with time for 4 metal surfaces contacted with cesium-contaminated, flowing sodium at 200°C.

curves vary from 0.20 to 0.28 in the time period 2 to 200 h.

The fact that some redistribution of activity is occurring during test, as illustrated by Figs. 462-4 and 462-5, indicates that the assumption of constant cesium concentration during a test is invalid. This condition is confirmed by radiochemical analyses of bulk sodium before and after each test, showing that the ^{137}Cs concentration in solution decreases 20-50% over a 500-800 h period. The inactive cesium level also is changing, but at levels which cannot be detected by the analytical method used at present. Therefore, the activity deposition rate data, which do not take the varying concentration of cesium in solution into account, are suspect.

Although these experiments can be rearranged rather simply to avoid the large shifts in liquid phase cesium concentration, the measurement of total cesium concentration will require a more sensitive analytical technique than has been used. The period during which another technique is developed for determination of inactive cesium in sodium will be used to extend the present experiments to higher temperature. It is anticipated that only minor differences in adsorption behavior will be found among the four metals, and that Type 316 stainless steel will be selected for a study of the variables of sodium flow rate, cesium concentration, degree of cold work, and temperature on adsorption.

b. Trace Irradiated Fuel Loop

Another small, forced-convection sodium loop, whose principal sections can be scanned for gamma-emitting isotopes, has been operating satisfactorily for 8000 h. The loop will be used to study the release and distribution of fission products ($\tau \geq 8$ d) from trace-irradiated plutonium-containing fuels. However, mechanical, electronic, and vacuum difficulties were encountered with the gamma scanning equipment. These have been resolved, but there has been a delay in the use of the loop for its original purpose. During part of this delay, the loop has been used for a limited experiment to examine the attrition of unirradiated $(U,Pu)O_2$ particles in flowing sodium.

Approximately 2 g of partially sintered $(U_{0.8}Pu_{0.2})O_2$ powder, with an O/M of 2.015 ± 0.010, were added to the loop with the hot leg operating at 600°C and the cold leg operating at 325°C. The 600°C section contained a removable zirconium hot trap and a stainless steel specimen. A stainless steel specimen also was located in the 300°C section. After 2880 h of operation, the stainless steel specimens, the zirconium hot trap, and a stainless-steel-mesh-packed section were removed for chemical analyses. Samples of bulk sodium were withdrawn from the loop after 4, 29, 55, and 120 days of operation and samples filtered through 10μ screens were withdrawn after 29, 55, and 120 days. The 4-day bulk sample

contained ~20 ppm uranium and ~5 ppm plutonium, indicating that a portion of the powder was circulating even at the low sodium velocities (~1 fps, max) of this loop. The remainder of the samples contained 6 ppm uranium and < 0.1 ppm plutonium, indicating (1) that if any suspended material was present, it was $\overline{<}$ 10 μ in size, and (2) that the original mixed oxide had undergone some chemical change, as reflected by the change in U/Pu between the 4- and 29-day samples. Analysis of the traps and specimens have not been completed.

B. Study of Fission Product Gettering in Capsule Experiments
(H. A. O'Brien, C. R. Cushing)

1. General

Capsule experiments have been designed to determine the distribution of gamma-active isotopes in the sodium/stainless steel/helium/adsorber system as a function of time and temperature. Gamma ray scanning permits a study of transport rates, adsorption and desorption phenomena, and the equilibrium distribution between phases to be made. The isotope ^{137}Cs is the first radioisotope to be studied in these experiments because it is a major fission product released from irradiated nuclear fuels, and its long (27.7-yr) half-life simplifies measurements. Other candidates for study, using these experimental techniques, are ^{131}I and ^{140}Ba-^{140}La.

In the present series of experiments, the ^{137}Cs gettering capacities of carbon and various oxides are to be determined. In each capsule tested a basket containing one of the materials to be tested, will be introduced into the sodium after the cesium and sodium have come into equilibrium. The capsule will be scanned with a collimated NaI(Tl) crystal in order to determine the amount and rate of cesium pickup by the getter.

2. Current Results

a. Graphite and Activated Charcoal

In comparing cesium adsorption on graphite with that on activated charcoal at 500°C, the following observations were made.

(1) Both graphite and charcoal showed an initial rapid adsorption during the first ¼ h after the material was introduced into the sodium.

(2) Following the initial adsorption, the quantity of cesium picked up on the graphite appeared to be proportional to t^2, where t is time in hours, until equilibrium was approached. On charcoal, on the other hand, the quantity adsorbed was proportional to t^3 from 0.1 to 0.5 h, after which the rate was proportional to t.

(3) Graphite reached equilibrium after the first 24 h, while 400 to 500 h were required for charcoal to reach equilibrium.

(4) At equilibrium, graphite had adsorbed only about 40% of the charcoal value, which was greater than 99% of the ^{137}Cs in the sodium.

(5) Radiochemical analysis showed that the sodium from the charcoal experiment had a ^{137}Cs concentration of 0.33 μCi/g at the conclusion, while that from the graphite experiment was 3.3 μCi/g.

It is apparent from this study that activated charcoal is more effective than graphite as a decontaminating agent for the fission-product cesium in sodium.

b. Aluminum and Chromium Oxides

A study of aluminum and chromium oxides as possible gettering agents for cesium in sodium showed that both were impractical. After a slight adsorption of cesium on these materials during the first 24 h, the cesium began to accumulate in the vapor region above the sodium in appreciable quantities. In both experiments, no appreciable amount of cesium had been observed in the vapor region during the preliminary equilibration period, which was, in general, longer than the period of time the oxides were in the sodium. The gradual accumulation of cesium in the vapor region after the oxides were introduced into the sodium suggests that the cesium was reduced, distilled from the sodium, and deposited on the cooler wall of the capsule above the sodium, No accumulation of cesium in the vapor region was observed in the experiments with charcoal or graphite.

V. ON-LINE MONITORING METHODS

A. Plugging Meter Studies
(C. C. McPheeters, J. C. Biery)

1. General

Plugging meters have been used on sodium systems for many years. They are relatively simple to design, install, and operate; however, the meaning of the data obtained from these instruments has

not always been clear, and as a result, the value of the instrument has sometimes been questioned. Work previously reported[2] indicates that the plugging meter is a valuable instrument and that it can be used with confidence. The three areas of investigation indicated below are continuing to better understand the meter.

a. Studies of the bare orifice meter.

b. Observations of the operating characteristics of the oscillating plugging meter.

c. Determination of mass transfer coefficients from plugging meter data.

2. Current Results

a. Effects of Velocity and Nucleation

A series of plugging runs made on the cold trap system plugging indicator was analyzed to determine the dependence of the mass transfer coefficient on the velocity of sodium through the orifice. (The meter contains four orifice holes with 0.052 in. diam.) Three types of runs were analyzed. In each run the orifice temperature was held constant at 209°C while the saturation temperature was 218°C. The impurity was assumed to be oxygen, and these temperatures give a driving force of 3.3 ppm. In the three runs the sodium throttling was incrementally increased, left unchanged, and incrementally decreased to give a range of velocities through the orifice. The results are shown in Fig. 462-6. For partially developed plugs, the mass transfer coefficient varied with the 0.8 power of the Reynold's number based on the bare orifice diameter.

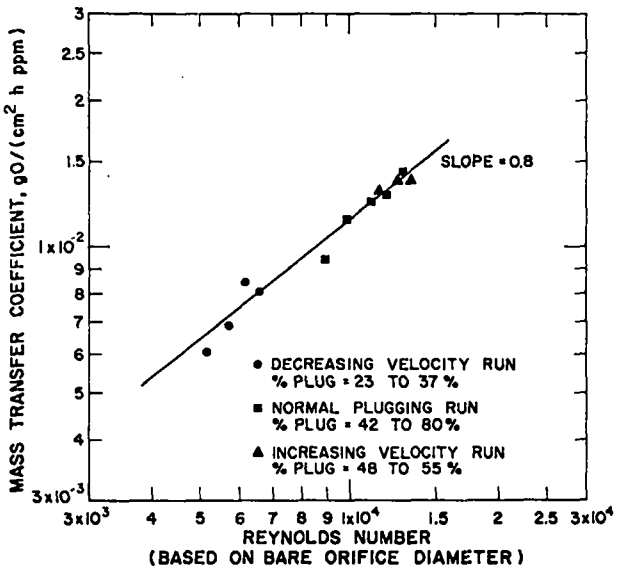

Fig. 462-6. Mass transfer coefficient as a function of Reynold's number of Na_2) precipitation on a 0.052 in. plugging meter orifice.

For plugs below 25% and above 80%, the mass transfer coefficients deviated significantly from the 0.8 power line. The probable reason for the deveiation is that the growth of the plug in its early and late stages of development does not follow the model proposed in the mass transfer coefficient calculations. This model proposes that the Na_2O precipitates on the cylindrical surface of the orifice and grows uniformly inward as an annular layer. If some other type of growth occurred, then the coefficient would reflect that growth pattern by being too large or too small depending on whether the relative surface area of precipitate as compared to the cylindrical surface increased or decreased. As an example of this effect, calculations were made by assuming the number of nuclei precipitated on the cylindrical surface of the orifice and grew inward as square cylindrical blocks. The expression for the ratio of the surface area of the nuclei to the surface area of the cylinder at the same percentage plug can be developed as follows:

$$na^2 = P_f \pi r^2 \qquad (1)$$

n = number of nuclei

a = dimension of side of square crystal, cm

P_f = fraction of orifice plugged

r = radius of bare orifice, cm.

Equation 1 expresses the equivalence of the two cross-sectional areas of the two types of plugs, blocks and cylindrical layer. Equation 2 is a rearrangement of Equation 1. In formulating Equation 1, the curved nature of the base of the block crystals was ignored.

$$a = r\sqrt{\frac{P_f \pi}{n}} \qquad (2)$$

The precipitation areas for the two cases are expressed as follows:

$$A_a = 3\ an\ell \qquad (3)$$

$$A_r = 2\pi r\sqrt{1-P_f\ell} \qquad (4)$$

A_a = area of precipitation for n cylindrical square blocks

A_r = area of precipitation for continuous cylindrical annular layer

ℓ = thickness of orifice plate, cm.

The ratio of the two areas is obtained by dividing Equation 3 by Equation 4. Equation 5 results

$$\frac{A_a}{A_r} = \frac{3}{2}\sqrt{\frac{nP_f}{(1-P_f)\pi}} = 0.847\sqrt{\frac{nP_f}{1-P_f}} . \qquad (5)$$

A restraint exists such that the sum of the inward face dimension of the blocks cannot be greater than the inner circumference of the orifice available for growth. Equation 6 expresses this restraint.

$$n < 2\pi\left[\left(\frac{1}{P_f} - 1\right) + \sqrt{\left(\frac{1}{P_f} - 1\right)^2 - 1}\right] \qquad (6)$$

Equations 5 and 6 were used to calculate the data in the following table which gives the ratio A_a/A_r as a function of n and P_f.

Table 462-II

Area Ratio, A_a/A_r, As A Function Of P_f And n

P_f ↓ / n →	1	2	6	16	28	50	113	> 113
0.1	0.283	0.401	0.693	1.13	1.50	2.00	3.01	X(1.0)
0.2	0.424	0.600	1.040	1.70	2.24	3.00	X(1.0)	
0.3	0.554	0.784	1.36	2.22	2.93	X(1.0)		
0.4	0.691	0.978	1.69	2.76	X(1.0)			
0.5	0.847	1.198	2.08	X(1.0)				
0.6	1.038	1.465	X(1.0)					
0.7	1.291	X(1.0)						
0.8	X(1.0)							

The values of n were chosen to meet the restraint imposed by Equation 6, and the X's indicate that restraint. (Note: Equation 6 is valid for $P_f \leq 0.5$. Above 0.5, the simple geometric model used to derive the equation breaks down, and the individual cases for $n < 6$ must be considered separately as special cases.)

When the restraint of Equation 6 is met, the A_a/A_r ratio drops to 1.0. This condition implies that the individual crystals have grown together and have formed a relatively smooth inner cylindrical surface. At this point the simple model used to calculate mass transfer coefficients applies directly.

The experimental data from the three plugging runs seemed to indicate that a small number of nuclei intially precipitated on the orifice. In all cases, the mass transfer coefficient started below the 0.8 slope line in Fig. 462-6, approached it as the plug fraction increased, and finally merged with it at plug fractions near 0.40. If the 0.8 slope line is taken as the $A_a/A_r = 1.0$ condition, the initial mass transfer coefficients at 10% plug were a factor of 2.9 low. A comparison of these data with those given in Table 462-2 indicates that for these conditions of flow and ΔC driving force of 3.3 ppm very few nuclei initially formed on the orifice surface. Possibly as few as 1 to 3 nuclei were formed. If many nuclei formed, the rate constant would be expected to initially increase or remain constant and then decrease as the cylindrical plug was formed. With only 1 to 3 nuclei formed, the rate constant should increase and then approach smoothly the 0.8 slope line. This latter condition was that observed experimentally.

The effect of ΔC driving force should be tested on the above postulated nucleation model. A larger ΔC should nucleate more crystals, and the behavior calculated for a large number of sites given in Table 462-2 might be followed. In this case the rate constant should not increase much with plug growth and might even decrease some at the 0.1 to 0.2 plug fraction range.

b. Visits to Other Sites

J. C. Biery and C. C. McPheeters visited two sodium research installations, General Electric at San Jose, California, and Liquid Metal Engineering Center near Canoga Park, California, to study the dynamic characteristics of operating plugging meters of varying designs. By determining mass transfer coefficients, times to nucleation, and oscillation characteristics for these meters, their capabilities can be compared, and the general utility of the plugging meter on operating multi-impurity systems can be evaluated.

(1) General Electric Company, San Jose, California

Characteristics of Plugging Indicator:

Mass transfer Loop 8 Plugging Meter

No. of holes: 4

Diam of holes: 0.035 in.

Length of holes: 0.035 in.

Type of Meter: Regenerative, flow down outside, up inside, orifice plate at bottom of inside tube.

Mass Transfer Loop 9 Plugging Meter

No. of holes: 4

Diam of holes: 0.025 in.

Length of holes: 1/16 in.

Type of Meter: Regenerative, flow down outside annulus, up inside pipe, orifice plate in annular section at bottom of inside pipe.

Plugging meter runs were made on mass transfer loops 8 and 9. Loop 8 indicated only one precipitable impurity, and the behavior of the impurity was studied in some detail. Loop 9 probably contained more than one impurity, and the one which was studied exhibited equilibrium temperatures much above the cold trap temperature of the loop. (Cold trap temperature = 280°F, equilibrium temperature varied from 430°F to 700°F.)

(a) Summary of Loop 8 Plugging Indicator Behavior (Cold Trap Temperature = 320°F)

Oscillating Runs (Partially Plugged)

Six sets of five minima and maxima were run. The average values of the indicator saturation temperatures were as follows: 320°, 322°, 320°, 317°, 311°, and 309°F. The last two sets were obtained after a set point change which increased the amount of plug and lowered the flow. (The 320°F temperature is equivalent to 3.2 ppm of oxygen from the Rutkauskas curve.)

The reason for the above behavior of changing saturation temperature is not clearly understood. However, the probable reason may be the trapping of Na_2O in the flow reversal region of the plugging indicator. A rough calculation was made, and the result indicated that there was sufficient area in the cool region of the plugging indicator to significantly affect the concentration in the 12-gal system. The above saturation temperature change is equivalent to 0.3 ppm oxygen change (Rutkauskas curve), and the calculations indicated that a change in the 1 to 10 ppm might be expected.

Mass transfer coefficients were calculated from portions of the partially plugged runs. The results are as follows:

Table 462-III

Mass Transfer Coefficient Variation with Reynold's Number

Velocity (cm/sec)	Reynold's Number (Based on the bare orifice diam of 0.035 in.)	Coefficient (g O/cm^2 h ppm)
557	8.40×10^3	1.04×10^{-2}
690	1.04×10^4	1.12×10^{-2}
810	1.22×10^4	1.30×10^{-2}
1000	1.50×10^4	1.96×10^{-2}

The Rutkauskas solubility curve was used to calculate the ΔC values in the mass transfer calculations. These results are in very good agreement with similar calculations run on partially plugged dynamic data obtained from a plugging meter at LASL. The investigators feel that the impurity being studied was probably Na_2O and was the same impurity observed in the LASL studies.

Cooling Rate Effect on Bare Orifice Nucleation

Normal plugging runs were made at varying cooling rates. The saturation temperature was 320°F and the indicated plugging temperatures required to nucleate a detectable quantity of precipitate are indicated below in Table 462-IV.

Table 462-IV

Effect of Cooling Rate on Nucleation Temperature

Cooling Rate (°F/min)	Plugging Temperature	Temperature Depression
2.3	279°F	41°F
4.7	275°F	45°F
6.3	265°F	55°F
12.0	262°F	58°F

Effect of Temperature Depression on Nucleation Time

The effect of temperature depression on nucleation time was briefly studied. The results are presented in Table 462-V.

Table 462-V

Time to Nucleation as Function of Temperature Depression

Time to Plug Detection (min)	Constant Orifice Temperature	Temperature Depression
10.0	283°F	37°F
8.25	274°F	46°F

(b) Summary of Loop 9 Experience

No dynamics were calculated; however, the meter was run overnight in the oscillating mode on the high temperature impurity. The flow change was very erratic and temperature changes were quite variable. The indicated saturation temperature varied from 470°F down to 430°F overnight. When the temperature was raised to dissolve the plug off, the plug size increased. The reason was obscure but may have been because of extensive upstream precipitation in the meter itself. With the temperature increase, the upstream impurity dissolved and produced an apparent increase in concentration at the orifice.

(2) Liquid Metal Engineering Center

The plugging meter on the primary system of the SCTI (Sodium Components Test Installation) was investigated. The meter consisted of a 1-in. valve with a fluted plug. The plug had 10 square slots, 0.040 in. deep. The impurity concentrations in the primary loop were quite low, and an impurity plug had not been obtained in about two to three months by the SCTI operating crews. The cold trap had been initially run at temperatures between 220°F and 240°F some months before and was at the time of the test valved out of the system.

Because of the low impurity content, only one precipitation run was made. By making a long term (5 h) constant temperature run at approximately 220°F, a plug was formed and was allowed to grow to the 40 to 50% plug level. The kinetics of precipitation were very slow, and as a result, an oscillating flow pattern was difficult to form. However, a few long period oscillations were developed near the end of the run, and a saturation temperature of 282°F to 285°F was indicated. If the precipitable impurity were Na_2O, the concentration indicated by the Rutkauskas curve[3] was 2.1 ppm if the curved portion was used and 0.9 ppm if the linear extrapolation was utilized.

The rate constants were a factor of 5 smaller than similar constants for the GE and LASL rates. The design of the fluted plug valve meter may reduce the turbulence at a given orifice Reynold's number and thus produce lower transfer rates.

B. Direct Current Resistivity Meter Study
(G. E. Meadows)

1. General

The dc resistivity meter has the capability of detecting dissolved, particulate, and gas-bubble impurities in system sodium if the temperature of the sodium in the meter can be adequately controlled. The present work involves the testing of a LASL designed dc meter which includes a thermostated section for careful temperature control. The instrument will be tested on Analytical Loop No. 2 and will be used to detect oxygen in cold trapped and soluble gettered systems. CaO particulates may be detected with the meter.

2. Current Results

The dc resistivity meter has been installed on Analytical Loop No. 2. No data will be obtained until the remaining portions of the loop are completed.

C. Evaluation of UNC EMF Cells
(G. E. Meadows, C. C. McPheeters)

1. General

The UNC thoria-yttria solid electrolyte EMF cell has demonstrated the capability of indicating oxygen activity in sodium. However, such characteristics as life time, sensitivity, response time, drift, temperature coefficients, effects of vibration, and of H and C impurities have not been clearly determined. At LASL EMF cells have been installed on the cold trap loop and Analytical Loop No. 2 for use in the cold trap kinetic studies and soluble getter studies. Many of the above characteristics will be determined for these particular instruments as the indicated research progresses.

2. Current Results

a. Analytical Loop No. 2

Two meter housings are installed; however, no data on the meters will be obtained until the loop is completed.

b. Cold Trap Loop

Two new ceramic tubes are being installed in the cell housings in the cold trap loop. This loop is being modified. However, the loop and the EMF cells should be operating by the middle of the next quarter.

VI. SAMPLING AND ANALYSIS - Laboratory Methods

A. Vacuum Distillation Studies
(G. E. Meadows, L. A. Waldschmidt, D. N. Rodgers)

1. General

The vacuum distillation technique has been shown to be a valuable method for analyses of oxygen in sodium.[3] As a result, the method is routinely used on many of the experimental loops at LASL. However, the versatility of the method can be increased as the interaction on the analytical result of other sodium impurities such as NaH and Na_2CO_3 is better understood. Also, the method may be expanded to include analysis of metallic impurities in sodium such as Ca, Fe, Ne, and Cr. The research at LASL

is directed toward refinement of the oxygen analysis methods and the determination of these metallic impurities with vacuum distillation.

2. Current Results

a. Off-Gas from Distillation

Observations conducted on sodium samples removed for vacuum distillation analysis for dissolved oxygen have indicated that there is a small quantity (10^{-5}-10^{-6} liters) of gas evolved from the 5 g sodium metal sample during the final stages of distillation. The evolution occurs while the sample is being distilled at constant temperature (~360°C) and is associated with the removal of the final portion of the metallic sodium from the nonvolatile residue. Samples analyzed by gas chromatographic techniques have shown the evolved gas to be composed primarily of hydrogen with traces of methane.[4]

Based on these observations it was postulated that the gas evolved might be a decomposition product of sodium hydride. Therefore, hydrogen was added to the sodium sample before distillation to determine whether the amount of gas evolved would increase.

To add the hydrogen, the sodium sample was pulled from the loop and allowed to cool under about 2 psig of high purity helium. After the sodium had solidified, the helium was pumped out and replaced with a 6 v/o H_2, 94 v/o He mixture. The sample was heated to ~175°C, and after 15 min the distillation chamber was evacuated. The distillation then proceeded normally. The amount of hydrogen that reacted was calculated from the composition of the H_2-He mixture before and after the sample was heated. The amount of gas evolved was compared to the amount evolved in a normal distillation.

A residual gas analyzer (Atlas "Gasdetektor") was connected to the vacuum system to analyze the distillation off-gas. The analyzer can be set to monitor a single component of the off-gas.

Hydrogen was analyzed in a preliminary run. Since the background was quite high, the input had to be throttled to keep the readings on scale (maximum 10,000 divisions). At the beginning of the distillation the hydrogen level seemed to parallel the total system pressure. However, the hydrogen concentration did not show any significant increase during the pressure peak at the end of the distillation. This observation indicated that the pressure peak is not primarily composed of hydrogen.

In a second preliminary run nitrogen was monitored. Although the background was much lower (less than 50 divisions with no throttling) the nitrogen concentration paralled the system pressure throughout the distillation.

It is planned to analyze other possible components of the distillation off gas and to record the analysis concurrently with the system pressure by comparing the size of the peaks in the pressure vs time curves recorded during the distillation.

Preliminary results indicated that the hydrogen addition did increase the amount of gas evolved. However, analysis showed that these results were due to sample contamination. More careful work eliminated the contamination and showed that, in fact the amount of gas evolved at the end of the distillation did not increase with the addition of hydrogen.

B. Study of Gamma Ray Activation Analysis for C and O
(D. M. Holm, G. E. Meadows, W. J. Heyman, B. K. Barnes, J. L. Parker)

1. General

Many analytical techniques for the analysis of oxygen such as vacuum distillation and amalgamation methods are not specific for a given compound and give oxygen concentrations by assuming the nature or form of the final residue being extracted or analyzed by flame photometry. Thus, analytical techniques are required which can give concentrations of oxygen and other impurities such as carbon directly without making assumption about the chemical form of the impurity.

Photon activation of oxygen and carbon has this property of determining total impurity concentration regardless of its chemical nature. The sodium sample is irradiated by high energy photons (~20 MeV); the sodium is extruded and then is transported pneumatically to the counter where the positron annihilation radiation is detected in a very large segmented NaI crystal. The resulting count rate vs time curve is decomposed by computer analysis into O, C, and K decay curves. Thus, O and C can be determined from one sample if the interferences of K and Na are kept at low levels.

2. Current Results

A sodium sample was irradiated in the LASL linear electron accelerator facility in an attempt to detect carbon by photon activation. The sample was irradiated at about 18 MeV for about 5 min (1mA average current). After a 30-min decay, the sample was counted in the gated 4π mode. Some 20.4-min activity (from ^{11}C) was observed along with substantially more ^{22}Na and a large amount of ^{24}Na. The ^{24}Na is from neutron capture in ^{23}Na. The absolute amount of ^{12}C in the sample could not be determined because of the variable energy of the electron beam during the radiation. Also, the source of the neutrons which produced the ^{24}Na is not known at the present time. A redesign of the electron target may help to eliminate the neutron generation. Preparations are being made for additional activation runs to be made in January.

C. Absorption Spectrophotometry Development for Metal Impurity Analyses
(G. E. Meadows, L. A. Waldschmidt)

1. General

Soluble getter and corrosion studies require that various metal impurity concentration be known as a function of operating conditions. One technique for determining these concentrations is absorption spectrophotometry. Refinement of this technique is being made to detect low level concentration (~1 ppm) both in vacuum distillation residues and in bulk sodium samples. The impurities to be studied are Ca, Mg, K, Fe, Ni, and Cr.

2. Current Results

Procedures have been developed for the determination of Ca in vacuum distillation residues and also bulk sodium samples. Precision for Ca in the residue samples is ± 0.05 ppm in the 0.1 to 10 ppm range, and for bulk sodium samples ± 0.5 ppm in the 1 to 10 ppm range. Some data obtained indicates that part of the Ca in sodium can be carried over with the sodium in the distillate.

Fe, Ni, and Cr are determined in the vacuum distillation residues (a Ta distillation cup is used and the residues are leached with aqua regia). Samples taken form Analytical Loop No. 1 for K determinations have run 150 ± 20 ppm in bulk samples. Residue determinations for K have been < 1 ppm. The K is found to be carried over with the sodium in the distillate.

D. Total Carbon Analysis Development
(K. S. Bergstresser)

1. General

The low temperature combustion technique for total carbon analysis is being refined. By using a high sensitivity gas chromatograph for quantitative measurement of the CO_2 produced, it is hoped that carbon concentrations in the 1 ppm range can be determined.

2. Current Results

An all-metal system for the determination of C at the 1 to 10 ppm concentration level was tested by measuring background or apparatus blank levels of CO_2. The system, which was designed for the low-temperature combustion of Na, has a Ni chamber for burning the Na at 700°C to ensure conversion of all C traces to CO_2. The CO_2 is measured by gas chromatography following separation by acidification of the basic combustion products (Na_2O and Na_2CO_3) and collection of the released CO_2 in a molecular sieve trap. Determinations of backgrounds were made by flowing He gas through the metal system and measuring the amount of CO_2 picked up in the He. The background levels of CO_2 initially were high. Possible sources of contamination will be investigated before combustion of Na in the burn chamber.

Successful operation of the gas chromatograph (Varian Aerograph Model 1532-2B) was delayed considerably by a faulty gas-handling system in the instrument. Replacement of the system and a long "conditioning" period reduced the high background current to a reasonable level. Methods were tested for removal of moisture from the He carrier gas and for collecting the CO_2 in traps cooled in liquid N_2. Preliminary calibrations of the chromatograph were obtained by measuring known amounts of CO_2 added to He with a syringe.

E. Development of Remotely Operated Distillation Samplers for EBR-II
(W. R. Wykoff, D. N. Dunning, J. R. Phillips, H. M. Ruess, E. O. Swickard, J. M. Reilly, E. L. Duran)

1. General

At the request of the AEC, part of the effort directed to a study of in-line sampling associated

with the vacuum distillation analytical method has been redirected to the design and construction of remotely operated, integral sampling and distillation units for installation on the primary coolant loop of EBR-II. A version of the sampling system is also being developed for the nonradioactive secondary sodium system of EBR-II. The sampling system design is a modified engineering loop version of the laboratory model integral full-flow vacuum distillation sampling system currently in use on the Analytical Loop No. 1 and cold trap experimental facilities at the LASL. The entire sampling system will be fabricated of Type 304 stainless steel, and separation of sodium from the nonvolatile impurities will be accomplished by induction heating. The work coil of the induction heater is located within the metal envelope surrounding the distillation zone.

2. Current Results

The sample transfer mechanism of the EBR-II sodium sampler (Fig. 462-7) was designed and a

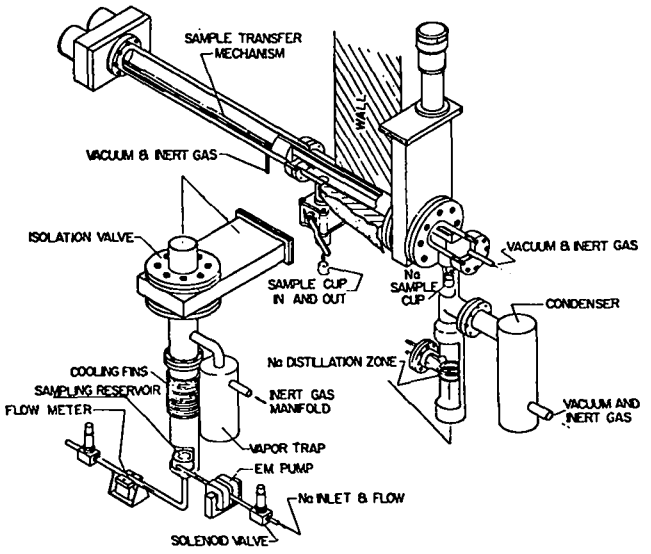

Fig. 462-7. Skematic drawings of sample transfer mechanism and distillation unit of the EBR-II sodium sampled.

mockup completed. Checkout of the system revealed that no modifications are necessary for the production model. Layouts and detailed drawings for the production model are complete, and the Mark I unit is in fabrication and scheduled for completion at the end of February 1969.

A design layout of the vertical leg of the sodium sampler has been completed, and a layout of the entire sodium sampler for Cell A of Reactor Building No. 767 at NRTS has been 80% completed. The sodium overflow chamber is being designed, as is a sodium dump tank.

A water model of the sodium flow system has been built and tested.

Design of the basic sampler assembly is nearly completed, and design and fabrication of the prototype instrumentation and control system is in progress. The complete prototype sampler system is expected to be installed on the LASL test loop by July 1, 1969.

A paper describing the sampler system was presented at the International Conference on Sodium Technology and Large Fast Reactor Design at Argonne National Laboratory on November 7-9, 1968.

VII. COVER GAS AND MAINTENANCE ATMOSPHERES

A. Development of a High Temperature Quadrupole Mass Spectrometer for Cover Gas Analysis (J. P. Brainard, D. C. Kirkpatrick, C. R. Winkelman)

1. General

The purpose of this research is to develop a method for continuous on-line analysis of high temperature (up to 650°C) cover gas in an LMFBR. The analyzer must be capable of detecting impurities such as nitrogen, oxygen, hydrogen, carbon dioxide, methane, and fission products in the cover gas with a sensitivity varying from the part-per-million range to the percent range. A response time of about 1 min is necessary if the analytical data are to serve as the error signal furnished to activate devices for continuous control of cover gas composition.

A quadrupole mass spectrometer was obtained in order to meet the above requirements. It is believed that reasonably representative sampling can be accomplished by transporting the sample gas in sodium loop containment materials and at sodium loop temperatures until it has passed through the spectrometer for analysis.

2. Current Results

The apparatus to measure gas flux distribution from various molecular beam sources was completed

and pre-tests proved it to be functioning properly. Gas beam distributions for the long 7-mil i.d. tube and collimated hole structure were measured in the apparatus and the results are shown in Fig. 462-8.

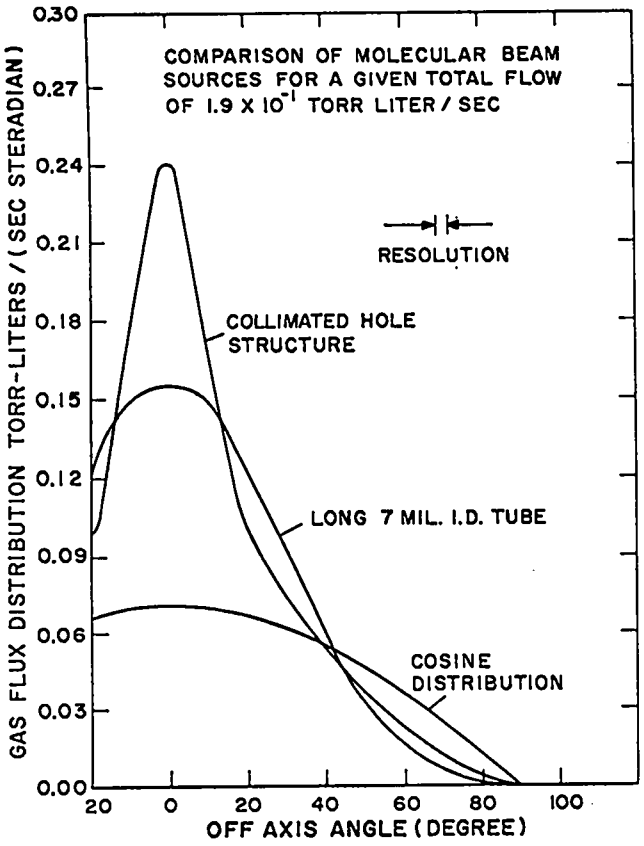

Fig. 462-8. Gas flux distribution of various sources for a fixed total flow.

Another collimator was received this quarter, it consists of 5,500 holes of 0.65 mil i.d. in a stainless steel disc 80 mils in diam by 70 mils long. The distribution follows the theory within the resolution of the instrument. The results show that the multi-hole collimator structure is superior to the long tube type.

Apertures for these molecular gas beams have been designed and fabricated. The gas distribution has been measured for the collimated hole structure with an aperture of 0.08 in. diam at 0.8 in. from the source. Also, the distribution of the 7 mil i.d. tube with an aperture of 7 mils i.d. at 70 mils from the source has been measured. The results are as expected, with the beam intensity being zero beyond 6° from the beam axis and the maximum intensity being the same as the peak intensity without the apertures.

The diffusion pumps and the high-quality stainless steel for the future high temperature gas analyzer have been received. Cold traps are being adapted to the diffusion pumps.

REFERENCES

1. George G. Libowitz, The Solid-State Chemistry of Binary Metal Hydrides, W. A. Benjamin, Inc., New York, 1965

2. "Quarterly Status Report on the Advanced Plutonium Fuels Program," April 1 - June 30, 1968, Report LA-3993-MS, Los Alamos Scientific Laboratory.

3. V. J. Rutkauskas, "Determination of the Solubility of Oxygen in Sodium Using the Vacuum Distillation Analytical Technique," Report LA-3879, Los Alamos Scientific Laboratory, 1968.

4. "Quarterly Stuatus Report on the Advanced Plutonium Fuels Program," July 1 - September 30, 1968, Report LA-4073-MS, Los Alamos Scientific Laboratory.

PROJECT 463

CERAMIC PLUTONIUM FUEL MATERIALS

Person in Charge: R.D. Baker
Principal Investigator: J.A. Leary

I. INTRODUCTION

The principal goals of this project are to prepare pure, well characterized plutonium fuel materials, and to determine their high temperature properties. Properties of interest are (1) thermal stability, (2) thermal expansion, (3) thermal conductivity, (4) phase relationships by differential thermal analysis, (5) structure and phase relationships by x-ray diffraction, high temperature x-ray diffraction, neutron diffraction and high temperature neutron diffraction, (6) density, (7) hardness and its temperature dependence, (8) compatibility including electron microprobe analysis, (9) compressive creep (deformation).

In addition to phase equilibria and general properties, specific thermodynamic properties such as free energy of formation by vaporization equilibria in the 1000-2000°C temperature range with mass spectrometer identification of vapor species, free energy of formation by electromotive force measurements in the 450-1200°C temperature range, and heat capacity and heat of transition are being determined.

II. SYNTHESIS AND FABRICATION

(M.W. Shupe, A.E. Ogard, R.L. Nance, D. Kelley)

1. Carbides

A variety of carbide compositions have been prepared by methods described in previous reports. These materials were used for properties measurements. The following compositions were prepared: $U_{0.8}Pu_{0.2}C$, $U_{0.8}Pu_{0.2}C_{1.1}$, $PuC_{0.98}$, $PuC_{1.32}$, $PuC_{1.41}$, $PuC_{1.65}$, $PuC_{2.1}$, $PuC_{2.2}$, and $PuC_{4.0}$.

During last quarter the effect of several binders on the sintered pellet microstructure of (U, Pu) C was examined. It was found that 0.5 w/o additions of Carbowax 4000 changed the microstructure from single phase MC to MC and M_2C_3. The pellet in which paraffin was used as the binder was single phase and exhibited the fewest microcracks. This period the effect of increasing paraffin binder concentration on $U_{0.8}Pu_{0.2}C$ was determined. No lessening of microcracks was found with increasing paraffin concentration. Also, the amount of irregular-sized pores increased with increasing binder. As indicated in the next paragraph, binders are not necessary and will therefore not be used in the future.

Powders of two particle sizes were pre-slugged (without binders), cold compacted at several pressing pressures, sintered, and examined for microcracks. Both powders were screened to < 64μ size. The courser powder (lot 7-93-1) was ground in a oscillating mill, while the finer powder (lot 7-87-1) was further pulverized by ball milling 16 hr. Particle size analysis is being done. The pellets prepared from the course powder were free of microcracks when pressed at pressures up to 20 tsi. Pellets from the finer powder were found to be free of microcracks up to 10 tsi pressing pressure. These effects are shown in Figures

463-1 and 463-2. It is concluded 10 tsi pressing pressure is optimum for preparing pellets of good integrity.

Using the same two powder lots, the effect of pressing pressure on densification and diametral control was determined. It can be seen that the sintered density has very little dependence on pressing pressure. Results are shown in Figures 463-3 and 463-4. The pellets were prepared in duplicate using pre-slugged, binder free powders. Pellet densities of 93 and 94 percent of theoretical are attainable with the coarse and finer powders, respectively, at 10 tsi. In addition, densification to 95% of theoretical can be obtained by pressing the finer powder at 20 tsi. Future ceramic engineering studies will be directed towards generation of time-temperature-density curves using existing materials.

Compatibility experiments at other laboratories have indicated that compatibility of UC_{1+x} with stainless steels may depend on the form of the higher carbide, i.e., U_2C_3 or UC_2. In order to evaluate this for $(U, Pu)C_{1+x}$, efforts are being directed towards determining the conditions necessary to convert completely the acicular phase observed in $U_{0.8}Pu_{0.2}C_{1+x}$ into the reprecipitated M_2C_3 structure. The $2\,MC_2 \rightarrow M_2C_3 + C$ transformation occurs at $\sim 1660^{\circ}C$. Pellets of the composition $U_{0.8}Pu_{0.2}C_{1.2}$ and $U_{0.8}Pu_{0.2}C_{1.1}$ contain some of the acicular phase (MC_2) after sintering at $1800^{\circ}C$ for 4 hr followed by $1400^{\circ}C$ for 2 hr as shown in Figures 463-5 and 463-6, respectively. The surface "rind" shown on the photomicrograph in the upper left figure 463-5 is typical of pellets of this composition. Heating at $1600^{\circ}C$ for 24 hr or $1400^{\circ}C$ for 24 hr does not significantly change the amount of acicular phase as shown in Figure 463-5. A small but measureable reduction in amount of this phase was found on holding at $1400^{\circ}C$ for 36 hr as shown in Figure 463-6. Apparently complete transformation is extremely slow. Annealing the higher carbides at $1250^{\circ}C$ for 36 hr did not completely eliminate the appearance of the acicular phase, as shown in Figure 463-7. In this sample, only the MC phase was detectable by x-ray diffraction analysis. The higher carbides can be formed essentially free of acicular phase by sintering compacted powders below the transformation temperature such as $1525^{\circ}C$ as shown in Figure 463-8. Densification to approximately 93% of theoretical occurred after 24 hr at $1500^{\circ}C$. A slight trace of platelets in the pellet interior was found even after additionally heating $1400^{\circ}C$ for 36 hr.

$U_{0.8}Pu_{0.2}C_{1.2}$ pellet no. 7-60-3C was prepared from powder treated at $1800^{\circ}C$ for 4 hr followed by $1600^{\circ}C$ for 24 hr in Ar. Pellets prepared from this powder were sintered at $1525^{\circ}C$ for 4 hr in Ar. The lattice dimensions of a sample so prepared was found to be 4.964 A for MC and 8.098 A for M_2C_3. The unit cell size is higher than previously obtained with $(U_{0.8}Pu_{0.2})_2C_3$. This would be possible if Pu were enriched in the M_2C_3 phase relative to the MC phase. In order to test this, pellets of the same composition were sintered for 24 hr in Ar at $1500^{\circ}C$. Electron microprobe examination of these pellets indicated that the Pu and C x-ray intensities were approximately 100 and 45% greater, respectively, and the U x-ray intensity approximately 25% less, from the M_2C_3 phase than from the MC phase. Thus a high enrichment of Pu in the M_2C_3 phase occurred.

A typical single phase $^{235}U_{0.8}Pu_{0.2}C$ carbide pellet was examined for homogeneity by three techniques. Alpha radiography found complete homogeneity to the limit of detection. Metallographic examination indicated single phase homogeneous monocarbide. Electron microprobe examination of a typical region detected a few percent variation in U and Pu x-ray intensities, as shown in Figure 463-9.

2. Nitrides

Specimens of PuN have been prepared from powder lot PuN-16 for low temperature calorimetry at AERE Harwell and for high temperature calorimetry at this Laboratory. The properties of the PuN powder are shown in Table 463-I. The Harwell specimens were 0.37 in. dia x 0.33 in. tall with a 0.13 in. dia axial hole. The density was 12.2 g/cc after sintering at $1900^{\circ}C$ for 2 hr in N_2. The high temperature calorimetry pellets were 5/8 in. dia x 0.4 in. tall after sintering

EFFECT OF PRESSING PRESSURE
ON $(U, Pu)C$ PELLETS

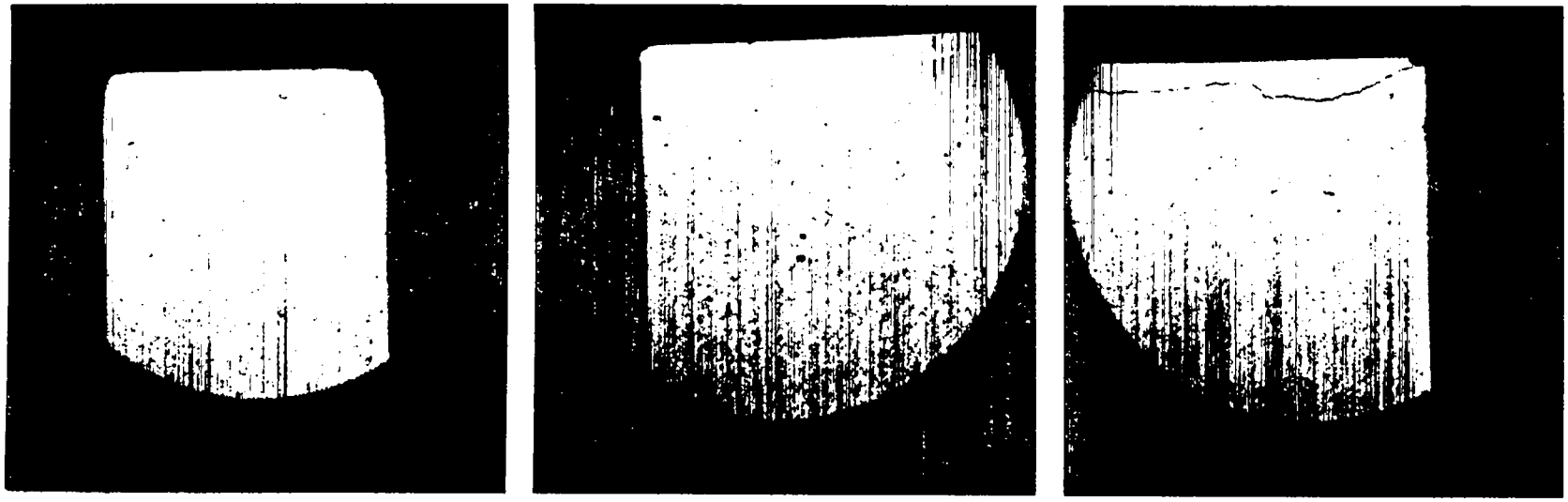

14 X

14 X

14 X

PRESSING PRESSURE 10 TSI

20 TSI

40 TSI

FROM OSCILLATING MILLED POWDER 7—93--1

Figure 463-1

EFFECT OF PRESSING PRESSURE ON (U,Pu)C PELLETS

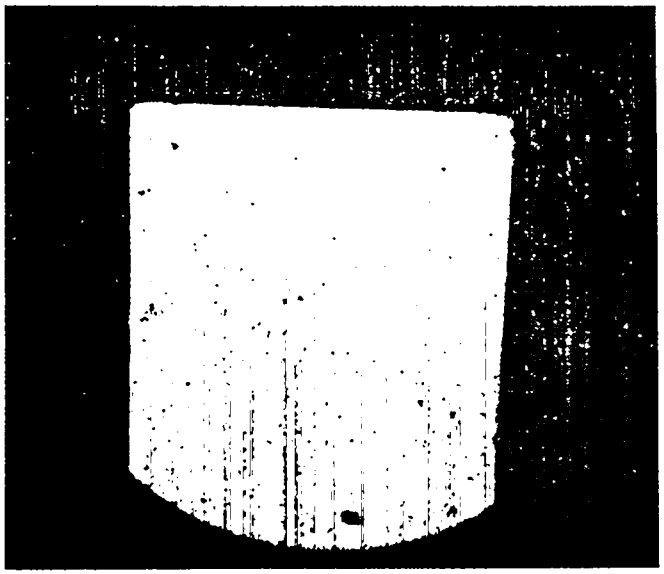

14 X

PRESSED 10 TSI

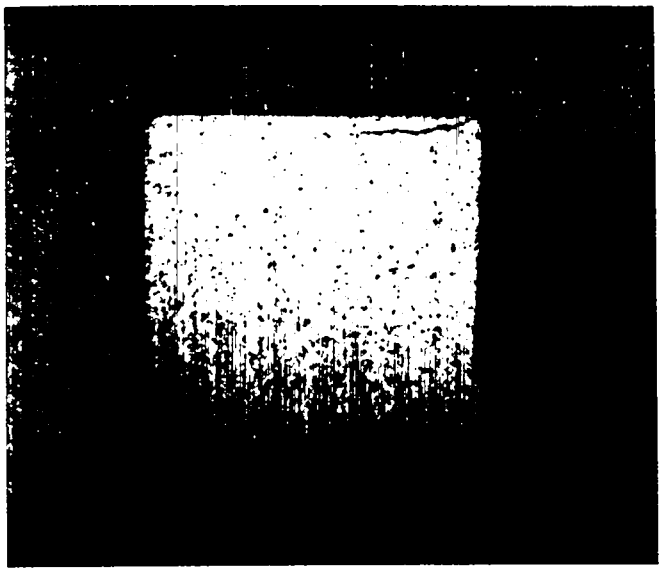

14 X

PRESSED 20 TSI

FROM BALL MILLED POWDER 7-87-1

Figure 463-2

DENSIFICATION CURVE

LOT NO. 7-87-1

SINTERING CYCLE 1800°C 4 HRS, Ar

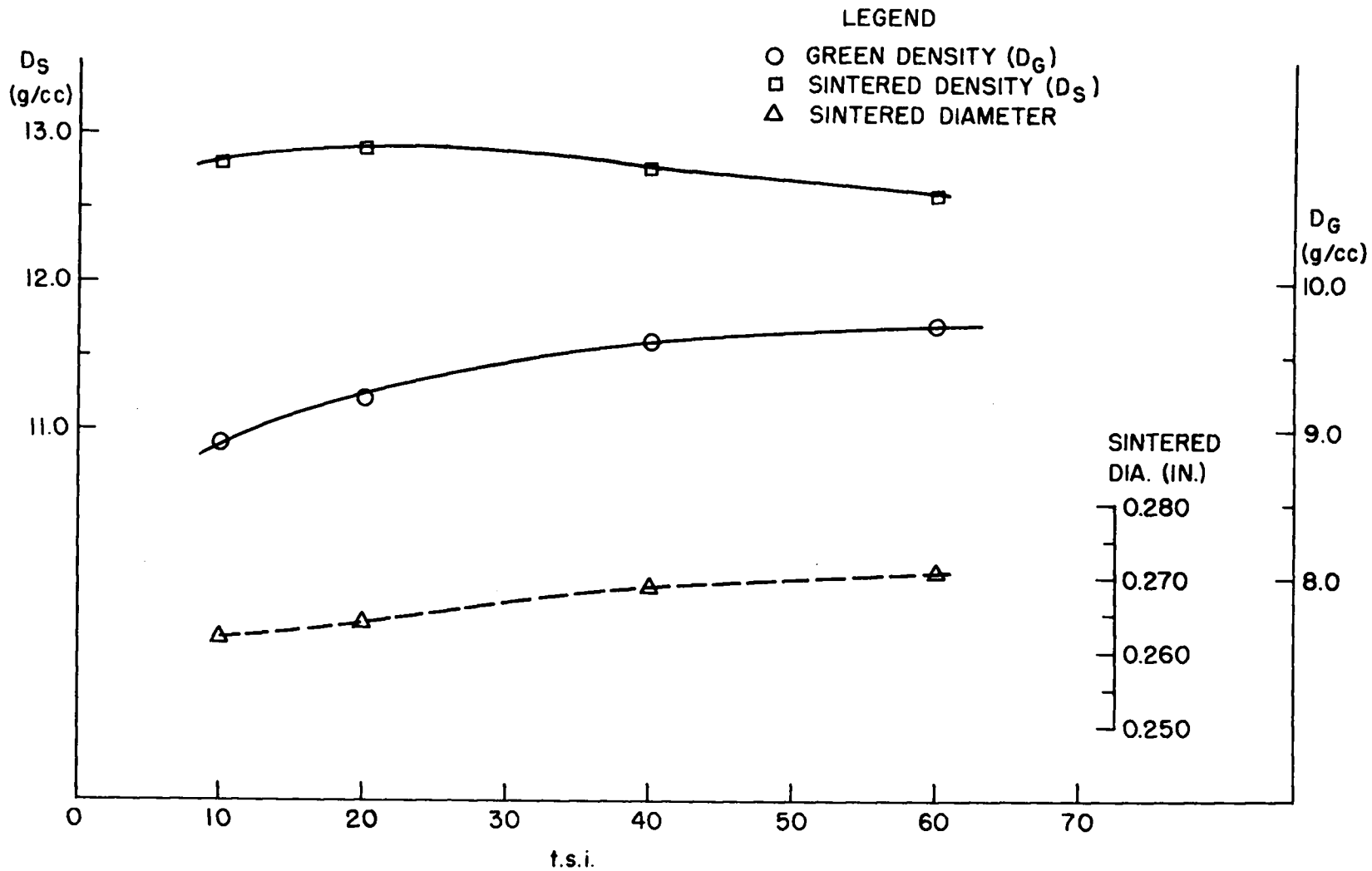

Figure 463-3

DENSIFICATION CURVE

LOT NO. 7-93-1

SINTERING CYCLE 1800°C 4 HRS, Ar

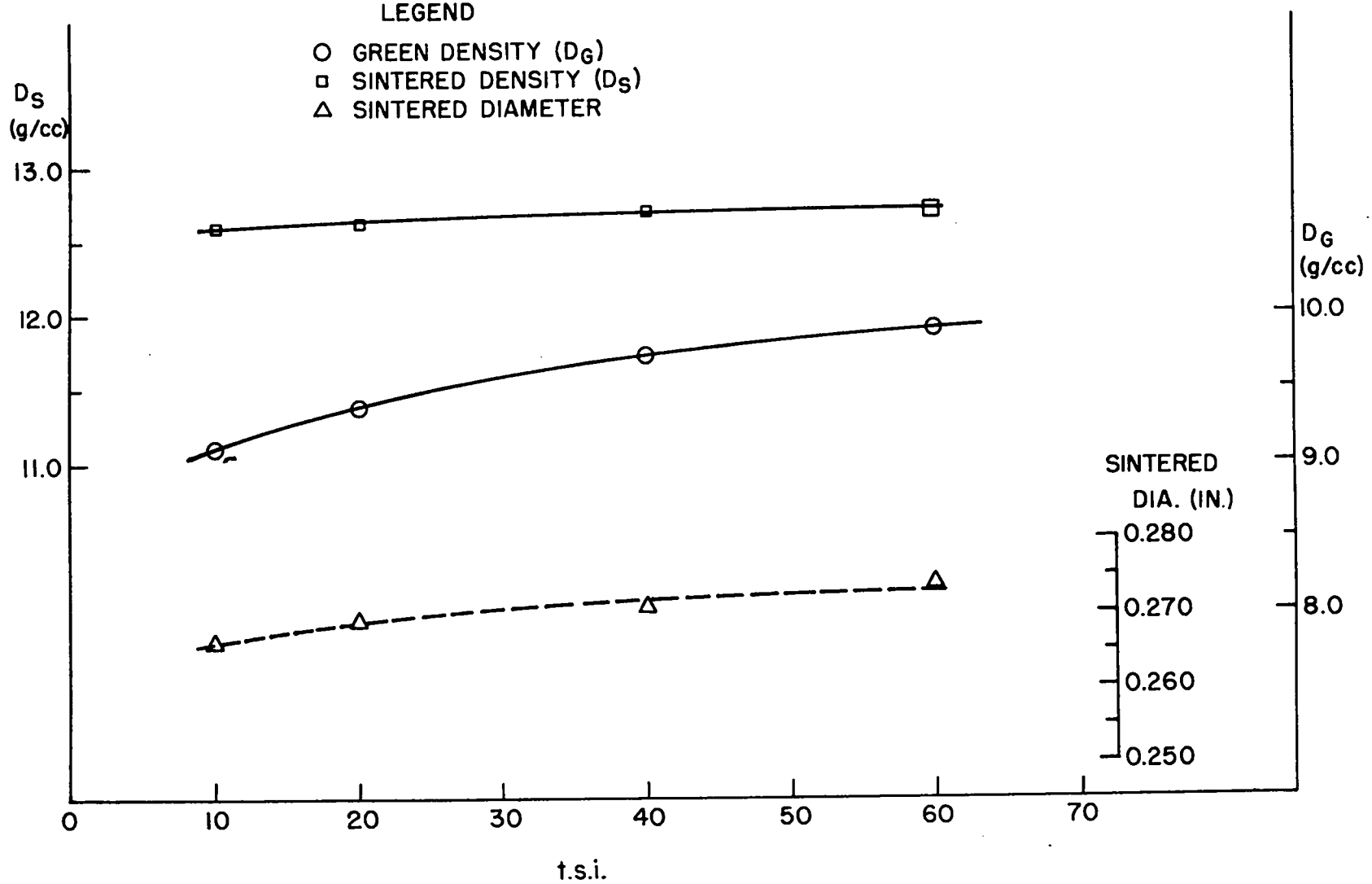

Figure 463-4

$U_{0.8}\ Pu_{0.2}\ C_{1.2}$

LOT 7-60-3

CONTROL

380X ELECTROLYTIC ETCH

CONTROL

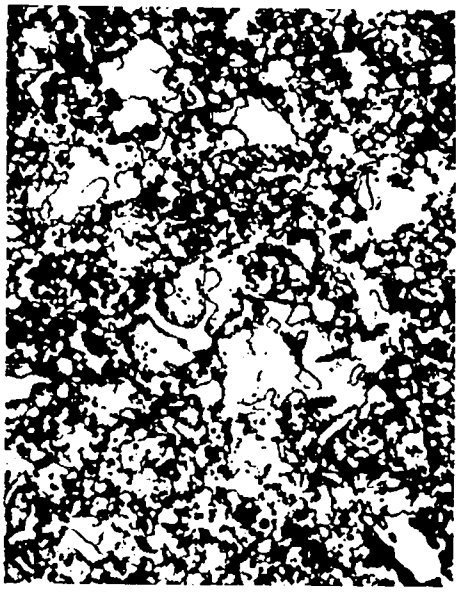

380X ELECTROLYTIC ETCH

HEATED 1800°C – 4 HR – Ar
1400°C – 2 HR – Ar

TREATMENT 1

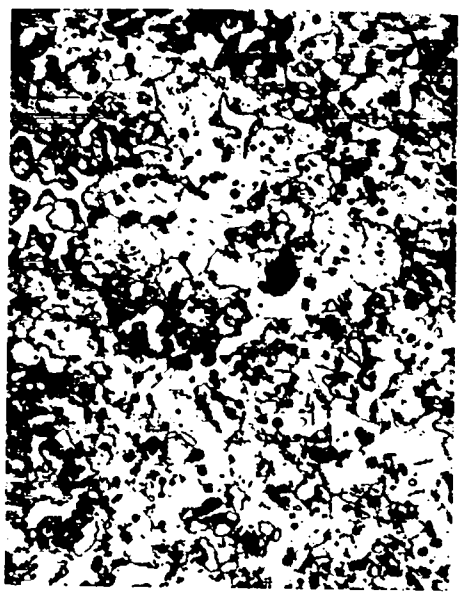

380X ELECTROLYTIC ETCH
ADDITIONALLY HEATED
1400°C – 24 HR – Ar

TREATMENT 2

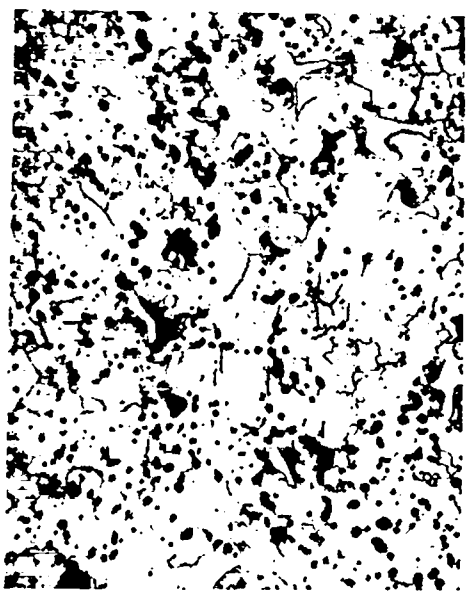

380X ELECTROLYTIC ETCH
ADDITIONALLY HEATED
1600°C – 24 HR – Ar

Figure 463-5

$U_{0.8}Pu_{0.2}C_{1.1}$

LOT 7-60-2

CONTROL

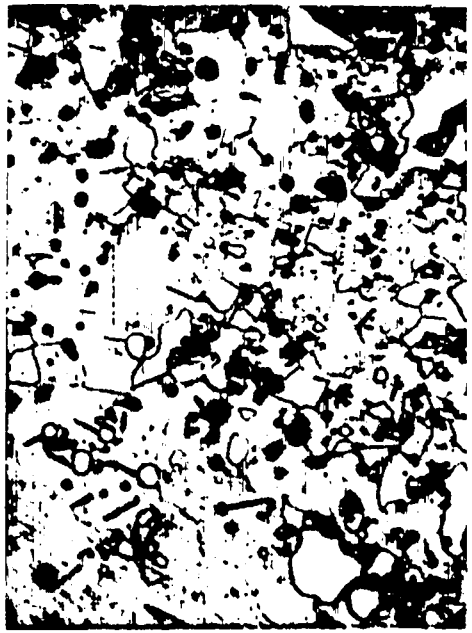

900X ELECTROLYTICALLY ETCHED

HEATED 1800°C - 4 HR - Ar

1400°C - 2 HR - Ar

TREATED

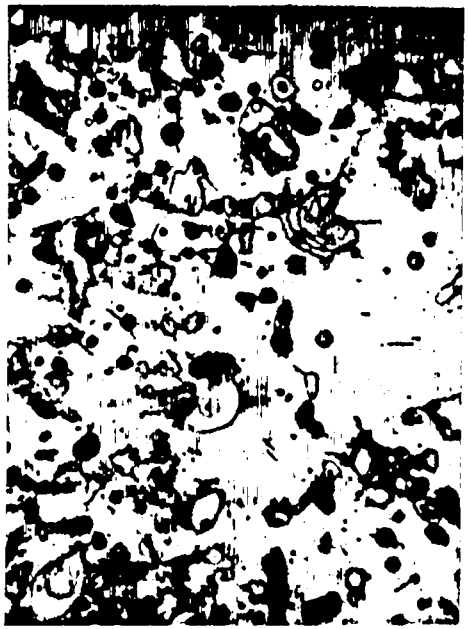

900X ELECTROLYTICALLY ETCHED

ADDITIONALLY HEATED

1400°C - 36 HR - Ar

Figure 463-6

$U_{0.8}Pu_{0.2}C_{1\pm x}$

LOT 7-71-1C

CONTROL

380X ELECTROLYTICALLY ETCHED

HEATED 1625°C - 4 HR - Ar

TREATED

380X ELECTROLYTICALLY ETCHED

ADDITIONALLY HEATED

1250°C - 36HR - Ar

Figure 463-7. An x-ray powder diffraction photograph obtained from this material shows it to consist of a single detectable crystalline phase, face-centered isometric with lattice dimension a_o 4.9652 ± 0.0004Å: (U, Pu)C solid-solution phase.

$U_{0.8}\ Pu_{0.2}\ C_{1.2}$

LOT 7-60-3

CONTROL

900X STAIN ETCHED
HEATED 1525°C – 4 HR – Ar

TREATED

900X STAIN ETCHED
ADDITIONALLY HEATED
1400°C – 36 HR – Ar

CONTROL

900X ELECTROLYTIC ETCH
HEATED 1500°C ± 50 – 24 HR – Ar

Figure 463-8

EXAMINATION OF (U,Pu)C BY THREE TECHNIQUES FOR HOMOGENEITY

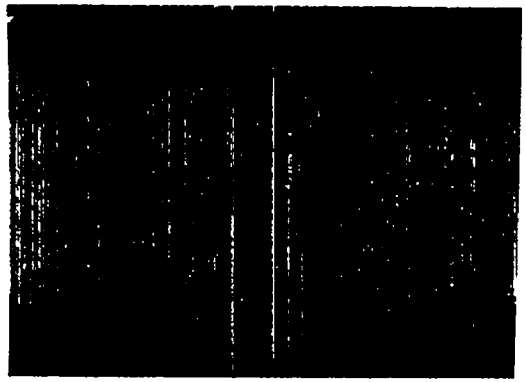

4X ALPHARADIOGRAPH

380X PHOTOMICROGRAPH

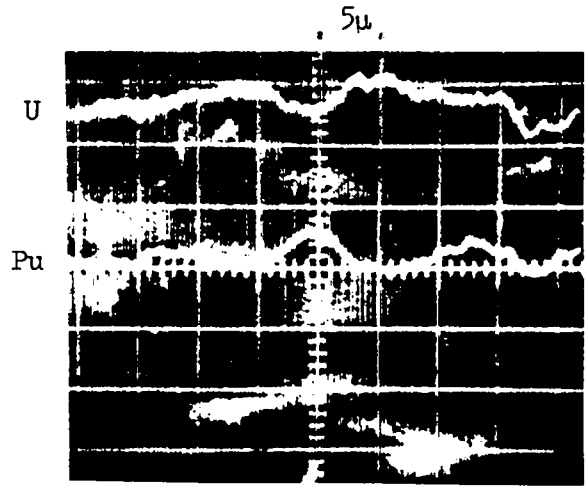

Line scan analyses showing distribution of U and Pu across a grain (2000x).

ELECTRONMICROPROBE

Figure 463-9

Table 463-I

COMPOSITION OF PuN-16 POWDER

Lattice dimension, A	4.9044 ± 0.0002
w/o N (theor. = 5.53)	5.50 ± 0.05
w/o Pu (theor. = 94.5)	94.48 ± 0.23
O content, ppm by wt.	50 ± 14
Fe content, ppm by wt.	50
Cr content, ppm by wt.	0.5
Am content, ppm by wt.	413

Emission spectrochemical analysis:

Element	ppm by wt.	Element	ppm by wt.
Li	< 0.005	Ni	< 0.5
Be	< 0.001	Cu	2-3
B	< 0.5	Zn	≈ 10
Na	1	Rb	< 0.5
Mg	≈ 2	Sr	< 0.1
Al	1-2	Y	< 0.1
Si	10-15	Zr	1
K	< 0.5	Mo	< 0.5
Ca	< 2	Cd	< 0.5
Ti	< 0.5	Sn	< 0.5
V	< 0.5	Cs	< 5
Ba	< 0.1	La	< 1
Hf	< 0.5	Ta	< 25
W	50-65	Re	< 0.5
Pb	4	Bi	< 0.5
Co	< 0.5		

in the same manner as the small annular pellets for the UK. X-Ray diffraction analysis indicated single phase PuN having a unit cell size of 4.9046 ± 0.0004 A. Chemical analysis was 5.49 w/o N, 330 ppm O.

3. Oxides

Reference pellets of $(U, Pu)O_2$ are required for an exchange with AERE Harwell. Pure UO_2 and PuO_2 powders were blended and ball milled for 24 hours, then pressed and sintered at 1600°C for 6 hr in Ar - 6% H_2 that contained 0.4 mm H_2O. Geometric densities of these pellets were 10.0 g/cc. The 88 pellets produced in this first lot have been sampled for complete characterization before shipping to Harwell.

III. PROPERTIES

(J.G. Reavis)

1. Differential Thermal Analysis

Transition Temperature of PuC_2: DTA observations have been made using a high purity sample of $PuC_{2.1}$. Calibration of the apparatus was rechecked by observation of the melting point of Pt and the eutectic temperature of Pt + C immediately after observation of the $PuC_{2.1}$ sample. The Pu_2C_3 + C/PuC_2 transition temperature was found to be 1660 ± 10°C and liquid phase formation was seen at 2232 ± 10°. Previously PuC_{2+x} samples have shown arrests at 1650 ± 20° and 2235 ± 20°. This concludes study of these transitions. The Pu_2C_3/PuC_2 transition temperature is independent of the C concentration over the range C/Pu = 1.6 to 8 (atom ratio). The solidus temperature also is independent of the C concentration over the range C/Pu from 2.0 to 8.

DTA Furnace Development: Previous DTA observations have been made using a sample located in approximately the center of the furnace and a reference temperature point near the top of the furnace. This highly unsymmetrical location of the two points of observation gave rise to a gradual and somewhat unpredictable change in the ΔT base line. A new and larger furnace having symmetrical location of sample and reference compartments has been developed, tested, and put into the glovebox. It appears that the larger furnace will not attain temperatures as high as those attained by the smaller furnace, but should make possible the precise determination of very small heat effects up to about 2000°C.

Another change made possible by use of the new furnace is the use of thermocouples to extend the range of the apparatus down to room temperature. The optical system used in the conventional system (and which will continue to be used at high temperatures) was not sensitive at temperatures below 1000°C.

2. X-Ray Powder Diffraction

(C.W. Bjorklund, R.M. Douglass)

Self-Irradiation Damage

The parameters in the equation expressing the lattice expansion of PuO_2 as a function of time and temperature were recalculated to reflect additional data. This equation

$$a_t = \frac{P_1 P_2 a_o}{P_2 + P_3 e^{-P_4/T}} \left[1 - e^{-(P_2 + P_3 e^{-P_4/T})t} \right] + a_o$$

was described in a previous report. a_t is the lattice dimension measured at time t and absolute temperature T, and P_1, P_2, P_3, P_4, and a_o (the lattice dimension at time 0) are the parameters calculated by a least squares routine. An error was found on one of the data cards in the -198° PuO_2 data deck which had been reproduced for the original calculations. After correction of the error and addition of the new data, the values of

the parameters were found to have changed only slightly, but the standard deviations were decreased by a factor of 10. The revised values are:

Parameter	Value	Standard Deviation
P_1	$3.22_1 \times 10^{-3}$	$0.02_8 \times 10^{-3}$
P_2	$1.13_8 \times 10^{-2}$	$0.02_3 \times 10^{-2}$
P_3	$6.2_{03} \times 10^{-2}$	$0.5_3 \times 10^{-2}$
P_4	$1.32_1 \times 10^{3}$	$0.05_0 \times 10^{3}$
a_o	5.3953_6	0.00009

Because $(a_t - a_o)$ at saturation varies exponentially with 1/T, it seemed that there would be a minimum temperature below which any change in Δa would not be detected experimentally. Assuming that a change in Δa of 5×10^{-5}Å would be the absolute minimum change detectable, it was calculated that the minimum temperature occurs at ~ 176°K (-97°C). Conversely, the equation would permit a Δa at saturation of 0.006Å at 1273°K (1000°C), which seems unlikely. Upon comparing data calculated from the equation with annealing data reported by Rand, et al,[1] it would appear that a practical upper temperature limit exists at approximately 500-600°C.

The effects of energy deposition (dose) on the lattice expansion of different plutonium compounds were recalculated to include additional data obtained during the past quarter. The results confirmed those obtained previously, i.e., only in the case of PuO_2 was the rate of expansion as a function of total energy deposition independent of the dose rate. (For the two sets of PuO_2 samples studied the dose rates differed by a factor of 10.)

No significant changes were observed in the lattice dimensions of the enriched compounds measured during this period.

3. High Temperature X-Ray Diffraction
(J. L. Green)

Work has been initiated on the study of the high temperature crystallographic properties of PuC_{1+x} compositions. Preliminary investigations have been carried out on a sample having a nominal composition of $PuC_{2.2}$. Since the data were derived from only one sample, the results must be regarded as tentative.

Thermal expansion data for carbon-rich Pu_2C_3 have been obtained in the temperature interval from 800 to 1600°C. A least squares fit of this set of data yields

$$\frac{\Delta a}{a_o} = 1.2 \times 10^{-5} T + 2 \times 10^{-9} T^2$$

where T is the temperature in °C and a is the lattice dimension in Angstrom units. This corresponds to a thermal expansion coefficient that is relatively large, e.g., $\bar{\alpha}_{0-1600^o}$ 16×10^{-6} °C^{-1}. No data have been reported by other workers that can be used for comparison at high temperatures; however, two determinations have been reported for lower temperature ranges. Rand and Street[2] reported an average expansion coefficient of 16.22×10^{-6} °C^{-1} (20°-935°C) and Pallmer[3] reported a value of 14.8×10^{-6} °C^{-1} (20°C-780°C). The average low temperature expansion coefficient computed for data from the present study is ~ 14×10^{-6} °C^{-1} (0°C-800°C), which is somewhat smaller than those reported in the earlier works.

Attempts to determine an independent value for the temperature at which the transition

$$PuC_{1.5} + 0.5\ C \rightarrow PuC_2$$

occurs have been unsuccessful to date. The kinetics of this reaction appear to be very slow. For instance, at 1750°C, the transition takes place at an observable rate, but intensity changes occur very slowly. Transition rates below the reported transition temperature have not been investigated to date.

The only stable structure existing above the temperature at which the transition is observed is the cubic modification of PuC_2. This is in agreement with results reported in the UK.[4] No indication of the tetragonal modification has been observed at or near the transition temperature. However, it is possible that a region of stability for this structure exists and is being obscured by kinetically sluggish transitions. Furthur work will be necessary to clarify this point.

Obtaining accurate lattice parameter data for PuC_2 (cubic) will be somewhat difficult. To date, all reflections observed for this structure have been

entirely limited to the front reflection region. This problem is probably due to intensity and resolution losses arising from thermal effects. A small amount of preliminary thermal expansion data have been obtained for PuC_2 (cubic), but, only a crude expansion coefficient may be calculated, due to the small number of observations and to scatter in the data. The average expansion coefficient estimated for the temperature range 1750°C to 2000°C is $21 \times 10^{-6}\ ^{\circ}C^{-1}$. No comparable data on PuC_2 are available, but Bowman[5] has reported $25.2 \times 10^{-6}\ ^{\circ}C^{-1}$ (1765°C - 2300°C) for UC_2 (cubic).

Two metastable phases have been observed in quenched samples of PuC_2. The first of these is the tetragonal modification of PuC_2[6,7] and the second is a material of unknown composition and structure.[8] PuC_2 (tet.) typically results from rapid quenching rates ($\sim 10^3\ ^{\circ}C$/min). Although the furnace being used in the present study is capable of very rapid quenching only relatively slow cooling ($\sim$ 500-600°C/min) has been carried out to date. Under these circumstances, no PuC_2 (tet.) has been observed, while samples containing the unknown phase are easily prepared. The reported diffraction patterns of samples containing PuC_2 (tet.) virtually always contain extra lines which correspond to this unknown phase. It would seem reasonable to postulate that the unknown species is a kinetically trapped metastable intermediate involved in the mechanism of the decomposition of PuC_2 to Pu_2C_3.

4. Thermodynamic Properties of Plutonium Compounds by Electromotive Force Techniques
(G. M. Campbell)

Emf measurements have been made on the Pu_2C_3 vs Pu system using a galvanostatic technique to determine the Pu equilibrium potential in fused $PuCl_3$, LiCl-KCl. The experiments were made in the temperature range 917-1047°K. Since emf measurements on this system do not show good correlation with vapor pressure measurements, the experiments were continued over long periods of time to insure equilibrium conditions and to allow any possible oxygen impurities to react with the $PuCl_3$ in the electrolyte. This was done with the consideration that Pu_2O_3 should be more stable than any of the Pu-C-O derivatives. Since Pu_2O_3 is insoluble in the electrolyte and a nonconductor of electrons, oxygen should be eliminated by equilibrating an oxygen contaminated electrode with the electrolyte. The procedure used was as follows. A Pu_2C_3 + C pellet used as an electrode was equilibrated with the $PuCl_3$, LiCl-KCl electrolyte for a period of 506 hours. A second Pu_2C_3 + C electrode made from the same stock material was then introduced and the emf of the second electrode recorded vs the emf of the first electrode. At the same time the emf of either electrode against the Pu reference was determined using the galvanostatic technique.

After 95 hours the second Pu_2C_3 + C electrode was 0.008 volts more positive than the first. This indicated that the Pu activity was slowly increasing with time. After 650 hours both electrodes were at the same potential and the activity of Pu was slightly increased in either electrode. The electrodes were very stable over a period of 1006.4 hours at which time the experiment was interrupted due to slow vaporization and condensation of the electrolyte. The discontinuities were observed as might be expected if oxygen or some other impurity were being titrated.

The results of these experiments still do not show good correlation with the vapor pressure studies although, of course, these measurements are at a much lower temperature than the vapor pressure measurements.

Further studies will be carried out to determine if the Pu_2C_3 + C system can be reasonably correlated with the U_2C_3 + C and the $(U, Pu)_2C_3$ + C systems. Although some studies[9] have been made on the U_2C_3 + C system in this temperature range, they were done with solid UF_3 as electrolyte without a means of detecting oxidation to UF_4 at these temperatures. This system will be re-examined using a molten salt electrolyte.

5. Thermodynamic Properties from Vaporization Studies
(R. A. Kent)

The mass spectrometer-Knudsen cell assembly described previously has been utilized to study the

vaporization of Pu metal, PuN and various plutonium carbide compositions.

Pu:

Plutonium metal was effused from both W Knudsen cells and ThO_2 cups contained in W Knudsen cells over the range 1426-1658°K. The experimental results indicate that Pu(ℓ) vaporizes to the monomer with the Pu pressure given by the equation

$$\log_{10} P_{Pu}(atm) = (4.924 \pm 0.120) - \frac{17420 \pm 184}{T^{o}K} . \quad (1)$$

The Pu pressure data are presented in Figure 463-10. The results of this investigation are in excellent agreement with those of previous studies [10, 11] and when the data from all the vaporization studies are combined, the heat and entropy of vaporization obtained are $\Delta H^{o}_{v\,298} = 83.0 \pm 0.5$ kcal mole^{-1} and $\Delta S^{o}_{v\,298} = 29.1 \pm 0.5$ eu. The boiling point of Pu is calculated to be 3466°K.

A manuscript detailing the results of this investigation has been submitted for publication in the Journal of High Temperature Science.

PuN:

A Knudsen effusion study has shown that, in the range 1658-1976°K, plutonium mononitride decomposes congruently to the elements according to the reaction

$$PuN_{0.98}(s) = Pu(g) + 0.49\, N_2(g) . \quad (2)$$

The Pu partial pressure data can be represented by the equation

$$\log_{10} P_{Pu}(atm) = (6.452 \pm 0.055) - \frac{21958 \pm 98}{T^{o}K} \quad (3)$$

and are presented in Figure 463-11. The vapor pressure data lead to a third law heat of formation for PuN of $\Delta H^{o}_{f\,298} = -71.0$ kcal mole^{-1}. This value is in agreement with the values derived from the combustion study of LaPage and Bunce[12] at Harwell and the EMF investigation at this Laboratory,[13] -70.2 and -72.4 kcal mole^{-1}, respectively.

The standard heat and entropy of formation for PuN are taken to be $\Delta H^{o}_{f\,298} = -71.2 \pm 2.5$ kcal mole^{-1} and $\Delta S^{o}_{f\,298} = -19.9 \pm 2.0$ eu. A manuscript detailing the results of this investigation has been submitted for publication in the Journal of High Temperature Science.

Pu-C System:

As a first step in the study of the Pu-U-C ternary system the vaporization behavior of the Pu-C binary system is being investigated as a function of the C/Pu ratio. To date a series of experiments have been performed with samples ranging in composition from Pu to PuC_2 + C. In addition to vapor pressure data, some information pertaining to the Pu-C phase diagram has been attained.

Plutonium monocarbide vaporizes to yield gaseous

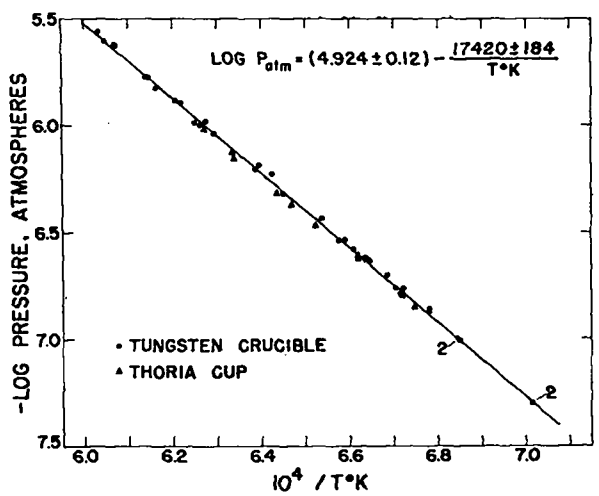

Figure 463-10. The vapor pressure Dependence of Pu(g) over Pu(ℓ) as a Function of T^{-1}.

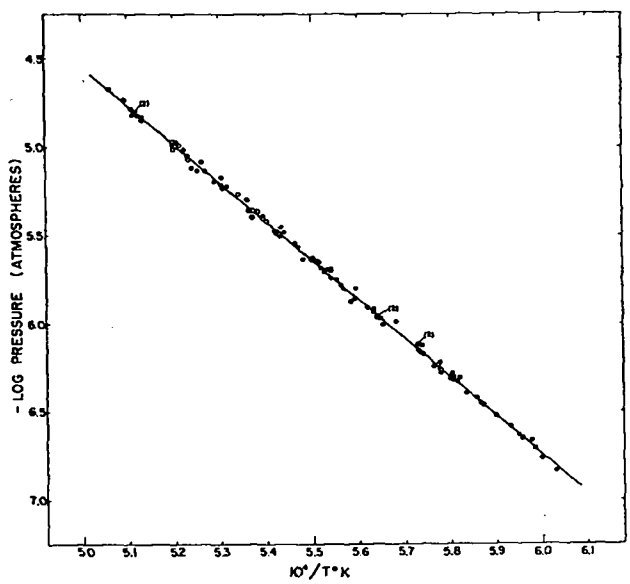

Figure 463-11. The partial pressure of Pu over PuN. as a function of T^{-1}.

Pu and solid Pu_2C_3. A series of samples having original stoichiometries ranging from $PuC_{0.85}$ to $PuC_{1.34}$ were heated in W Knudsen cells. The results indicate that the vaporization process is invarient, i.e., the Pu pressure is independent of composition so long as the condensate consists of both the mono- and sesquicarbide. The Pu vapor pressure data are in good agreement with those attained in previous studies.[14, 15] The sesquicarbide low carbon-side line in the Pu-C phase diagram curves towards the PuC composition at high temperatures, passing through the stoichiometry $PuC_{1.41}$ at approximately 1550°C.

The vapor pressure data attained for samples consisting of Pu_2C_3 + C are in poorer agreement with published data.[14] At 1669 ± 15° the sesquicarbide transforms to the dicarbide. When a sample consisting of the dicarbide plus graphite is heated both Pu and PuC_2 appear in the vapor phase. However, the sensitivity and resolution of the mass spectrometer now in use are such that quantitative data pertaining to $PuC_2(g)$ are difficult to obtain. Hopefully, this problem will be resolved when the new magnetic mass spectrometer has been delivered and installed. This instrument, which has a resolving power of $M/\Delta M = 500$ for the present unit, is scheduled to be delivered to LASL on February 1, 1969.

6. High Temperature Calorimetry
(A. E. Ogard, G. Melton)

The high temperature heat contents of UO_2, $U_{0.8}Pu_{0.2}O_{1.98}$ and $U_{0.8}Pu_{0.2}O_{2.00}$ are being determined as a part of a cooperative program with G.E.-Sunnyvale. To date the measurements have been completed up to ~ 2400°K in a drop calorimeter that was not enclosed in a glovebox. The calorimeter has been relocated in a Pu handling enclosure and a W mesh heating element incorporated as part of the furnace in order to increase the temperature limit.

Above a temperature of ~ 2400°K there are no standards for calibration of drop calorimeters. In order to determine the heat content of a material that could be used as a standard and which is also the container material used in the experiments, the apparent heat content of W is being determined as a function of temperature, container size, and weight. The results to date are shown in Table 463-II. When further data is available corrections for radiative heat loss during free fall of the crucible may be applied to give a true heat content of W.

7. Adiabatic Calorimeter
(D. G. Clifton)

The development of a small adiabatic calorimeter is being continued. The calorimeter will operate up to 1400°C and will permit energy measurements upon condensed phase samples of a cylindrical shape that are about 1.6 cm high and 1.2 cm O.D. This system will allow the measurement of heat capacities, and heats of reaction and of transformations for processes which progress at a reasonable rate in this temperature range.

The calorimeter housing with its vacuum system is mounted on a temporary work bench in the laboratory. It will ultimately be installed in a glovebox. An associated cold He flush system with a uranium-chip furnace for He purification has also been installed. The entire system has been leak tested and is now tight. The heater systems for the calorimeter have been wound and these together with the sample crucible radiation shields, control thermocouples, and temperature sensing thermocouples are presently being installed. The instrumentation is being assembled and will soon be mated to the calorimeter, at which time calibration tests will be performed using heat capacity

Table 463-II
Apparent Heat Content of Tungsten

Temp., °C	Sample	$H_T - H_{298}$, cal/g	Temp., °C	Sample	$H_T - H_{298}$, cal/g
1013	A	33.9	1963	B	71.2
1085	B	36.6	2100	B	75.5
1211	B	41.4	2114	A	77.6
1305	B	45.2	2135	A	78.6
1437	A	50.0	2165	B	79.7
1504	B	51.8	2195	B	80.4
1711	A	61.1	2330	A	86.6
1750	B	62.2	2340	B	86.6
1770	B	62.8	2620	A	101.0
1932	A	69.4			

Notes: A - 103.9 g W crucible, area = 17.1 sq cm
B - 111.8 g crucible, area = 36.1 cm²

measurements on standard materials such as synthetic sapphire.

8. Intermediate Temperature Drop Calorimeter (D.G. Clifton)

The fabrication of parts for this calorimeter which were necessary to provide a better constant temperature heating zone have been completed. This entire system is being assembled for check-out.

IV. ANALYTICAL CHEMISTRY (G.R. Waterbury, E.A. Hakilla, et. al.)

Electron microprobe examinations were made on samples of (U, Pu) C to determine homogeneity and to identify impurities.

Controlled-potential coulometric methods were applied to the determination of U and Pu in samples of (U, Pu) C with a precision (1σ) of 0.2 to 0.3 percent.

Analyses were made for U, N, O, C, Pt, and spectrographic impurities in various materials such as PuO_2, PuN, (U, Pu) C, PuC, and Na.

V. TOPICAL REPORTS AND PUBLICATIONS

1. G.M. Campbell, "Thermodynamic Properties of PuN by Galvanostatic Potential Determination," LASL Report No. LA-3945 (1968).

2. R.A. Kent and J.A. Leary, "Mass Spectrometric Studies of Plutonium Compounds at High Temperatures. I. The Heats of Vaporization of Gold and Plutonium and the Heat of Decomposition of Plutonium Mononitride," LASL Report No. LA-3902 (1968).

VI. REFERENCES

1. C.S. Griffin, K. Mendelssohn, E. King, J.A. Lee, M.H. Rand, R.S. Street, "Self-Irradiation Damage in Transuranic Elements and Compounds," in "Plutonium 1965," A.E. Kay and M.B. Waldron, pp. 189-204 (1967).

2. M.H. Rand and R.S. Street, AERE-M 973 (1962).

3. P.G. Pallmer, HW-72245 (1962).

4. E.A. Harper, H.J. Hedger, J.T. Dalton, Nature 219, pp. 151 (1968).

5. A.L. Bowman, J. Inorg. Nucl. Chem., 19, 111 (1966).

6. D.M. Chackraburtty and N.C. Jayadevan, Acta. Cryst., 18, 811 (1965).

7. J.G. Reavis, M.W. Shupe, C.W. Bjorklund, and J.A. Leary, Transactions of the American Nuclear Society, Annual Meeting, p. 111 (1967).

8. R.N.R. Mulford, F.H. Ellinger, G.S. Hendrix and E.D. Albrecht, Plutonium 1960, p. 301, Cleaver-Hume Press Limited, London (1960).

9. W.K. Behl and J.J. Egan, J. Electrochem. Soc., 113, 376 (1966).

10. T.E. Phillips, G.W. Sears, R.L. Seifert, and O.C. Simpson, U.N. Int. Conf. PUAE 7 (1956) p. 382.

11. R.N.R. Mulford, Thermodynamics, Vol. 1, IAEA, Vienna, 1965, p. 231.

12. R. Lapage and J.L. Bunce, Trans. Faraday Soc., 63, 1889 (1967).

13. G.M. Campbell, to be published in J. Phys. Chem., Feb. 1969.

14. W.M. Olson and R.N.R. Mulford, Los Alamos Scientific Laboratory Report LA-DC-8012 (1967).

15. P.S. Harris, B.A. Phillips, M.H. Rand, and M. Tetenbaum, United Kingdom Atomic Energy Authority Report AERE-R 5353 (1967).

PROJECT 464

STUDIES OF Na-BONDED (U,Pu)C AND (U,Pu)N LMFBR FUELS

Person in Charge: D. B. Hall
Principal Investigators: R. H. Perkins
G. H. Best

I. INTRODUCTION

(U,Pu)C and (U,Pu)N are regarded as attractive alternates to mixed oxides as fuels for commercial LMFBR application. The high heavy-atom densities and thermal conductivities of the mixed carbide and nitride make it possible for these fuels to outperform mixed oxides. Full exploitation of carbides and nitrides dictates the use of a gap between fuel and clad to accommodate fuel swelling (with minimal fuel-cladding mechanical interactions) and a high thermal conductivity path across the gap to limit fuel temperature. The conditions can be met by filling an annulus between fuel and clad with sodium.

Before a satisfactory sodium-bonded fuel element can be developed, however, information is required that will identify the number and severity of problems associated with sodium bonding and will suggest solutions to these problems. Problem areas that are being studied in this experimental program are:

1. The mechanisms and kinetics of carbon transfer to claddings through the sodium bond.
2. The significant fuel and sodium variables that affect compatibility.
3. The consequences of exposing fuel to coolant sodium.
4. The behavior of sodium-bonded fuel elements under irradiation.
5. The performance limitations of the sodium bond under high-heat-flux conditions.

Efforts are now concentrated on the mixed carbide fuel. Type 316 stainless steel is the base cladding material being studied, though vanadium alloys are also being tested.

As prerequisites for this compatibility program, a number of developmental efforts have been undertaken. These include establishment of (1) techniques for the production of single-phase monocarbide pellets of known composition and dimensions, (2) techniques and equipment for fuel pin loading, bonding, and inspection, and (3) techniques and equipment for determining the distribution of fission products in irradiated fuel pins.

II. SYNTHESIS AND FABRICATION OF (U,Pu)C PELLETS (M. W. Shupe, J. A. Leary, A. E. Ogard, R. W. Walker, S. McClanahan, H. G. Moore, C. Gilley)

A. General

Standardized procedures for producing single-phase monocarbide pellets of known composition and dimensions have been developed. These pellets will be utilized in EBR-II irradiation experiments and compatibility testing. Basic process steps are:

1. Multiple arc melting of a physical mixture of ^{235}U, Pu, and C on a 60-g scale using a graphite electrode.
2. Solution treatment of the arc melted ingot for 24 h at 1600°C.
3. Crushing and grinding of the ingot in a WC vibratory mill, followed by screening of the resulting powder to $\leq$ 62 μ size.
4. Blending of several powder batches.
5. Elimination of excess carbon by reaction with H_2 at 850°C.
6. Cold compaction at 20 tsi into pellets

without the use of binders and sintering aids.

7. Sintering of the pellets in Ar at 1800°C.
8. Characterization of the pellets by linear dimensioning, weighing, density (by immersion technique), metallography, x-ray powder diffraction analysis, chemical analysis including U, Pu, C, N, O, H, and spectrochemical analysis for trace impurities, electron microprobe analysis, x-ray radiography for determination of possible internal cracks, and isotopic analysis of the uranium and plutonium.

B. Current Results

A campaign has been completed wherein a total of approximately 925 carbide pellets were prepared for irradiation studies in EBR-II and for out-of-pile compatibility tests. These are being transferred to the fuel pin loading facility. Characterization of these pellets by randomized sampling techniques indicates the following:

1. No cracks and chips could be detected by x-ray radiography (all pellets were radiographed).
2. The composition of the pellets is controlled within narrow limits. The averaged results of analyses of 39 samples are shown in Table 464-I. All deviations shown are standard deviations.

Table 464-I

Chemical Composition of 39 Samples of (U,Pu)C

Element	Concentration	
	g atom/mole carbide[(a)]	w/o
U	0.796 ± 0.001	75.3 ± 0.4
Pu	0.204 ± 0.004	19.57 ± 0.18
C	0.97 ± 0.01	4.70 ± 0.06
O	0.006 ± 0.003	0.027
N	0.005 ± 0.001	0.037
H	< 0.001	

(a) ± one standard deviation.

3. Concentrations of metallic impurities are maintained at low levels. The average concentrations of impurities in 45 random samples are shown in Table 464-II.
4. All samples were single phase. The average lattice dimension from 45 samples was found to be 4.965 ± 0.001 Å.

Table 464-II

Average Spectrochemical Analysis of $(U_{0.8}Pu_{0.2})C$ Pellets

Element	ppm	Element	ppm
Li	< 1	Ni	19
Be	< 1	Cu	40
B	< 1	Zn	< 10
Na	< 2	Sr	< 5
Mg	< 5	Zr	< 100
Al	< 10	Nb	< 50
Si	94	Mo	12
P	< 50	Cd	< 10
Ca	< 5	Sn	< 2
Ti	< 50	Ba	< 10
V	< 5	Ta	< 25
Cr	< 10	W	19
Mn	3	Pb	< 2
Fe	55	Bi	< 2
Co	< 5		

Note: The "<" sign is a normal limit of detectability.

5. The average density obtained by immersion techniques on 43 samples was 89.8 ± 1.5% of theoretical (13.62 g/cm^3). Target densities were 90 ± 1% of theoretical. Of the same 43 samples, the average density obtained by dimensioning and weighing was 89.0 ± 1.5% of theoretical.
6. Single phase monocarbide microstructures were found by metallographic examination. No uncombined metal or higher carbide phases were present. The grain size was generally less than 55 μm wide. In some pellets, inclusions were found to be present to < 0.5 v/o as determined by point counting methods. Generally they contained impurity elements such as Si, Fe, Cu, or W in combination with Pu. In up to 50% of the metallographic examinations, microcracks of approximately 20 microns width were found. These microcracks appeared as short necklaces of interconnected porosity. These were below the limit of detectability by x-ray radiographic examination.

7. Examinations of chemically etched samples by electron microprobe techniques revealed that the pellets were homogeneous on a macro scale and on a grain-to-grain basis. On a micro scale some heterogeneous distribution with respect to uranium and plutonium was found within some of the selected grains. These "mottled" areas are thought to be "cored" remnants, in which the plutonium intensity generally varied 10 to 20% while the uranium intensity varied 30 to 20%. No quantitative correlation between x-ray intensities and element concentrations are available at this time. Small inclusions, a few microns in size, were found to be enriched in plutonium and depleted in uranium and carbon. In addition, they usually contained one or more impurities such as Si, Fe, Ni, Cu, or W. A typical pellet microstructure is shown in Fig. 464-1.

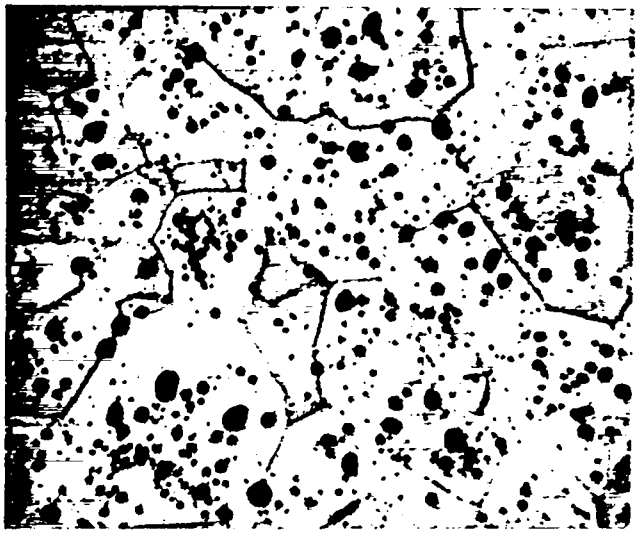

Fig. 464-1. Typical single phase $(U_{0.8}Pu_{0.2})C$. Electrolytic etch, 380X.

8. Results of heavy metal isotopic analysis of 22 samples have been averaged and are shown in Table 464-III. (These are documented individually but only averages are listed here.)

Table 464-III

Averaged Results of Isotopic Analysis for $(U_{0.8}Pu_{0.2})C$ Pellets

Mass No.	U (a/o)	Pu (a/o)
234	1.01 ± 0.2	...
235	93.08 ± 0.15	0.34 ± 0.30
236	0.36 ± 0.06	...
238	5.50 ± 0.12	0.038 ± 0.02
239	0.151	94.25 ± 0.23
240	...	5.30 ± 0.04
241	...	0.30 ± 0.002
242	...	0.016 ± 0.002

Note: The deviations shown are standard deviations.

9. The distribution of pellet diameters is shown in Fig. 464-2. Pellet diameters were obtained using profilometric techniques when the equipment was available.

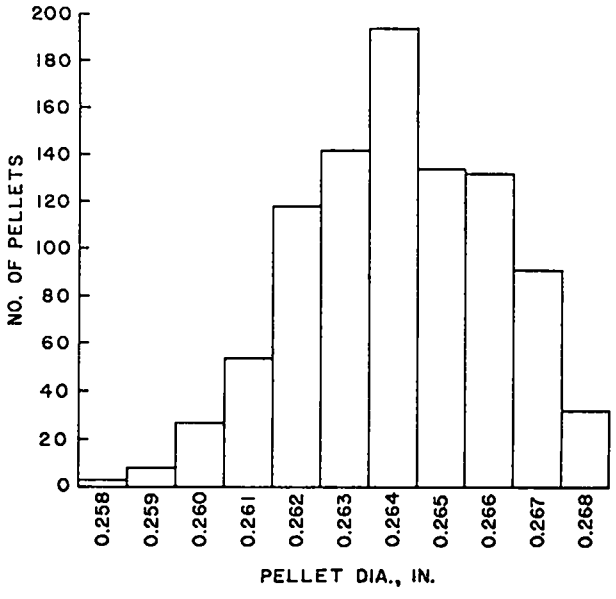

Fig. 464-2. Histogram of $(U_{0.8}Pu_{0.2})C$ pellet diameters (fully enriched uranium-plutonium carbides for EBR-II irradiation fabrication campaign No. 1).

Archive sample pellets are being stored under helium in welded steel containers.

In addition to the (U,Pu)C pellets, 104 insulator pellets of depleted UC were delivered for this project. Characterization of these pellets

indicates the following:

1. The lattice dimension taken from representative samples was 4.959 ± 0.006 Å. All samples were found to be single phase by x-ray powder diffraction analysis.
2. Chemical composition was 0.0335 ± 0.0015 w/o N, 0.0406 ± 0.0056 w/o O, 95.56 ± 0.56 w/o U, and 4.74 ± 0.01 w/o C, which corresponds to $UC_{0.983}O_{0.006}N_{0.006}$.
3. The immersion density of a typical specimen was found to be 90.9% of theoretical. The minimum density calculated from pellet dimensions was 90.4% of theoretical.
4. Average results of spectrochemical analysis of two samples are shown in Table 464-IV.

Table 464-IV

Composition of Single-Phase UC
(Average Spectrochemical Analysis)

Element	ppm	Element	ppm
Li	< 1	Co	< 5
Be	< 1	Ni	< 10
B	< 1	Cu	< 2
Na	< 2	Zn	< 10
Mg	< 5	Sr	< 5
Al	<10	Zr	< 100
Si	<20	Nb	< 50
P	<50	Mo	< 10
Ca	< 5	Cd	< 10
Ti	<50	Sn	< 2
V	< 5	Ta	<1000
Cr	<10	W	15 ± 5
Mn	< 2	Pb	< 5
Fe	<20	Bi	< 2

The "<" sign indicates lower limits of detectability.

5. Essentially single-phase UC was found metallographically in representative samples. In some samples a few inclusions, much less than 0.5 v/o, were found, but no uncombined metal or higher carbide phases were detected. A typical single-phase UC microstructure is shown in Fig. 464-3.
6. Uranium isotopic analysis is shown in Table 464-V.

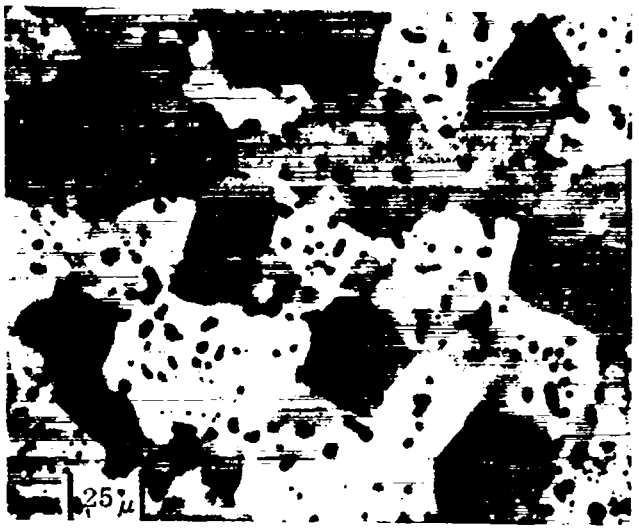

Fig. 464-3. Typical single-phase UC. Stain etched, 380X.

Table 464-V

Results of Isotopic Analysis on UC Pellets

Mass No.	Atomic Percent
233	< 0.0005
234	0.003
235	0.429
236	0.006
238	99.56

III. LOADING FACILITY FOR TEST CAPSULES
(D. N. Dunning)

A. General

A prerequisite to a compatibility program involving (U,Pu)C and sodium is a satisfactory capsule loading and bonding facility. There is little point to obtaining well-characterized materials for testing if these materials are contaminated before they are placed in test. Sodium and (U,Pu)C are sufficiently reactive that all operations must be performed either in vacuum or in a high-quality inert atmosphere. The loading facility for handling these materials has been constructed; it consists of inert-atmosphere gloveboxes equipped with inert-gas clean-up systems to provide an environment for handling fuel pellets and bonding sodium with a minimum of contamination.

B. Current Results

Final installation of the fuel loading box

and checkout of the box systems have been completed, and several capsules have been loaded using the entire facility. (Some difficulty has been experienced in maintaining the inert gas purity level in this box within the desired impurity limit of 10 ppm oxygen plus moisture.) Figure 464-4 shows the facility and the flow diagram for fuel and sodium loading. This procedure differs from previous loading schemes in that no fuels are loaded into capsules in the sodium box. The (U,Pu)C fuel pellets are brought into the loading box in an "alpha transfer can," and measurement and visual examination of the fuel pellets are accomplished in this box. The fuel pellets are then loaded into capsules by passing them through a valve in the wall of this two-compartment box. Alpha contamination is contained in the examination and measurement section of the fuel box; the other section remains free from alpha contamination. The capsules containing the fuel pellets are then transferred to the sodium box where solid sodium rod is loaded into the capsules. The closure weld is then made in the welding chamber. Helium leak testing and sodium bonding of the capsule are done external to the loading area.

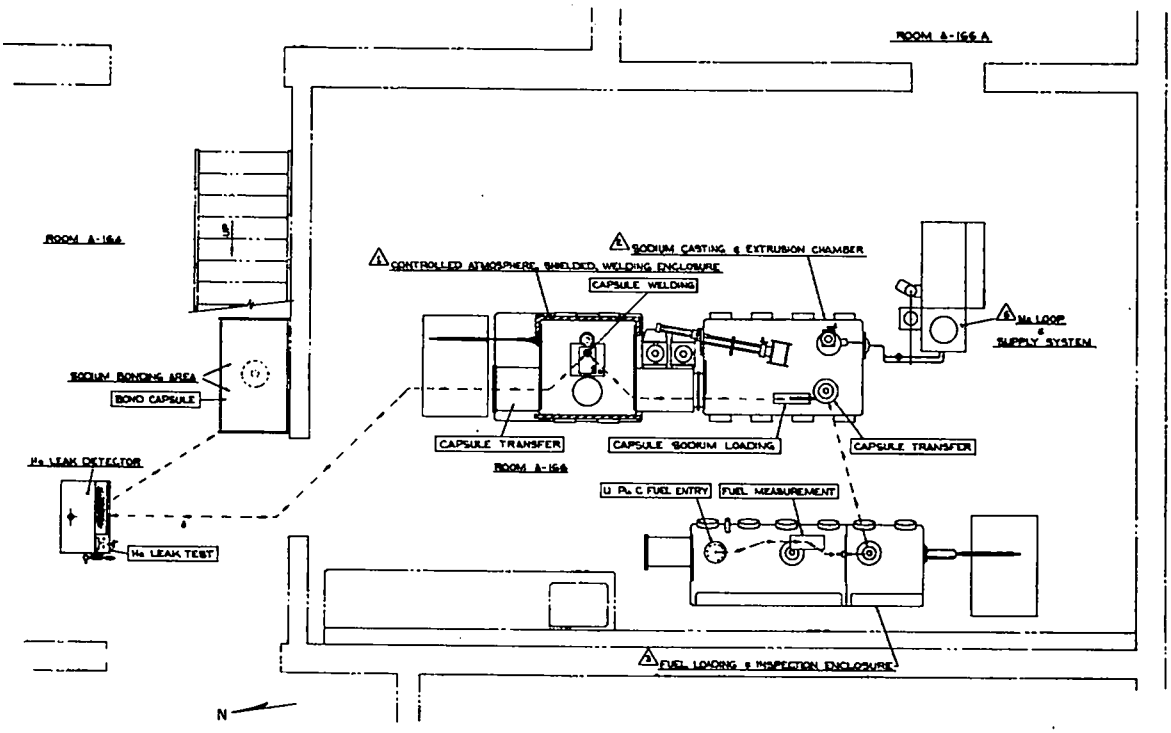

Fig. 464-4. Fuel pellet flow diagram.

IV. CARBIDE FUEL COMPATIBILITY STUDIES

(F. B. Litton, H. A. O'Brien, L. A. Geoffrion, J. H. Bender)

A. General

The objectives of this program are to study the interactions among single-phase mixed (U,Pu)C, a sodium bond, and potential cladding materials, i.e., to investigate the technology related to sodium-bonded fuel elements. There are two approaches to the experimental work. One approach is to determine the reactions occurring between $(U_{0.8}Pu_{0.2})C$ and potential cladding materials, using Type 316 stainless steel and a high-strength vanadium-base alloy as the first and second choices of

cladding material, respectively. A second concurrent set of experiments is designed to study the mechanism of carbon transport through sodium, the effect of impurities such as oxygen, and the carburizing potential of sodium in mutual contact with carbides and the preferred cladding materials.

Capsules containing sodium-bonded, single-phase (U,Pu)C are tested in sodium loops at 750°C for periods up to 10,000 h. High-purity, thoroughly-characterized sodium is used for the studies. Fuels of known composition are used in all tests. Most of the testing is performed on single-phase (U,Pu)C fuel in which the Pu/U ratio is maintained at 0.25, but some experiments are being carried out on material containing a second phase (either metallic or carbon-rich). Other experiments are being carried out on stoichiometric and hyperstoichiometric UC to determine the effect of plutonium addition on the behavior of the carbide fuel.

B. Current Results

1. Calculations Related to the Measurement of Carbon Activity in Carbide Fuels

As part of the program of determining the compatibility of sodium-bonded carbide fuel with Type 316 stainless steel and high strength vanadium alloys, information is needed on the activity of carbon in the fuel. One possible technique for measuring the activity of carbon in off-specification fuel is by reducing the fuel with hydrogen, and comparing the amount of methane produced with that in equilibrium with $Cr_{23}C_6$ at the proposed operating temperature. (The activity of carbon in $Cr_{23}C_6$ as a function of temperature is known.) The hydrogen-carbon reaction was selected in preference to the sodium-carbon reaction because the thermodynamics of the latter reaction are relatively unknown.

A series of thermodynamic calculations to evaluate the feasibility of this experimental technique was completed. The calculations were based on the standard free energy of formation of the carbide fuel and that of CH_4 in the temperature range 400-700°C. By application of Hess' law and the equation

$$\Delta G^\circ = - RT \ln K_{eq}$$

where $K_{eq} = P_{CH_4}/P_{H_2}^2$, the following reactions were investigated.

(a) $$UC_2 + 2H_2 \rightarrow UC + CH_4$$

(b) $$\tfrac{1}{2}UC_2 + 2H_2 \rightarrow \tfrac{1}{2}U + CH_4$$

(c) $$\tfrac{1}{3}Pu_2C_3 + 2H_2 \rightarrow \tfrac{2}{3}Pu + CH_4$$

(d) $$\tfrac{1}{3}U_2C_3 + 2H_2 \rightarrow \tfrac{2}{3}U + CH_4$$

(e) $$\tfrac{1}{3}(U_{0.8}Pu_{0.2})_2C_3 + 2H_2 \rightarrow \tfrac{2}{3}(U_{0.8}Pu_{0.2}) + CH_4$$

(f) $$yPuC_{0.87} + 2H_2 \rightarrow yPu + CH_4 \quad (y = 1.149)$$

and

(g) $$UC + 2H_2 \rightarrow U + CH_4$$

The results indicated that the pressure of methane would be too small to be detected in all cases except reaction (a), and that an experimental program is not warranted.

2. Calculated Fuel Compatibility with Chromium, Vanadium, and Iron

These calculations were performed to obtain an indication of the relative thermodynamic compatibilities of fuel carbides with chromium, vanadium, and iron. Previously reported standard free energies of formation equations were used to compute the equilibrium constant for the decomposition of the fuel carbide and the transfer of one mole of carbon to either chromium, vanadium, or iron. The temperature range considered was 400-750°C. The method of calculation used here was similar to that described in the previous section, except that the equilibrium constant was here defined as the ratio of the product of the activities of the reaction products to that of the reactants.

The following trends were indicated from the results:

1. In all cases, the heavy metal carbide is more stable in contact with vanadium than with chromium. Thus it appears that, if carbon were transferred to a vanadium-chromium alloy cladding, the carbon would react preferentially with the chromium.
2. Uranium sesquicarbide, uranium monocarbide and uranium-plutonium sesquicarbide appear to be compatible with vanadium.
3. Uranium dicarbide is more likely to decompose to uranium monocarbide plus carbon

rather than to uranium metal plus carbon.

4. It appears unlikely that carbon would be transferred from fuel carbides to iron.

Although these calculations yield the value of the thermodynamic equilibrium constant, they give no information about the reaction kinetics, i.e., whether or not the reaction, as written, will take place within a finite period of time.

3. Vanadium Alloy Compatibility

Compatibility tests were performed on V-15Ti-7.5Cr alloy capsules containing three sodium-bonded (U,Pu)C pellets. The tests consisted of heating two capsules at 650° and three capsules at 750°C in hot-trapped sodium loops for 1000-h periods. Metallographic examination of the test capsules showed that reaction had occurred between the fuel and clad in one of the capsules heated at 750°C. A reaction product was not observed at the contact surface on the other capsules. A diffusion zone approximately 50 μm thick was observed on the outer surface of all the capsules in contact with loop sodium.

Chemical analysis of the fuel pellet in contact with the reaction zone indicated that the fuel was hypostoichiometric prior to test. Its free metal content apparently was responsible for the observed reaction product. The pellet analyzed 77.1% U, 18.4% Pu, 4.61% C, 0.08% O, and 180 ppm N, corresponding to an interstitial to metal ratio of 0.963. The desired composition for single-phase carbide fuel is an interstitial to metal atom ratio of 0.97 with maximum oxygen and nitrogen contents of 250 and 350 ppm, respectively.

Electron microprobe analyses confirmed the presence of uranium and plutonium throughout the attack area and to an appreciable depth (~ 0.007 in.) in the capsule wall. A higher concentration of plutonium than uranium was observed in the reaction product and along the grain boundaries. The uniform zone on the outside of the capsule wall was attributed to the diffusion of interstitials, particularly oxygen and carbon, from the sodium in the loop. The extent of carbon diffusion was about 10 μm. Precipitates of titanium carbide were detected in this layer.

4. Behavior of Vanadium Alloys in Hot-Trapped Sodium

Vanadium alloys have been proposed as a backup cladding material for Type 316 stainless steel for the liquid-metal fast breeder reactor. The information being developed in this experimental work will aid in the screening of vanadium alloys for this application.

Information obtained from free energy calculations was used to determine the most suitable alloying elements to form vanadium alloys that are stable in oxygen-bearing sodium. Studies of vanadium-titanium binary alloys in zirconium-gettered sodium have shown that these alloys absorb oxygen, carbon, and, most probably, nitrogen. Although tensile properties have not been investigated after corrosion testing, it is likely that absorption of interstitials will increase the yield strength, decrease the ductility, and adversely affect the corrosion resistance.

The variation in free energy of formation as a function of temperature for the reaction

$$2Na + \frac{1}{2}O_2 = Na_2O$$

was calculated from the relation

$$\Delta F_T' = \Delta F_T^\circ + RT \ln a[Na_2O]$$

where

$$RT \ln a[Na_2O] = 4.575\ T \log_{10} [\text{assumed oxygen concentration}] - 4.575\ T \log_{10} [\text{oxygen concentration at saturation}].$$

This treatment was reported by Evans and Thorley[1] assuming unit activity of oxygen at saturation. The solubility of oxygen in sodium is expressed by Rutkauskas[2] as

$$\log_{10}[\text{wt \% oxygen}] = 4.25 - 3499/T.$$

The standard free energy for the reaction

$$2Na + \frac{1}{2}O_2 = Na_2O$$

is reported by Wicks and Block[3] to obey the relation

$$\Delta F_T^\circ = -99{,}300 + 6.02\ T \ln T - 7.02 \times 10^{-3}T^2 + 0.85 \times 10^{-6}T^3 - 0.10 \times 10^{5}T^{-1} - 1.61T.$$

Substitution of these equations in the expression for $\Delta F_T'$ allows this term to be calculated. Values of $\Delta F_T'$ become more negative with decreasing oxygen activity. In a similar manner, the standard free energy for the reaction

$$V + \frac{1}{2}O_2 = VO$$

may be calculated from the relation[3]

$$\Delta F_T^\circ = -99{,}100 - 2.34\ T\ \ell nT - 0.36 \times 10^{-3}T^2 + 0.53 \times 10^{5}T^{-1} + 38.64T.$$

At 10 ppm oxygen, $\Delta F_T'$ for Na_2O is approximately equal to ΔF_T° for VO at 450°C (-82.9 kcal for the reaction involving vanadium and -83.1 kcal for the sodium reaction). At this temperature conditions indicate that vanadium is stable in sodium containing less than 10 ppm oxygen.

As shown in Fig. 464-5, the free energy curves

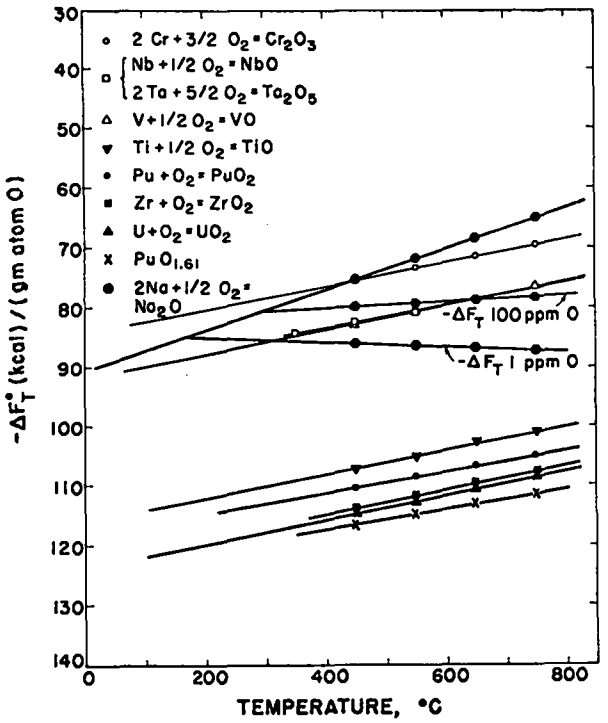

Fig. 464-5. Comparison of the free energies of formation of Na, V, C, Nb, Ti, Zr, Pu, and U oxides as functions of temperature.

for the formation of tantalum[3] and niobium[4] oxides overlap the curve for vanadium oxide. The curves for zirconium,[3] titanium,[3] uranium,[3] and plutonium[5] oxides are more negative (~ 30 kcal) than for sodium containing 1 ppm oxygen. These calculations indicate that the binary vanadium-chromium alloys probably are stable in cold-trapped sodium, and that refractory metal additions should be kept to a low level. A vanadium alloy containing 16% Cr and 2% Zr that is under development in Germany[6] may be satisfactory for use in cold-trapped sodium.

The weight changes that have been obtained for V, V-10Ti, V-20Ti, V-40Ti, and V-15Ti-7.5Cr alloys in hot-trapped sodium are shown in Fig. 464-6 as a

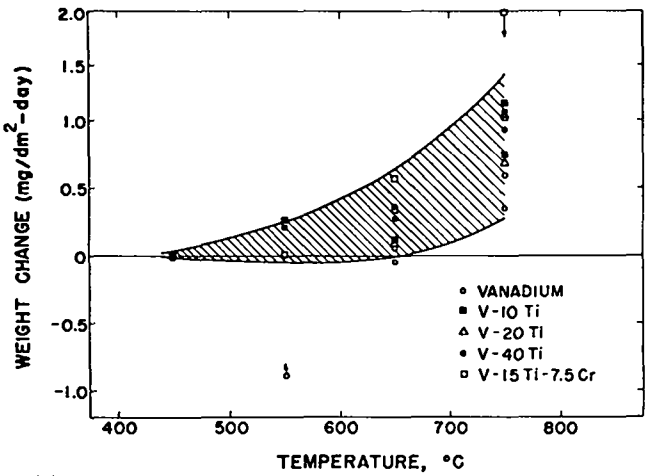

Fig. 464-6. Weight change of vanadium alloys in hot-trapped sodium as a function of temperature.

function of temperature. The curve includes data from 500, 1000, and 4000 h tests. In general, weight losses were observed in tests of short duration at low temperature, while weight gains were observed in tests of long duration at higher temperatures.

V. EBR-II IRRADIATION TESTING
(J. O. Barner)

A. General

The purpose of these irradiations is to evaluate candidate fuel/sodium/clad systems for the LMFBR program. In the reference design, pellets of single-phase (U,Pu)C are separated by a sodium bond from a cladding of Type 316 stainless steel or other high-temperature alloy. Seven fuel-element tests are planned in the initial group of a continuing series of EBR-II irradiation experiments.

The capsules are to be irradiated under the following conditions:

1. Lineal power: 29.15 to 30.20 kW/ft (max).
2. Fuel composition: $(U_{0.8}Pu_{0.2})C$ (single-phase, sintered, fully enriched).
3. Fuel density: 90% of theoretical.
4. Smear density: 80%.
5. Clad size: 0.300 in. o.d. x 0.010 in. wall.
6. Fuel size: 0.265 in. diam x 0.25 in. high.
7. Clad type: 316 SS.

8. Maximum clad temperature: 1250°F.
9. Maximum fuel centerline temperature: 2130°F.
10. Burnup: 0.22 to 0.66 g fissioned per cm^3.

B. Current Results

LASL-42B has operated in the EBR-II reactor at ~ 29.5 kW/ft to a maximum burnup of ~ 1.4 a/o. The capsule is currently out of the reactor because other experiments in the subassembly were scheduled to be terminated. After nondestructive examination, LASL-42B is scheduled to be reinserted for an additional burnup of 2.5 to 3.5 a/o.

The remaining six EBR-II capsules in this series are being loaded.

VI. GAMMA SCANNING AND RELATED STUDIES
(D. M. Holm, W. M. Sanders, B. M. Moore, B. K. Barnes)

A. General

Gamma scanning is a nondestructive technique for obtaining information on the distribution of fission products and activation products in fuel elements. A new advanced semiconductor detector system has been constructed for this purpose. ^3He activation has also been studied as a method of determining the concentration and distribution of impurities in materials.

B. Current Results

1. Computer Code Development

Many of the fuel elements being examined have had a large number of spectra taken for detailed analysis. However, for well-behaved fuel elements, it is not necessary to perform such a sophisticated analysis to determine whether gross mass transfer of fission products or activation products has occurred.

In order to minimize the time required for data analysis, a new code has been written that simulates multiscaler analysis (from the spectral data recorded on magnetic tape). Energy windows are set by the computer instead of using a single-channel pulse height analyzer. Since isotopic effects are being studied, only the counts in certain peaks are of real interest. Therefore, the operator selects the peaks of interest and specifies the channels occupied by these peaks. A working magnetic tape is written by the IBM 7094 in which only the channels with peaks of interest are listed. The new code enables the operator to integrate the counts in the peaks and to plot their area (including background) as a function of position.

This code is not as accurate as multispectral analysis by unfolding complex spectra, but it is faster, and can therefore be used to determine when more complex analysis is needed.

2. Semiconductor Detector System

One of the important problems in the maintenance of Ge(Li) gamma-ray spectrometers is keeping the detector at dry ice temperature or below. Since the vacuum is maintained in the Dewars by cryogenic pumping with a molecular sieve, even slight warming will cause the insulating vacuum to be lost. A loss of this vacuum causes a rapid and generally catastrophic warming of the detector. Although it is sometimes possible to revive the detector, there is no guarantee that this can be accomplished. Tests were conducted to determine the usefulness of a vapor pressure thermometer as a disaster alarm on the Ge(Li) detector Dewars. In the temperature range of interest (75 to 85°K), the vapor pressure thermometer can be used to measure temperatures to a fraction of a degree without the problems of electromechanical devices.

A vapor pressure thermometer was constructed as shown schematically in Fig. 464-7. Oxygen was

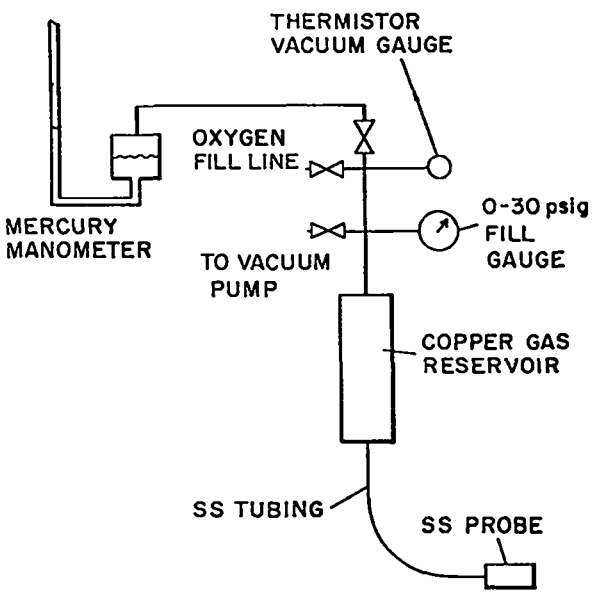

Fig. 464-7. Schematic of vapor pressure thermometer.

chosen as the fill gas for three reasons:

1. It does not freeze in the temperature region of interest.
2. Its operating pressures are small and easily measured with a simple mercury manometer.
3. The normal pressure is not atmospheric, so the device can be made fail safe.

Some tests have been made using the probe shown in Fig. 464-7. Figure 464-8 shows the vapor

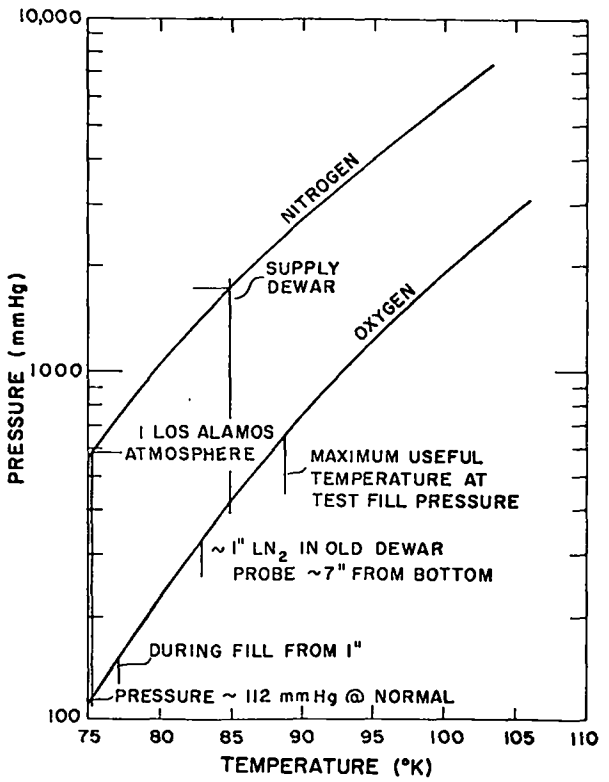

Fig. 464-8. Vapor pressures for Dewar disaster alarm.

pressure versus temperature curves for nitrogen and oxygen. The probe was placed in a detector Dewar at a position approximately 7 in. above the bottom of the liquid nitrogen container. As the liquid nitrogen level decreased from ~ 7 in. to ~ 1 in., the pressure in the manometer increased from ~ 112 to ~ 325 mm Hg. This indicates a temperature increase in the boil-off gas of about 8°K for these conditions.

The effects of filling with pressurized liquid nitrogen and the possible contamination of the oxygen in the thermometer remain to be determined.

3. ^{3}He Activation

^{3}He activation analysis is being used as a very sensitive analytical method for investigating the surface contamination of materials. Data obtained from the activation of four germanium crystals by 10.0-MeV ^{3}He and two germanium crystals by 6.5-MeV ^{3}He were analyzed.

The samples activated at 10.0 MeV were found to have too much interference probably due to radioactive isotopes from the interactions of the ^{3}He with germanium for accurate analysis of the surface oxygen. A spectrum (4 π NaI detector) of a sample bombarded at 10.0 MeV is shown in Fig. 464-9. The

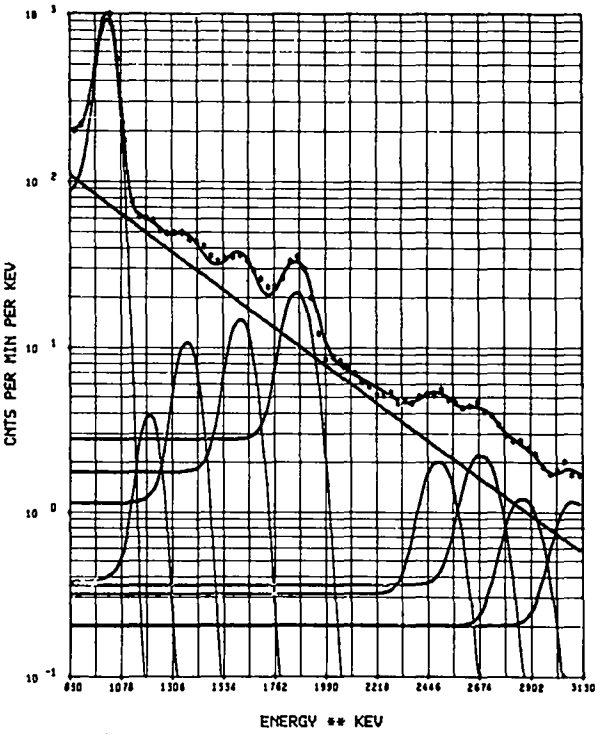

Fig. 464-9. Gamma-ray spectrum from germanium bombarded by 10.0-MeV ^{3}He.

interfering reactions were reduced by nearly an order of magnitude for the samples bombarded at 6.5 MeV. A spectrum (4 π NaI detector) of a sample bombarded at 6.5 MeV is shown in Fig. 464-10. This reduced interference allowed a determination to be made of the oxygen in the two samples bombarded at 6.5 MeV. The peak at 1.022 MeV is the peak of

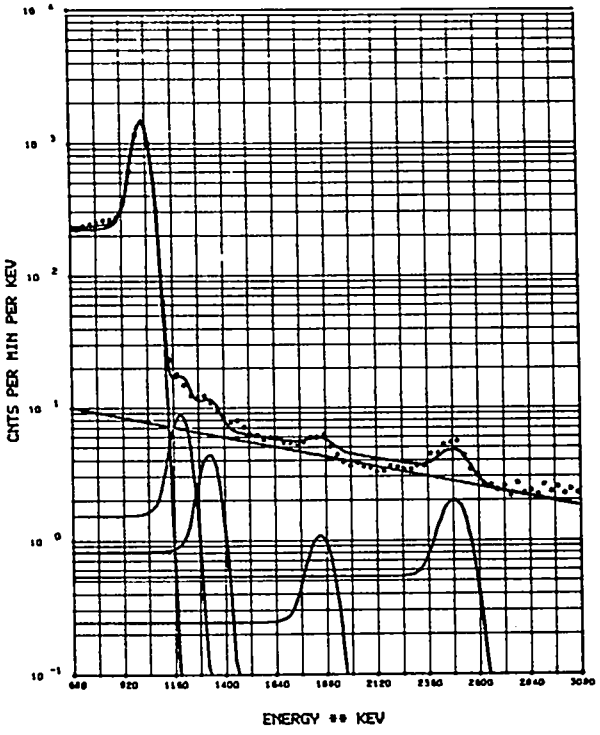

Fig. 464-10. Gamma-ray spectrum from germanium bombarded by 6.5-MeV ^{3}He.

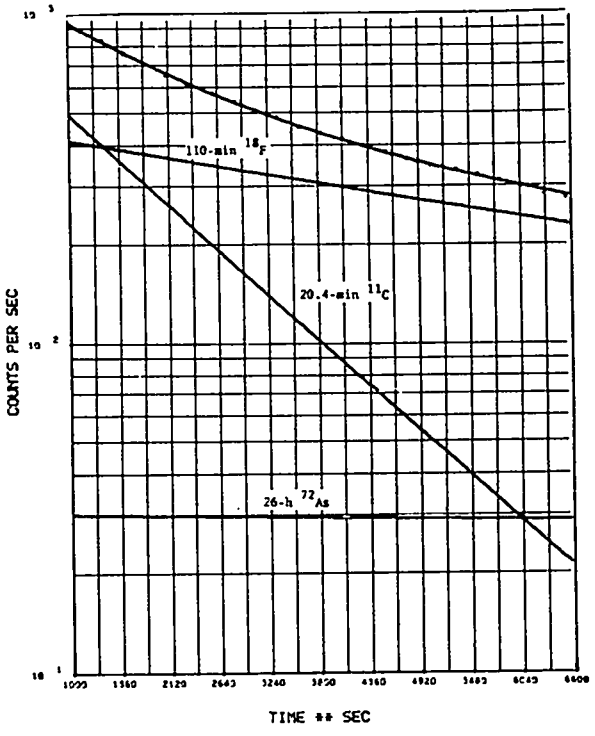

Fig. 464-11. Decay curve for 1.022-MeV positron annihilation peak.

interest for determining oxygen content. The other peaks are probably from germanium activation products, but the isotopes have not yet been positively identified. Figure 464-11 shows an exponential decay fit to the counts under the 1.022-MeV positron annihilation peaks for one of these samples as a function of time. Each point represents the area under the 1.022-MeV peak from a fit to the data.

The following conclusions about the oxygen content of the two samples may be drawn from the tests:

First sample

2.5 ± 0.5 μg/cm^2 if all oxygen is surface oxygen

$1.6 \times 10^3 \pm 0.3 \times 10^3$ ppm oxygen if all oxygen is "volume" oxygen

Second sample

3.1 ± 0.6 μg/cm^2 if all oxygen is surface oxygen

$2.0 \times 10^3 \pm 0.4 \times 10^3$ ppm oxygen if all oxygen is "volume" oxygen

The amount of oxygen present is such that a significant portion of it must be present as a surface layer. Experiments are now in progress to differentiate between the surface oxygen and that present in the body of the germanium crystal.

Work has also been done on the design and construction of a heated target holder to allow the germanium crystal to be heated *in situ* to clean the surface as much as possible prior to bombarding.

VII. SODIUM-BOND HEAT TRANSFER STUDIES
(J. O. Barner, K. Meier)

A. General

The purpose of this project is to evaluate methods for determining the effects of fuel-pin defects on heat transfer properties of the sodium bond. Such defects could arise in a number of ways. For example, a void in the sodium bond could: (1) be present before insertion in the reactor, (2) come from dewetting of the pellet due to change in composition as fission products are formed, (3) form from a hot spot on the pellet and consequent local

vaporization of the sodium, and/or (4) be produced from desorbed or fission-product gases. Of these, probably the most serious defect would be the presence of fission gas bubbles in the bond region.

There appear to be three methods of obtaining the high heat fluxes necessary for "defect analysis": (1) in-pile experiments, (2) out-of-pile experiments utilizing a central, high-heat-flux heater, (3) out-of-pile experiments utilizing an induction heat source with the heat flow direction reversed. These three methods are all receiving consideration for use in sodium-bond heat transfer studies.

B. Current Results

Design, construction, and testing of portions of the apparatus for out-of-pile testing of sodium bonds utilizing a central, high-heat-flux heater are underway. The graphite rod heater was tested at a heat flux of 1.5×10^6 Btu/h-ft^2 at the heater surface. This will produce a heat flux of 1.0×10^6 Btu/h-ft^2 at the cladding tube surface. The heater functioned satisfactorily throughout a 35-min test. Further testing will be done when the UC cylinder, sodium bond, and cladding tube are placed around the heater. This will be a more stringent test, because heater temperatures will increase about 400°F.

The UC cylinder was pressed and eloxed to size. It was fabricated in three sections, each about 1-1/2 in. long. Inspection showed that the finished dimensions meet specifications.

Design and drafting work was completed on the bubble injection apparatus. It consists of a micrometer syringe which injects bubbles of helium gas into the sodium bond through a 0.008 in. o.d. tube. After a bubble is injected, an electromagnet will pull the tube away from the bubble to prevent any unwanted constraints on the bubble. Fabrication of the bubble injection apparatus is 75% complete.

A glass tube mockup of the cladding was built. The UC cylinder, heater, and sodium bond fit inside the glass tube. The mockup will be operated at 100°C and will allow visual testing and calibration of the bubble injection apparatus. The mockup will also give data on the behavior of bubbles in a sodium annulus at 100°C.

Design was completed and drafting has begun on the transition section of the experiment. This portion is at the top of the heater and makes the transition from the sodium to the atmosphere. Stainless steel bellows are being used to seal the sodium bond annulus and the heater to allow for thermal expansion.

Design has started on the rotating section. This section supports and rotates the 40 thermocouples that measure the cladding temperatures. Intercomparison of these temperatures will identify the presence of bubbles in the sodium bond.

VIII. ANALYTICAL CHEMISTRY

A. General

Specific analytical techniques have been dedeloped and evaluated to cope with the problems encountered in the investigation of fuel/clad compatibility. The results of many of these special analyses are given in several sections of the report in Project 464. A brief summary of some of the techniques, and the problems to which they were applied, is given below.

B. Current Results

1. Electron Microprobe Examination
(E. A. Hakkila, H. L. Barker)

Variations in uranium and iron concentrations were determined through a U-Fe diffusion couple. Diffusion of iron into the uranium to a depth of approximately 550 microns had occurred preferentially along grain boundaries, but uranium had not diffused into the iron.

The following reaction products were identified in four samples of Type 316 stainless steel that had been exposed to (U,Pu)C and molten Na: (1) a white layer on the inner surface containing more Fe, Ni, and C, but less Mo and Cr than the matrix, (2) a brown layer containing less Fe, Cr, Ni, and Mo, but more C than the matrix, (3) narrow bands containing more Mo and C, but less Fe, Cr, and Ni than the matrix, and (4) a layer less than 5 μ wide on the outer surface that contained more Ni and C, but less Mo and Cr than the matrix. In the matrices of two samples, Fe, Cr, Ni, and Mo were heterogeneously distributed.

The surfaces of four (U,Pu)C specimens that had been tested in a sodium-bonded stainless steel

capsule contained slightly less uranium and more plutonium than the interiors of the samples. Grain boundary precipitates were composed predominantly of Si, W, and Pu. Small variations in uranium and plutonium concentrations in a few individual grains were observed.

The following reaction products were identified in five V, V-Ti, V-Ti-Cr, and Nb-W alloys exposed to molten Na: (1) precipitates that contained less V but more Ti than the V-Ti alloy, (2) a gray layer about 50-μ thick on the surface of the V-Ti-Cr alloy that contained more V and Cr, but less Ti than the matrix, and (3) carbides to depths of approximately 5 microns from the inner surfaces. Significant amounts of Cr had diffused from an unknown source into the V-Ti alloys. The W, Nb, and C in the Nb-W alloy were uniformly distributed.

2. Miscellaneous Support
(W. W. Wilson, N. L. Koski, L. E. Thorn, and G. R. Waterbury)

Controlled-potential coulometric and combustion gravjmetric methods were applied to measurement of U, Pu, and C in two pre-test (U,Pu)C samples and to one sample that had been held for 1000 h at 750°C in sodium in a V-Ti-Cr capsule. The coulometric methods for measuring U and Pu had a relative standard deviation of 0.2 to 0.3%, and the combustion gravimetric method for determining carbon had a precision (1 σ) of 0.5 relative percent. The methods performed satisfactorily.

Spectrophotometric methods were applied to measurement of tantalum in two pre-test (U,Pu)C samples, and to nitrogen in one (U,Pu)C pellet heated to 750°C for 1000 h in a V-Ti-Cr capsule. The relative standard deviation was 3% for measuring the nitrogen in the ppm concentration range. The tantalum concentrations were less than the lower limit of measurement, 25 ppm.

An inert-gas-fusion method, having a relative standard deviation of 10%, was applied without difficulties to the measurement of O_2 in 3 Nb-Zr alloys, 3 Nb-W alloys, 15 V-Ti alloys, 1 V-Ti-Cr alloy, 1 V metal, and 1 (U,Pu)C pellet. The samples had undergone testing in molten sodium at 450 to 750°C for 1000 to 4000 h. The O_2 concentrations ranged between 40 ppm and 0.18%.

Analyses for Zr, W, C, and N were made on corrosion test tabs of stainless steel, Nb-Zr, Nb-W, and Nb-Ti alloys. In addition, C was determined in samples of Na metal. Previously developed methods were used in all of this work.

Spectrographic analyses were made on samples of metallic Na, (U,Pu)C, PuO_2, Nb-W, and Nb-Zr alloys.

IX. REFERENCES

1. J. W. Evans and A. Thorley, "Corrosion of Niobium and Vanadium in Liquid Sodium," IGR-TN/C-1019, UKAEA, 1958.

2. V. J. Rutkauskas, "Determination of the Solubility of Oxygen in Sodium by Vacuum Distillation," Los Alamos Scientific Laboratory, Report LA-3879, Sept. 1968.

3. C. E. Wicks and F. E. Block, "Thermodynamic Properties of 65 Elements - Their Oxides, Halides, Carbides, and Nitrides," Bul. 605, U. S. Bur. of Mines, 1963.

4. H. L. Schick, Ed., "Thermodynamics of Certain Refractory Compounds, Vol. II," Academic Press, New York, 1966.

5. B. J. Seddon, "Physical Properties of Some Plutonium Compounds: A Data Manual," UKAEA, TRG-Report-1601, 1968.

6. Hans Ulrich Borgstedt, "Corrosion of V-Alloys in Liquid Na Up to 600°C," Institut fuer Material-und Festkoerperforschung. Translated by Elmar K. Wilip.

PROJECT 465

REACTOR PHYSICS

Person in Charge: D. B. Hall
Principal Investigator: G. H. Best

I. INTRODUCTION

Basic to the evaluation of various fast breeder concepts and proposals are the analytical techniques and physical data used in the analyses. Valid comparisons between different concepts and proposals depend on minimization of differences in results due to methods of analysis. To this end, the Los Alamos Scientific Laboratory is cooperating with other AEC laboratories and contractors in the development of evaluated cross-section data and associated processing codes. In addition, the Laboratory is working on the development and maintenance of digital computer programs pertinent to the nuclear analysis of fast breeder concepts. Finally, the Laboratory is evaluating the performance characteristics of various fast breeder reactor concepts.

II. CROSS-SECTION PROCUREMENT, EVALUATION AND TESTING (M. E. Battat, R. J. LaBauve, A. C. Niethammer)

A. General

Accurate predictions of reactor design parameters, such as critical mass, sodium worth, and spectral response, require the development and maintenance of up-to-date basic microscopic nuclear data files. To meet this need, a national cooperative program is in progress to prepare an evaluated nuclear data file (ENDF/B). The large amount of experimental data which are becoming available, together with the theoretical data, makes the maintenance of ENDF/B a continuing task. In addition, a large effort is needed in evaluating and testing the microscopic data prior to use in reactor calculations.

B. Data Testing

Forty-four materials from the current ENDF/B Data Tapes (released July 1968) were processed through all necessary codes and were merged into a single Library Data Tape #9 for MC^2.

This tape contains most of the materials for which data now exist in the ENDF/B format. Data for zirconium and U235R were not received on the a above data tapes but were received from Brookhaven on a special tape at a later date. The U235R differs from the ^{235}U in that it contains unresolved resonance data from Argonne National Laboratory.

Pointwise nuclear data for gallium obtained from the United Kingdom (UK) library[1] are being translated into the ENDF/B format. Files 1, 3, and 4 have been completed to date; work on File 5 is in progress.

Calculations of bare and reflected spherical experiments[2,3] have been completed at the Livermore Radiation Laboratory (LRL). These calculations differ mainly from those reported earlier in that the isotopic contents of oralloy and plutonium have been carefully reconstructed. Calculations were made using the current LRL evaluated library, and good agreement with experiment was obtained for the bare plutonium (JEZEBEL), oralloy (GODIVA) and ^{233}U assemblies.

For comparison purposes, calculations for these bare assemblies using the ENDF/B data were undertaken at LASL. Results for the JEZEBEL assembly are given in Table 465-I, and results for the other two assemblies are given in Table 465-II. Calculations were made using both the isotopic contents inferred from the information given in Ref. 2 and those supplied by LRL. Because the ENDF/B library does not contain gallium, calculations using

TABLE 465-I

PU-239 CRITICAL ASSEMBLY. SPHERICAL GEOMETRY. MONTE CARLO CALCULATIONS PERFORMED AT LRL. DTF-IV CALCULATIONS USED S-16 OPTION AND 1.0E-7 CONVERGENCE.

--CROSS SECTION SET--	----CODE----	-SPECIFICATIONS-	-CORE RAD (CM)	--K-EFF--
LRL	MONTE CARLO	LRL	6.2843	1.003
ENDF/B	DTF-IV	LRL(W/O GA)	6.2843	1.0037
ENDF/B	DTF-IV	LRL(W/O GA)	6.2575	1.0000
ENDF/B	DTF-IV	N S AND E	6.2296	1.0000
HANSEN-ROACH	DTF-IV	N S AND E	6.3023	1.0000
HANSEN-ROACH	DTF-IV	N S AND E PLUS GA	6.3023	1.0035
HANSEN-ROACH	DTF-IV	N S AND E PLUS GA	6.2763	1.0000

NOTE ATOM DENSITIES (1.0E+24 UNITS) SPECIFIED WERE---

	--PU-239--	--PU-240--	--PU-241--	--GALLIUM--
LRL	.037281	.001927	.000122	.001353
N S AND E (REF. 2)	.037684	.001776	--	--

Hansen-Roach cross sections were made to obtain the effect of gallium addition on criticality. Using the LRL specifications, the data shown in Table 465-I yield a k_{eff} = 1.0072 (= 1.0037 + 0.0035) using the ENDF/B data.

C. Processing Codes

A comparison of the Brookhaven National Laboratory (BNL) version of the MC^2 code with the Westinghouse (WAPD) version currently in use at LASL revealed that the BNL version was incorrectly computing the smooth slowly varying contribution to cross sections in the resonance region. The error was remedied by substituting the WAPD version of the subroutine SIGAVC for the BNL version in the BNL code. These findings were communicated to BNL and Atomics International, which is currently using the BNL version of MC^2. Also, the dimensions of our WAPD version have been increased so that the MC^2 "ultra-fine treatment" can be used for materials as beryllium.

The GLEN code, originally written as a thermal-group collapsing code, has been modified to accept

TABLE 465-II

ORALLOY AND U-233 BARE ASSEMBLIES. SPHERICAL GEOMETRY. ATOM DENSITIES SUPPLIED BY LRL. MONTE CARLO CALCULATIONS PERFORMED AT LRL. DTF-IV CALCULATIONS USED S-16 OPTION AND 1.0E-7 CONVERGENCE.

ASSEMBLY--	--CROSS SECTION SET--	---CODE---	--CORE RAD (CM)--	---K-EFF---
ORALLOY	LRL	MONTE CARLO	8.7100	1.005
ORALLOY	ENDF/B	DTF-IV	8.7100	1.0128
ORALLOY	ENDF/B	DTF-IV	8.5754	1.0000
U-233	LRL	MONTE CARLO	5.9647	1.002
U-233	ENDF/B	DTF-IV	5.9647	1.0304

**NOTE - ATOM DENSITIES (1.0E+24 UNITS) SPECIFIED WERE - - -

	--U-233---	--U-234---	--U-235---	--U-236---	--U-238---
ORALLOY	--	0.000482	0.045069	0.000191	0.002227
U-233	0.046745	0.000588	0.000014	--	0.000279

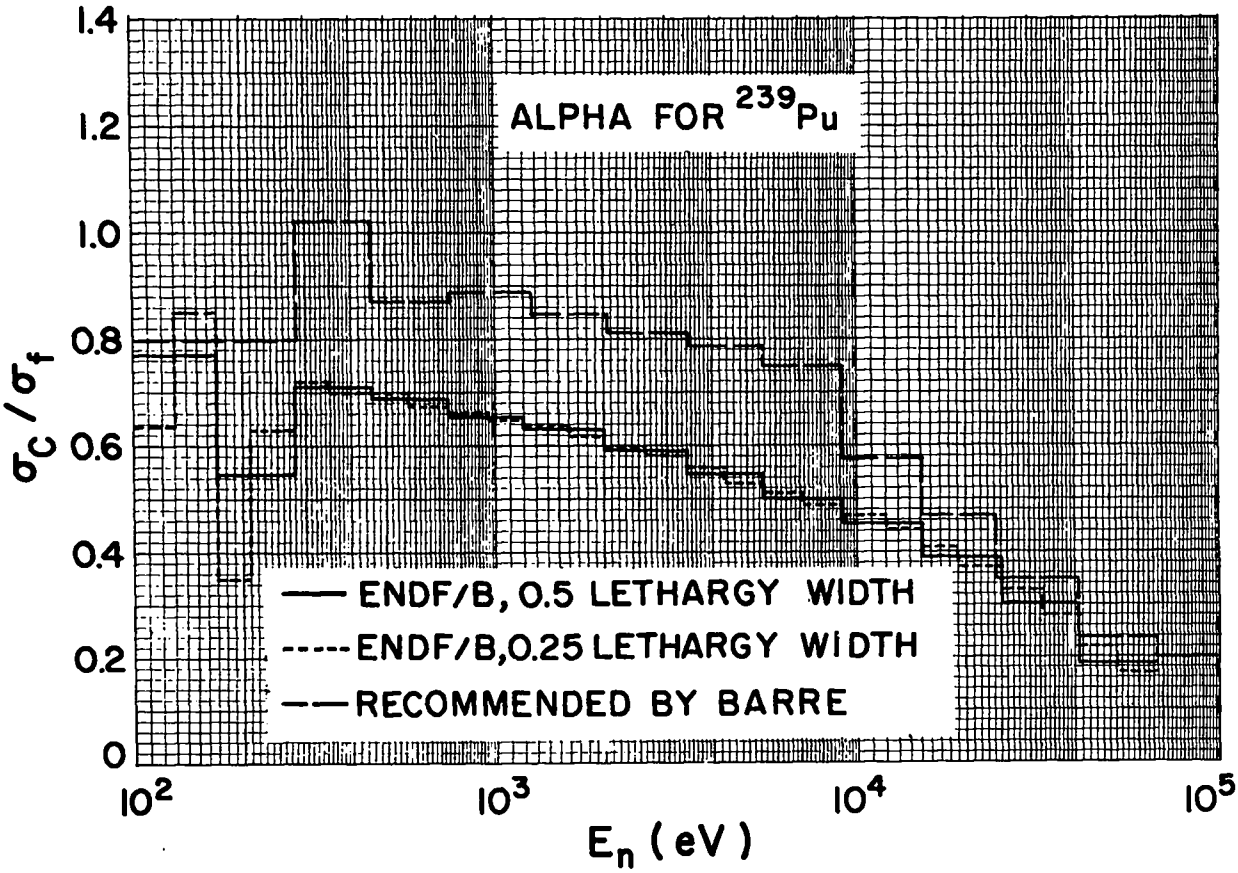

Fig. 465-1. Alpha for ^{239}Pu.

the output of FLANGE2, a thermal code used for processing ENDF/B moderator data. Also, MC^2 has been modified to supply the absorber data needed by GLEN. Thus, in principle, codes are now linked so that multigroup cross sections can be obtained from ENDF/B data for energies from thermal (about 0.001 eV) to 10 MeV. Thermal data in the ENDF/B format are presently available for H_2O, D_2O, beryllium, graphite, polyethylene, and ZrH. The FLANGE2 data for graphite is being compared with that from TOR, a code written as a companion to GLEN.

D. ^{239}Pu Alpha in the 100 eV to 10 keV Range

Recent experiments have indicated that the alpha (σ_c/σ_f) values for ^{239}Pu in the 100 eV to 10 keV range are, in general, higher than those used in many cross-section libraries, including ENDF/B. In order to define the problem, the ETOE-MC^2 processing codes were used to generate multigroup capture and fission cross sections for ^{239}Pu using the current ENDF/B data; the computed alpha values over the range of interest are shown in Fig. 465-1. The calculations were made using fine-group lethargy widths of 0.25 and infinite dilution. A flux weighting of 1/E within a fine group was used, except for the resolved resonance region (up to 300 eV for ^{239}Pu), where MC^2 uses a flux weighting proportional to the reciprocal of the total macroscopic cross section for the medium. Calculations were also performed to generate broad-group cross sections with lethargy widths equal to 0.50. Although the evaluation of the experiments which have yielded the high alpha values is still continuing, the ENDF/B alpha values are low compared to, for example, the values recommended by Barre et al.[4] A plot of the ENDF/B alpha values, and those recommended by Barre, is shown in Fig. 465-1.

III. REACTOR ANALYSIS METHODS AND CONCEPT EVALUATIONS

A. General

A continuing task in fast reactor analysis and evaluation is the improvement of computer programs and the development of new computational methods. In addition to new methods, advances are constantly being made in computer technology which make possible the extension of existing calculational techniques.

B. Variational Principles Applied to Transport Problems (R. E. Alcouffe)

The method for estimating transverse leakage effects when performing one-dimensional transport calculations as outlined in the last quarterly report[5] has been automated on the CDC 6600. The one-dimensional transport equations are solved by using DTF-IV[6] and iterating on the transverse leakage until convergence is achieved. In this program, two transverse calculations, R-Z or X-Y, are set up as for a normal DTF-IV run. From an input estimate of the transverse leakage, the adjoint and forward flux are calculated in one spatial direction. From this calculated angular flux and adjoint, parameters are computed for the transport equation in the transverse direction. The adjoint and flux for the transverse direction are then computed from these parameters. From this result, parameters are computed for the original spatial direction. This process is repeated until the eigenvalues for both spatial directions converge, hopefully to the same value.

The method is most effectively demonstrated on small fast systems in which leakage effects are large. Four such example calculations and the effects on the eigenvalue are given in Table 465-III. In this table,

- k(2DF) is the eigenvalue computed from 2DF,
- k_z is the eigenvalue resulting from an axial calculation using the transverse leakage correction,
- k_r is the eigenvalue resulting from a radial calculation using the transverse leakage correction,
- k_c is the eigenvalue resulting from a standard DTF-IV radial calculation using the core height as the buckling height, and
- k_R is the eigenvalue resulting from a standard DTF-IV calculation using the total core plus reflector height as the buckling height.

These calculations show that the eigenvalue is sensitive to the method used to estimate the leakage. The transverse leakage corrected method appears to be adequate, although the calculated eigenvalues are consistently high, except for the bare-dimension case.

TABLE 465-III

DESCRIPTION OF EXAMPLE SYSTEMS
AND RESULTS FROM DIFFERENT ESTIMATES OF TRANSVERSE LEAKAGE

	Case 1	Case 2	Case 3	Case 4
Geometry	Cylinder	Cylinder	Cube	Cylinder
Core				
diameter (cm)	5.7	15.2	10.16	12.1
height (cm)	50.0	3.9	10.16	12.4
% ^{240}Pu	5	6		
% ^{235}U		93.2	94	93.8
Reflector				
radial thickness (cm)	7.6	7.6	22.9	5.08
axial thickness (cm)	0	7.6	22.9	5.08
% ^{235}U	0.3	0.7	0.7	0.7
k(2DF)	1.0093 (618)[a]	1.0424 (1208)	1.0262 (1838)	1.0035 (1005)
k_z	1.0401	1.0832	1.0644	1.0391
k_r	1.0023 (262)	1.0621 (272)	1.0644 (198)	1.0352 (199)
k_c	0.9932 (74)	0.8434 (54)	0.8659 (42)	0.9102 (41)
k_R	-	1.1968 (54)	1.1950 (42)	1.0762 (41)

[a] Numbers in parentheses are CP time in sec.

C. Preparation and Maintenance of Code Packages

1. Buckling Perturbation in DAC1 (B. M. Carmichael). Leakage effects in a group g in directions transverse to the defined direction in a DTF-IV calculation[6] are approximated by adding to the total cross section σ_{Tg} the term

$$\frac{1}{3\sigma_{Tg}}\frac{\pi^2}{H^2}, \qquad (1)$$

where H is the effective transverse height. In general, perturbations in σ_{Tg} will cause the buckling correction term to be perturbed. Consequently, in order to make the DAC1 perturbation code consistent with DTF-IV, the buckling correction was recently added to DAC1.

2. Linked DTF-IV and DAC1 (B. M. Carmichael). Using punched cards as the link between DTF-IV and DAC1 is cumbersome, since both regular and adjoint flux dumps, as well as the input deck, are required to transmit DTF-IV results into DAC1. Moreover, for high-order S_n, the angular flux decks become prohibitively large. To overcome these inconveniences, DAC1 has been linked directly to DTF-IV. With the new system, the regular and adjoint DTF-IV problems and the DAC1 perturbation calculation can all be performed in one run on the computer, or the sequence can be interrupted at any intermediate stage, whereupon the interim results are dumped on tape for future resumption of the sequence.

In linking the two codes, it was necessary to use the overlay programming technique. By using overlays, a program may be divided into parts, each of which is called into the central memory in the computer and is executed separately. It was found that DTF-IV itself had to be separated into two overlays; namely, an input overlay and a run overlay. In contrast with a nonoverlay job, the loader must remain in core during program execution. Since DTF-IV in nonoverlay form occupies the full available core, including the space for the loader, it was too large as a single overlay.

The sequence followed in the linked program is

1. Call DTF-IV input overlay to read and print regular problem specifications.
2. Call DTF-IV run overlay to execute regular problem.
3. Call DTF-IV input overlay to print adjoint problem specifications.
4. Call DTF-IV run overlay to execute adjoint problem.
5. Call DAC1 overlay to read perturbation specifications and execute perturbation calculations.

The common A and IA data blocks in DTF-IV which contain all the problem specifications and results, except the angular fluxes, are dumped on tape. The angular fluxes are dumped separately on the same tape. Thus, results are available for subsequent DTF-IV and/or DAC1 problems. Other overlays may readily be added to perform additional processing of DTF-IV results as desired.

A spherical model of the JEZEBEL plutonium assembly was used for testing the DTF-IV and DAC1 link. The specifications for JEZEBEL (i.e., 15.66 g/cc Pu, 4.5% ^{240}Pu, and 16.28 kg critical mass) were taken from Ref. 2. Using the Hansen-Roach 16-group cross sections,[7] and the radius of 6.2843 cm implied by the above data, a k = 1.01019 is computed by DTF-IV for both regular and adjoint cases in the S_4 approximation.

From the perturbation calculation, the effective delayed neutron fraction is 0.00193 and the neutron lifetime is 3.03×10^{-9} sec, which may be compared to the experimental values of $0.0019_4 \pm 3\%$ and $2.9_8 \times 10^{-9}$, respectively.[2] The delayed neutron abundances and yield fractions for the plutonium isotopes were taken from Ref. 8.

The worth of the plutonium in ¢/cc obtained from DAC1 as a function of radius in the JEZEBEL sphere is plotted in Fig. 465-2. The effect of the spurious "flux transients" in DTF-IV calculations on the central plutonium worth is illustrated. The worth computed for the innermost mesh point lies about 2% below the curve fitted to the other data. This is one of the effects previously noted by G. Hansen[5] that contributes to the error in central worth calculations.

Some comparisons of worths computed by the perturbation technique with direct DTF-IV k-difference calculations are given in Table 465-IV. The perturbation in the core radius might be particularly sensitive to the order of n used in the S_n calculations. Further calculations are in progress to check this point.

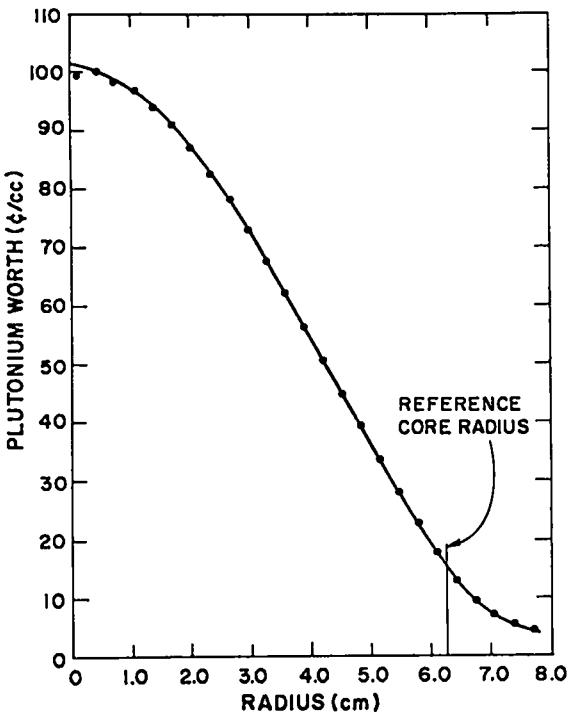

Fig. 465-2. Worth of plutonium in JEZEBEL.

TABLE 465-IV

PERTURBATION TEST CALCULATIONS

Perturbation	Δk/k: Worth from Perturbation Theory	Δk/k: Worth from k Difference	% Difference
1% increase in fuel density	0.00844	0.00837	0.81
5% increase in core radius	0.0407	0.0415	1.90
10% increase in core radius	0.0737	0.0821	10.2

3. Coupled Neutronic-Hydrodynamic Codes (M. E. Battat, J. C. Vigil). Two different computer programs that solve the coupled neutronic-hydrodynamic equations were compiled on the CDC-6600 computer, and test problems were run successfully with modifications of these programs.

The RAC code[9] was originally programmed at LASL to describe the coupled neutronic-hydrodynamic behavior of a graphite-uranium reactor core in space and time. This code was modified to describe excursions in a reactor composed of a UO_2 core and a BeO reflector. The input to the code consists of the initial geometry, temperature, relative power distribution, composition and disposition of materials, the reactivity worth per unit density of the materials, the equations of state of the materials, and the imposed reactivity above prompt critical. The code computes power, fission energy, kinetic energy, temperature, density, velocity, and pressure as functions of time in each zone. Four geometrical options are available: 1) slab, 2) cylinder with axial zones, 3) cylinder with annular zones, and 4) sphere.

During a time step, each zone is allowed to perform thermodynamic work on its neighbors through the common interface and to set the material in motion. Reactivity is decreased as the zones expand, the am amount of feedback being equal to a weighted sum of the fractional changes in density of each zone. Changes of state (solid-gas, solid-liquid, and liquid-gas) are allowed in the RAC code, but the power is assumed to vary exponentially in amplitude with a fixed spatial distribution specified in the input.

The AX-1 code,[10] as obtained from the Argonne Code Center, was coded for a step input of reactivity. It has been modified to include a ramp input of reactivity. Given a spherically symmetric, superprompt critical system, the AX-1 code computes the variation in time and space of the fission energy, temperature, pressure, density, and velocity. The code computes, as functions of time, reactivity, power, total fission, kinetic energies, and the positions of the various boundaries. The input information includes the initial geometry, initial velocities and temperatures of the zones, the composition and disposition of materials, the appropriate equation of state constants, and the neutron cross sections.

In the AX-1 code, the neutronics are calculated in S_4 approximation with up to seven energy groups. The neutronics portion of the code supplies to the succeeding portions of the program the reactivity feedback corresponding to that specific configuration. It also supplies a power distribution to be used in assigning the increase in energy within each spherical shell while this configuration remains a reasonable approximation. After a neutronics calculation, the code proceeds into the hydrodynamic and thermodynamic portions. During these portions of the calculations, the power is assumed to vary exponentially in amplitude with a period

determined from a time varying part (ramp) and a geometrical term (feedback) obtained in the S_4 calculation. If a change in configuration occurs because of motion of materials, the program returns to the neutronics portion to compute a new power distribution and feedback. Changes of state are not allowed in the AX-1 code.

In both the RAC and AX-1 codes, all delayed neutron effects are ignored, and no allowance is made for heat transfer by conduction or radiation. Tensions (negative pressures) are allowed in both codes.

Briefly, the major differences between the RAC and AX-1 codes are:

1. AX-1 computes reactivity feedback and fission distributions from S_4 neutronic calculations as the reactor expands during the transient. RAC uses a fixed relative fission distribution specified in the input, and feedback is proportional to the fractional change in density. Proportionality factors are specified as input and can be obtained from perturbation calculations of the original configuration.
2. RAC takes into account changes of state while AX-1 does not.

Considering the differences between RAC and AX-1, results obtained with the two codes for various test problems agree reasonably well.

4. Two-Dimensional Diffusion Theory Code Development (T. J. Hirons, R. D. O'Dell). Work has continued on the development of the variable basis representation[11] for the multigroup diffusion equations. The work has been restricted to two-dimensional (R-Z geometry) multigroup models with the same mesh spacing throughout all groups. A running version of the code has been developed, and parametric studies and comparisons with 2DB[12,13] have been performed.

In the variable basis method, an orthogonal transformation matrix is used for the expansion of the fluxes in a given axial region ν, i.e.,

$$\vec{\psi}_g^{\nu}(r) = Q_{\nu}\, \vec{\chi}_g^{\nu}(r) \ , \qquad (2)$$

where $\vec{\psi}_g^{\nu}(r)$ is a flux vector for group g of length $(N_{\nu} - 1)$ where N_{ν} is the number of mesh intervals in the νth axial region; Q_{ν} is the square transformation matrix of order $(N_{\nu} - 1)$; and $\vec{\chi}_g^{\nu}(r)$ is a vector containing the set of basis functions which are obtained from solution of the one-dimensional diffusion equation. This transformation couples the flux on a given interior line to the two interface fluxes bounding that region and gives region-to-region, rather than line-to-line, axial coupling. The mesh points in the axial direction are placed on the mesh boundaries rather than in the interior of the given mesh interval, and $(N_{\nu} - 1)$ is the number of interior mesh lines in the νth axial region. The basis functions for the interior mesh lines are obtained by the Crout reduction method, and the fluxes are then obtained as a linear combination of the basis functions according to

$$\psi_{g,k}^{\nu}(r) = \sum_{\ell=1}^{(N_{\nu}-1)} Q_{k,\ell}^{\nu}\, \chi_{g,\ell}^{\nu}(r) \qquad (3)$$

$$\text{for } k = 1, 2, \ldots, (N_{\nu} - 1).$$

The interface fluxes between axial zones are obtained directly by a second-order Taylor series expansion in which the flux at the adjacent interior line is expanded in terms of the interface flux. This operation is performed for the axial zone on both sides of the interface, and continuity of flux and current are then employed to obtain a consistent expression for the flux at the interface. Vacuum boundary conditions on the top and/or bottom exterior boundaries are also handled with a second-order Taylor series expansion. For the case of reflective boundary conditions on the top and/or bottom, a symmetry condition is employed for the flux on the adjacent interior line, and the diffusion equation on the boundary is then solved directly by the Crout reduction method.

The fluxes obtained from the variable basis method are point fluxes with respect to the axial direction, and a Simpson-rule integration technique is used to obtain the total fission source and other reaction rates which are needed for the source iteration.

Two reactor models were studied extensively in the evaluation of the variable basis method. The first is a relatively simple system consisting of a one-region core with axial reflector regions on the top and bottom and a single radial reflector. A 288-mesh array (16 radial and 18 vertical points)

was used to describe the system, which has both radial and axial symmetry. The second model is the 18-region 1000-MWe mixed oxide fast-breeder reactor referred to previously.[5] A 1462-mesh array (43 radial and 34 vertical points) was used for most of the studies on this model, which is considerably more complex than the other reactor.

For the 288-mesh, 4-region system, the variable basis representation gave similar results to those obtained from the 2DB code. Running times were 5 to 10% greater than with 2DB, but the variable basis technique gave slightly improved accuracy in the eigenvalue for a given mesh spacing. The converged eigenvalue from this method was fairly sensitive to the group flux distributions, and group rebalancing was required before each pass through the mesh to ensure a properly converged answer. The eigenvalue convergence pattern depended strongly on the acceleration schemes used, i.e., recycling through the mesh, and flux and fission-source over-relaxation. Various combinations of these acceleration techniques were tried, and results indicated that the optimum acceleration scheme depended on the problem. In general, 3 to 5 mesh cycles per group gave the best results, along with flux and fission-source over-relaxation factors which started low (1.0 to 1.1) and increased by some increment as the outer iterations increased to a final maximum value of 1.5 to 1.7.

With the 1462-mesh 18-region model, the running times for the variable basis model were significantly longer (20 to 35%) than those for the 2DB code. As before, slightly greater accuracy in the eigenvalue was obtained, but the sensitivity of the problem to acceleration schemes was greatly increased. For example, the use of an over-relaxation factor which gave good results with the 288-mesh problem often led to oscillations in the convergence pattern of the 18-region model, resulting in either an erroneous eigenvalue or no convergence at all. This behavior dictated the use of more conservative acceleration schemes, which, in turn, gave increased computer running times.

The results of the investigation of the variable basis method to date do not demonstrate improvement over the 2DB code, and, for more complex reactor models with large mesh arrays, significantly longer computer running times are required. Work is continuing in an attempt to improve the performance of this technique.

D. Fast Reactor Design Analysis (T. J. Hirons, R. D. O'Dell).

Detailed burnup analysis, using the 2DB code, is now in progress on the 1000-MWe mixed-oxide LMFBR.[14] The calculational model is shown in Fig. 465-3. An eight-group cross-section set generated from the core spectrum alone is being used. The breeding ratio and the isotopic contents of the various core and blanket zones are the most significant quantities being determined.

In order to achieve the desired 100,000 MWd/T burnup of the core fuel, the reactor is to be operated on a schedule consisting of a series of 146-d (100% load factor) refueling intervals. Each refueling interval should produce 25,000 MWd/T burnup in core zones 1 and 2 and 16,670 MWd/T burnup in core zone 3 (per fuel charge). A particular fuel charge must reside in the core for either four (core zones 1 or 2) or six (core zone 3) refueling intervals in order to achieve the design burnup. At the end of each refueling interval, a fraction of the

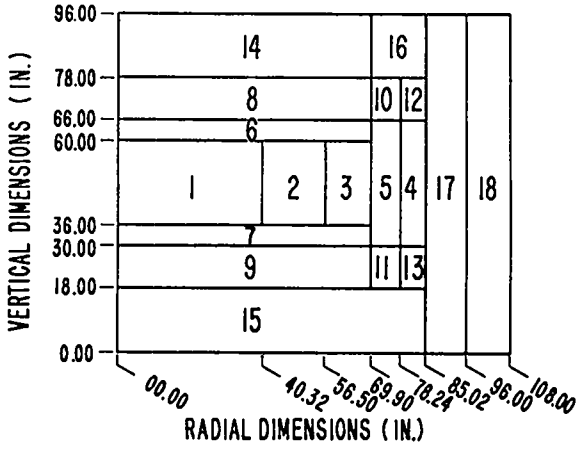

1. CORE ZONE 1
2. CORE ZONE 2
3. CORE ZONE 3
4. RADIAL BLANKET OUTER
5. RADIAL BLANKET INNER
6. UPPER AXIAL BLANKET INNER
7. LOWER AXIAL BLANKET INNER
8. UPPER AXIAL BLANKET OUTER
9. LOWER AXIAL BLANKET OUTER
10. UPPER RADIAL BLANKET
11. LOWER RADIAL BLANKET
12. VOID
13. VOID
14. UPPER AXIAL REFLECTOR
15. LOWER AXIAL REFLECTOR
16. UPPER RADIAL REFLECTOR
17. THERMAL SHIELD
18. RADIAL SODIUM REFLECTOR

Fig. 465-3. 18-region model of the 1000-MWe mixed-oxide reactor.

fuel in each core zone is removed and replaced with clean fuel. On the equilibrium cycle, the fuel removed and replaced at the end of each refueling interval will have undergone a burnup of 100,000 MWd/T. In accordance with the 146-d refueling interval, the fraction of the fuel removed and replaced at the end of each refueling interval on the equilibrium cycle is 1/4, 1/4, and 1/6 for core zones 1, 2, and 3, respectively.

The axial blankets above and below the core zones are refueled on the same schedule, since they are an integral part of the total fuel element assembly. The fuel management program calls for the radial blanket fuel assemblies to be replaced once every eight refueling intervals. The burnup schedule for a refueling interval on the equilibrium cycle is shown in Table 465-V.

TABLE 465-V

BURNUP SCHEDULE FOR A REFUELING INTERVAL ON THE EQUILIBRIUM CYCLE

(1000-MWe Mixed-Oxide LMFBR)

	Total Burnup (MWd/T)	
Fraction of Fuel	Begin Refuel Interval	End Refuel Interval
Core zones 1 & 2		
1/4	0	25,000
1/4	25,000	50,000
1/4	50,000	75,000
1/4	75,000	100,000[a]
Average	37,500	62,500
Core zone 3		
1/6	0	16,670
1/6	16,700	33,300
1/6	33,300	50,000
1/6	50,000	66,700
1/6	66,700	83,300
1/6	83,300	100,000[a]
Average	41,700	58,300

[a]Ready for discharge.

To be consistent with current schemes for economic analyses, the burnup process was begun with the reactor fully charged with clean fuel. Boron carbide was added to produce criticality, and the burnup for the first refueling interval was calculated by 2DB. Following this time step, 1/4 of the fuel in core zones 1 and 2 and 1/6 of the fuel in core zone 3 was removed and replaced with clean fuel. The boron content was readjusted to produce criticality, and a second burnup step was calculated. Following this step, the appropriate fraction of fuel in the core zones was removed and replaced with clean fuel. The fuel removed was only that which had undergone the maximum burnup of 50,000 MWd/T in core zones 1 and 2 and 33,300 MWd/T in core zone 3. After this refueling, the boron content was again adjusted to critical and another burnup step was calculated. This sequence was continued through at least six refueling intervals in order to achieve the equilibrium cycle.

To assure proper refueling before starting a new burnup step, two programs were written to calculate and punch the input atom densities for the next refueling interval. The program ATMDEN calculates the atom densities following refueling through six burnup intervals, assuming no flux shift in the reactor in progressing to the equilibrium cycle. A more general program, ATDENS, calculates both the atom density of the fuel fraction to be discharged, as well as the atom density following the refueling with a first-order correction for flux shift from interval to interval. Parallel burnup calculations have been performed using these two programs in conjunction with 2DB. In addition to the 18-region whole-core model, a 24-region half-core model was used.

Analysis and comparison of the results will be forthcoming.

REFERENCES

1. K. Parker, "The Aldermaston Nuclear Data Library as of May 1963," AWRE-0-70/63, UKAEA (1963).

2. G. A. Jarvis et al., Nucl. Sci. Eng. 8, 525 (1960).

3. H. C. Paxton, "Los Alamos Critical-Mass Data," LAMS-3067, Los Alamos Scientific Laboratory (1964).

4. J. Barre et al., "Examen Critique des Valeurs de $\alpha = \sigma_C/\sigma_F$ pour le ^{239}Pu au-dela de 1 keV et des Experiences Pouvant Ameliorer sa Connaissance," CEA-N-989, Saclay (1968).

5. "Quarterly Status Report on the Advanced Plutonium Fuels Program, July 1 to September 30, 1968," LA-4073-MS, Los Alamos Scientific Laboratory (1968).

6. K. D. Lathrop, "DTF-IV, a FORTRAN-IV Program for Solving the Multigroup Transport Equation with Anisotropic Scattering," LA-3373, Los Alamos Scientific Laboratory (1965).

7. G. E. Hansen and W. H. Roach, "Six and Sixteen Group Cross-Sections for Fast and Intermediate Critical Assemblies," LAMS-2543, Los Alamos Scientific Laboratory (1961).

8. G. R. Keepin, Physics of Nuclear Kinetics, Addison Wesley (1965).

9. C. G. Chezem and W. R. Stratton, "RAC, A Computer Program for Reactor Accident Calculations," LAMS-2920, Los Alamos Scientific Laboratory (1963).

10. D. Okrent et al., "AX-1, A Computing Program for Coupled Neutronics-Hydrodynamics Calculations on the IBM-704," ANL-5977, Argonne National Laboratory (1959).

11. R. A. Axford, private communication.

12. W. W. Little, Jr. and R. W. Hardie, "2DB, a Two-Dimensional Diffusion-Burnup Code for Fast Reactor Analysis," BNWL-640, Battelle Northwest Laboratory (1968).

13. W. W. Little, Jr. and R. W. Hardie, "2DB User's Manual," BNWL-831, Battelle Northwest Laboratory (1968).

14. "Liquid Metal Fast Breeder Reactor Design Study (1000 MWe UO_2-PuO_2 Fueled Plant)," GEAP-4418, General Electric (1963).

PROJECT 466

FAST REACTOR METALLIC FUEL STUDIES

Persons in Charge: R. D. Baker
D. B. Hall
Principal Investigators: W. J. Maraman
R. H. Perkins

I. INTRODUCTION

The objective of this program is the development of metal fuels for fast reactor application. Much of the primary effort is placed on preparation and fabrication development of the U-Pu-Zr alloys. Supporting effort is directed toward areas of physics and system evaluation, determining of physical and chemical properties of the fuel, and studying fuel-cladding interactions.

Irradiation testing is an essential part of the evaluation of a potential fuel alloy for fast reactor application. A knowledge of its intrinsic swelling rate as a function of alloy composition, metallurgical history, irradiation temperature, and total burnup must be obtained. The fission gas release rates and the limits of lattice-retained gas as a function of the above parameters are also required. In addition, the compatibility of fuels and claddings during irradiation at temperatures of interest to the LMFBR program must be determined.

II. FUEL PREPARATION AND FABRICATION
(D. R. Harbur, B. N. Robbins, A. K. Murdock, E. L. Grady)

A. General

The initial goals of this project are to prepare high purity, homogeneous U-15Pu-6Zr to U-15Pu-15Zr alloys, to fabricate these alloys into fuel pins of the EBR-II size and to fully characterize these pins. An alloy preparation and casting method for making high purity, homogeneous extrusion billets has been developed. Emphasis is now being placed upon the fabrication of these homogeneous billets into fuel pins with large length to diameter ratios. Characterization of these extruded alloys has been initiated.

B. Current Results

Homogeneous U-15Pu-6Zr to U-15Pu-15Zr alloys are now being prepared routinely by induction melting of the three elements in a NbC-coated graphite crucible at 1400°C, mechanically stirring the melt for 30 min and pouring into an ambient temperature aluminum mold. The chemical analyses of the feed materials and the top and bottom of a typical 0.75-in.-diam, 14-in.-long U-15Pu-12Zr chill-cast billet is shown in Table 466-I. The oxygen level of the alloys now being produced is between 40 and 120 ppm, which is the nominal range present in the feed materials. Figure 466-1 is a photomicrograph of a chill-cast U-15Pu-12Zr alloy showing essentially no α Zr(O) phase.

Two additional colloidal mold coatings of ZrC and Y_2O_3 with a high temperature silicate binder are being evaluated. Both of these coatings are easily applied with a spray gun and have exceptionally high adhesive strengths with good thermal shock properties.

A total of 29 extrusions have been made with the U-15Pu-6Zr to U-15Pu-12Zr alloys using a 60° die and less than 50 T of force. The material is being extruded at a 9 to 1 ratio (0.75 in. to 0.25 in. diam) in the α-phase temperature region at 570°C. Two extrusions were made at a 4 to 1 ratio in a shear die, and it was found that the internal friction within this alloy system is as high as the friction between the billet and the wall of the extrusion die. Curvature of the extruded rods has been eliminated by extruding the rods into a 0.312-in.-diam tube.

Table 466-I

Chemical Analyses[a] of Feed Material and As-Cast U-Pu-Zr Alloy

	Feed Material			As-Cast U-Pu-Zr	
Element	U	Pu	Zr	Top	Bottom
Pu	--	100%	--	15.00%	14.95%
Zr	--	< 0.1	100%	12.0%	12.1%
U	100%	41	--	73.0%	72.9%
O	50	20	170	110	85
C	70	20	110	90	60
H	--	10	80	10	5
Fe	40	4	50	240	210
Ga	--	2	--	45	20
Ta	--	< 5	< 20	< 25	< 25
Th	--	2	--	< 15	< 15
W	--	70	--	12	13
Li	< 0.1	< 0.005	< 30	< 2	< 2
Be	< 0.1	0.01	< 1	< 2	< 2
B	0.3	< 0.3	3	< 1	< 1
Na	1	1	< 100	< 5	< 5
Mg	40	1	10	< 5	5
Al	< 1	1	10	< 10	< 10
Si	25	4	30	25	25
P	< 50	--	--	< 50	< 50
Ca	< 2	2	< 100	< 5	< 5
Cr	1	< 0.5	< 10	25	25
Mn	3	< 0.1	< 3	8	8
Ni	5	0.5	< 10	40	35
Cu	2	0.6	< 10	5	5
Zn	--	< 10	< 30	< 10	< 10
Sr		< 0.1	--	< 5	< 5
Cd	< 1	< 0.5	< --	< 10	< 10
Sn	< 1	< 0.5	10	< 5	< 5
Pb	< 1	< 0.5	30	< 10	< 10
Bi	--	< 0.5	< 10	< 2	< 2
Nb	--	--	--	16	29

[a] Expressed as parts per million by weight, or percent, by weight, as noted.

Fig. 466-1 As-cast U-15Pu-12Zr chill-cast into an aluminum mold at 25°C. Oxygen content 70 ppm.

Severe grain orientation is obtained at extrusion rates higher than 1 in./min. Recrystallization of the extruded alloy occurs during extrusion at rates below 0.5 in./min. The recrystallized alloy is being examined by x-ray methods to determine if the preferred orientation has been completely eliminated. Thermal cycling experiments have also been initiated to determine if any preferred orientation exists which would cause anisotropic growth during temperature cycling through the phase transformation.

The swaging machine has been received and is now being enclosed in a glovebox.

Several extruded rods of the U-15Pu-6Zr to U-15Pu-12Zr alloys have been machined into tensile bars and tested at a standard strain rate of 0.015 in./in./min. The tensile strengths varied between 75,000 and 97,000 psi at 25°C with no measureable elongation. At 100°C the tensile strength of a

U-15Pu-12Zr extruded rod was 79,000 psi with no measureable elongation. At temperatures of 290 and 500°C the U-15Pu-6Zr alloy exhibited high ductility. At a load of 5,660 psi the specimen heated to 290°C was elongated by 33% giving the creep curve shown in Fig. 466-2. The secondary and tertiary stages

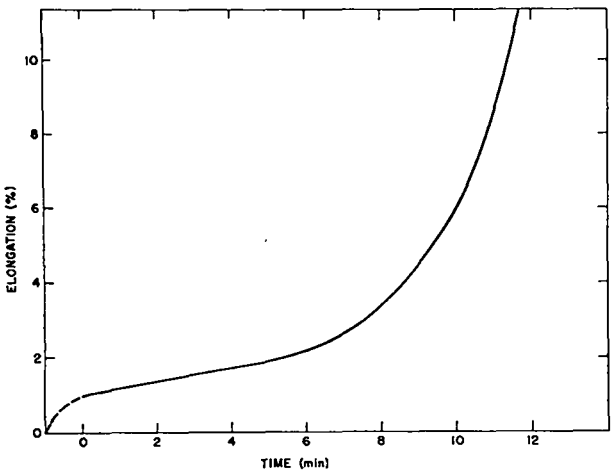

Fig. 466-2. Creep curve of U-15Pu-6Zr at 290°C and 5,660 psi. Total elongation 33%.

of creep are quite evident. The primary stage of creep is shown as a dashed line, since the load was increased slowly during this period to determine the minimum load at which creep would occur. The specimen heated to 500°C was elongated by 83% at a minimum stress of 1100 psi while the temperature was being increased. Figure 466-3 shows several

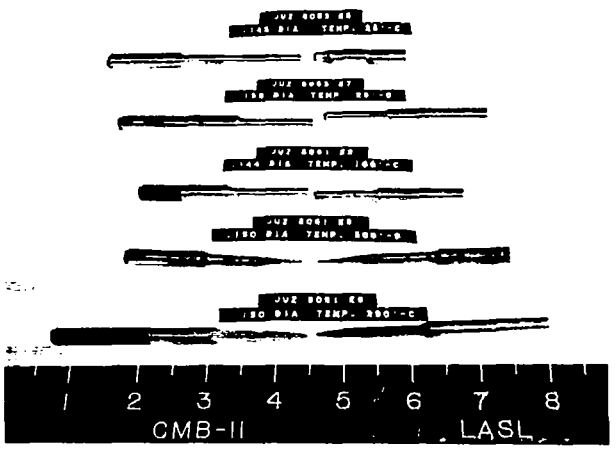

Fig. 466-3. Tensile specimens of extruded U-15Pu-6Zr (JUZ-8061) and U-15Pu-12Zr (JUZ-8053) tested at various temperatures. Note extreme ductility in specimens tested at 290 and 500°C.

tensile specimens which were made from 0.25 in. diam extruded rods and tensile/creep tested at various temperatures.

Compatibility samples from three different lots of the U-Pu-Zr alloys have been prepared. These consist of two lots of nominally U-15Pu-12.5Zr having oxygen contents of 180 and 820 ppm. The third lot is a U-14Pu-6Zr alloy containing 125 ppm oxygen. An additional batch of specimens received from ANL having the composition U-15.6Pu-10.7Zr and containing 650 ppm oxygen is now available for test. As-cast pins have also been prepared for irradiation tests.

III. METAL FUEL COMPATIBILITY TESTING (J. A. Horak)

A. General

The purpose of this task is to study the compatibility of potential fast reactor metallic fuels (e.g., U-Pu-Zr alloys) with potential cladding materials (e.g., Type 316 stainless steel). This will be accomplished by studying the mechanisms and kinetics of reactions between the fuels and cladding both in-pile and out-of-pile at temperatures of interest to LMFBR designers. The emphasis will be on out-of-pile studies with neutron irradiation being added as an experimental variable. To attempt to understand some of the reactions which will occur between the complex candidate fuel and cladding alloys, some experiments will be performed to study the reactions between the pure components of these alloys (e.g., U vs Fe).

B. Current Results

A series of out-of-pile compatibility tests for U-Pu-Zr fuels in Type 316 stainless steel clad has been planned. These tests are listed in Table 466-II. For the U-15Pu-12.5Zr alloys there are two levels of oxygen in the fuel; this is to study the effect of oxygen concentration on compatibility. An alloy that has only 6 w/o zirconium has been produced to determine the effect of zirconium concentration on the compatibility with Type 316 stainless steel. Eighteen specimens of the U-Pu-Zr produced by Argonne are included in the tests to determine the effect of the inhomogeneities resulting from injection casting on compatibility.

The fuel and cladding material for the tests

Table 466-II

U-Pu-Zr Alloys to be Tested with Type 316 Stainless Steel

Alloy	O_2 (ppm)	Temp (°C)	No. of Specimens 200 h	1000 h	4000 h
U-15Pu-12.5Zr	180	800	2	2	2
		750	2	2	2
		700		2	2
		650		2	2
U-15Pu-12.5Zr	820	800	2	2	2
		750	2	2	2
		700		2	2
		650		2	2
U-14Pu-6Zr	125	800	2	2	2
		750	2	2	2
		700		2	2
		650		2	2
U-15.6Pu-10.7Zr (Produced by ANL)	650	800	2	2	2
		750		2	2
		700		2	2
		650		2	2

indicated in Table 466-II have been prepared. They will be sealed in capsules and bonded as soon as the scheduled use of inert gas fuel loading facility permits. Sodium test loops and inert gas furnaces have been activated for these tests.

IV. IRRADIATION EFFECTS STUDIES
(J. A. Horak, R. L. Cubitt)

A. General

All long-term irradiations of metal fuel to date have had the effects of thermal cycling (due to reactor shutdowns and changes in power level) imposed upon the effects due to irradiation. Some of the detrimental effects to the fuel caused by this thermal cycling are:

1. The internal stresses produced by the volume changes associated with the alpha-gamma phase transformation in uranium-base alloys could be the source of microcracking.
2. Upon cooling, as alpha grains nucleate and grow from the existing gamma grains, the fission products (those that are insoluble and/or above their solubility limits) are swept ahead of the new alpha grains and end up in the alpha grain boundaries. The reverse process occurs on heating. The agglomeration of these elements produces a brittle and/or weak phase (usually intermetallic) resulting in a decrease in the mechanical strength and ductility of the fuel. This phase could exhibit a lower corrosion resistance to hot sodium than that typical of the parent fuel.
3. Possibly even more important is the relocation of fission gases during thermal cycling; the agglomeration of fission gases during repeated phase transformations could be responsible for the extensive swelling and cracking observed in many of the fuel alloys irradiated to date.

It is evident that thermal cycling of unirradiated material does not provide the information necessary to separate the effects due to irradiation from those due to combined irradiation and thermal cycling.

One of the prime objectives of this program is to determine the effects of irradiation in the absence of thermal cycling. Irradiations will be conducted in the Omega West Reactor where controlled temperature instrumented facilities are available.

Parallel experiments will involve thermal cycling to assess accurately the effects of thermal cycling during irradiation on the properties to be studied.

B. Current Results

The initial in-pile compatibility test will be on U-5Fs vs Type 304 stainless steel. The main purpose of this test is to determine the capabilities of the existing in-pile temperature control system. It is also necessary to determine the requirements of the proposed gas-filled "heat leak" system that will maintain constant temperature operation of the fuel with and without reactor power.

Three U-5Fs fuel specimens have been loaded into and sodium-bonded to the primary container (Type 304L stainless steel). They have been helium leak checked, radiographed, eddy current tested and loaded into the specimen holder. They are currently awaiting insertion into the secondary container. All of the hardware for the secondary insert system is complete and assembly of the experiment has begun. The major portion of the rehabilitation of the electrical and gas systems at OWR is complete and the experiment will be placed in the reactor early in calendar year 1969.

V. ANALYTICAL CHEMISTRY

1. Determination of Oxygen in U-Pu-Zr Alloys

(M. E. Smith, W. B. Hutchinson)

An inert-gas-fusion method was modified for the determination of oxygen in U-Pu-Zr alloys by substituting a Pt-20Sn bath at 1800°C for the customary molten platinum bath at 2000°C. The U-Pu-Zr samples dissolved more rapidly and completely in the Pt-Sn bath, which facilitated the release of oxygen as CO and improved the precision of the method. The evolved CO was oxidized to CO_2 and measured manometrically. Repeated analyses of a U-Pu-Zr alloy using each bath showed that the precision (1 σ) of a single determination of oxygen was 9 relative percent using the Pt-Sn bath as compared to 15 relative percent with the platinum bath.

2. Electron Microprobe Examinations of U-Pu-Zr Alloys

(E. A. Hakkila and H. L. Barker)

The electron microprobe was applied to the determination of the homogeneity of two U-Pu-12.5Zr alloys. Variations in the U, Pu, and Zr x-ray intensities measured at various locations showed that the alloys were heterogeneous. White areas contained significantly more zirconium than gray areas.

3. Miscellaneous Analytical Support

(C. S. MacDougall, W. Hutchinson, W. W. Wilson, L. E. Thorn, W. J. Baughman, G. R. Waterbury, C. J. Martell, C. B. Collier, and J. V. Pena)

A modified inert-gas-fusion method was applied to measurement of oxygen in 54 samples of U-Pu-Zr alloys. The oxygen content of these samples ranged from 40 ppm to 0.18%. No analytical difficulties were experienced.

Controlled-potential coulometric methods for measuring plutonium and uranium were applied without difficulty to analysis of 18 U-Pu-Zr alloys. The relative standard deviations were 0.2 to 0.3% in measuring either element.

A combustion-manometric method performed satisfactorily in measuring carbon in 20 U-Pu-Zr alloys. For the carbon concentration range between 30 and 850 ppm found in these samples, the precision (1 σ) was 10 relative percent.

Spectrophotometric methods were applied to measurement of zirconium in 39 U-Pu-Zr alloys; W, Th, Ta, Ga, and Fe in two of these alloys; and niobium in four alloys. The relative standard deviations were 1% in measuring zirconium and 2% in measuring W, Ga, Nb, and Fe. The thorium and tantalum concentrations were less than 15 ppm and 25 ppm, respectively, which were the lower limits of reliable measurement by these methods. Spectrographic impurities were determined in nine samples of U-Pu-Zr alloys.

SPECIAL DISTRIBUTION

Atomic Energy Commission, Washington

Division of Research

D. K. Stevens

Division of Naval Reactors

R. H. Steele

Division of Reactor Development and Technology

L. J. Colby
G. W. Cunningham
D. E. Erb
Nicholas Grossman
W. H. Hannum (2)
K. E. Horton
J. R. Humphreys
R. E. Pahler
J. M. Simmons (2)
E. E. Sinclair
Bernard Singer
C. E. Weber
G. W. Wensch
M. J. Whitman

Division of Space Nuclear Systems

G. K. Dicker
F. C. Schwenk

Idaho Operations Office

DeWitt Moss

Ames Laboratory, ISU

O. N. Carlson
W. L. Larsen
M. Smutz

Argonne National Laboratory

F. G. Foote
Sherman Greenberg
J. H. Kittel
W. B. Loewenstein
R. E. Macherey
M. V. Nevitt

Idaho Falls, Idaho

D. W. Cissell
R. C. Robertson

Atomics International

R. W. Dickinson, Director
Liquid Metals Information Center

J. L. Ballif

Babcock & Wilcox Co.

C. Baroch
J. H. MacMillan

Battelle Memorial Institute

D. L. Keller
S. J. Paprocki

Brookhaven National Laboratory

D. H. Gurinsky
C. Klamut

Combustion Engineering, Inc.

S. Christopher

Donald W. Douglas Laboratories

R. W. Andelin

General Electric Co., Cincinnati, Ohio

V. P. Calkins

General Electric Co., Sunnyvale, California

R. E. Skavdahl

Gulf General Atomic, Inc.

E. C. Creutz

Idaho Nuclear Corporation

W. C. Francis

IIT Research Institute

R. Van Tyne

Lawrence Radiation Laboratory

Leo Brewer
J. S. Kane
A. J. Rothman

LMFBR Program Office

Alfred Amorosi
D. K. Butler (Physics)
L. R. Kelman (Fuels & Materials)
J. M. McKee (Sodium Technology)

Mound Laboratory

R. G. Grove

NASA, Lewis Research Center

J. J. Lombardo

Naval Research Laboratory

L. E. Steele

Oak Ridge National Laboratory

G. M. Adamson
J. E. Cunningham
J. H. Frye, Jr.
C. J. McHargue
P. Patriarca
O. Sisman
M. S. Wechsler
J. R. Weir

Pacific Northwest Laboratory

F. W. Albaugh
E. A. Evans

FFTF Project

E. R. Astley
B. M. Johnson
D. W. Shannon (2)

U. S. Department of Interior

Bureau of Mines, Albany, Oregon

H. Kato

United Nuclear Corporation

A. Strasser

Westinghouse, Advanced Research Division

E. C. Bishop

Westinghouse, Bettis Atomic Power Laboratory

E. J. Kreigh